Distribution Agreement

In presenting this thesis or dissertation as a partial fulfillment of the requirements for an advanced degree from Emory University, I hereby grant to Emory University and its agents the non-exclusive license to archive, make accessible, and display my thesis or dissertation in whole or in part in all forms of media, now or hereafter known, including display on the world wide web. I understand that I may select some access restrictions as part of the online submission of this thesis or dissertation. I retain all ownership rights to the copyright of the thesis or dissertation. I also retain the right to use in future works (such as articles or books) all or part of this thesis or dissertation.

Signature:

_____ _____

Lauren Jeffers Date

Chronic Alcohol Consumption Induces Alveolar Epithelial Barrier Dysfunction *in vivo*

By

Lauren Jeffers
Doctor of Philosophy

Graduate Division of Biological and Biomedical Sciences
Biochemistry, Cell and Developmental Biology

_____
Michael Koval, Ph.D., Advisor

_____
Douglas C Eaton, Ph.D., Committee Member

_____
Andrew Kowalczyk, Ph.D., Committee Member

_____
Jennifer Kwong, Ph.D., Committee Member

_____
Bashar Staitieh, M.D., Committee Member

Accepted:

_____
Kimberly Jacob Arriola, Ph.D, MPH
Dean of the James T. Laney School of Graduate Studies

_____
Date

Chronic Alcohol Consumption Induces Alveolar Epithelial Barrier Dysfunction *in vivo*

By

Lauren Jeffers
B.S., University of Florida, 2011
B.A., University of Florida, 2011

Advisor: Michael Koval, Ph.D.

An abstract of
A dissertation submitted to the Faculty of the
James T. Laney School of Graduate Studies of Emory University
in partial fulfillment of the requirements for the degree of
Doctor of Philosophy in
Graduate Division of Biological and Biomedical Sciences
Biochemistry, Cell and Developmental Biology
2022

Abstract

Chronic Alcohol Consumption Induces Alveolar Epithelial Barrier Dysfunction *in vivo*

By Lauren Jeffers

Chronic alcohol abuse is a major risk factor for developing Acute Respiratory Distress Syndrome, a serious lung condition and a form of respiratory failure characterized by widespread airspace flooding and inflammation. One mechanism by which alcohol use weakens the integrity of the alveolar epithelial barrier is by changing the composition of tight junction proteins that are critically necessary to maintain a functional air-liquid interface. Previously, we have shown that alcohol exposure increases the paracellular permeability and decreases the transepithelial resistance across alveolar epithelial cells *in vitro*. Here, we first establish a novel model using Evans Blue dye to assess paracellular permeability across both epithelial and endothelial barriers *in vivo* using a murine animal model. We then tested the effects of alcohol and an endotoxemia injury on pulmonary function by comparing direct (intratracheal, IT) to indirect (intraperitoneal, IP) administration of lipopolysaccharide (LPS). Chronic alcohol ingestion primes the lung for increased alveolar macromolecular leak when coupled with either route of endotoxin injury and further compromises the vascular endothelial barrier when the LPS is administered directly (IT). Moreover, we show that nebulized treatment of a mimetic peptide of a tight junction-associated protein rescues the alcohol-mediated alveolar leak in mice treated with IT-administered LPS. Additionally, we begin to test *Klebsiella pneumoniae* as a model for infectious pneumonia and its effect on alcohol-primed lungs. We found a disease burden-dependent increase on alveolar permeability and that alcohol-fed mice had decreased bacterial clearance, providing a potential new infectious injury model against which barrier-enhancing therapeutics can be tested.

Chronic Alcohol Consumption Induces Alveolar Epithelial Barrier Dysfunction *in vivo*

By

Lauren Jeffers
B.S., University of Florida, 2011
B.A., University of Florida, 2011

Advisor: Michael Koval, Ph.D.

A dissertation submitted to the Faculty of the
James T. Laney School of Graduate Studies of Emory University
in partial fulfillment of the requirements for the degree of
Doctor of Philosophy in
Graduate Division of Biological and Biomedical Sciences
Biochemistry, Cell and Developmental Biology
2022

Acknowledgements

This work would not have been possible without the support of my current and former dissertation committee members: Drs. Douglas Eaton, Andrew Kowalczyk, Jennifer Kwong, Brian Petrich, and Bashar Staitieh. Additionally, I would like to extend my deepest gratitude for the years of support from my advisor, Dr. Michael Koval. The advice and recommendations from members of the Koval lab have been instrumental to my success as a graduate student. I would like to highlight my gratitude to Dr. Prestina Smith for her invaluable guidance over my project. I am thankful for my fellow graduate students in the Koval lab for the emotional support to thrive in graduate school, including Drs. Sabrina Lynn and Raven Peterson, Kristen Easley, and Yasmin Ibrahim. I would like to thank the animal care staff and administrative personnel of the Department of Animal Resources for maintaining my research animals and making my dissertation research possible. Additionally, I would like to thank the numerous medical students and undergraduate students who assisted me with various experiments through my graduate career.

Abbreviations

αCT1	Cx43 Carboxyl-Terminal Mimetic Peptide
CT	Claudin-5 peptide mimetic
EB	Evans Blue (dye)
IP	Intraperitoneal
IT	Intratracheal
IV	Intravascular
ZO-1	Zonula Occludens 1
Cx43	Connexin 43
AJ	Adherens junction
TJ	Tight junction
AJC	Apical junctional complex
PDZ	postsynaptic density protein, Drosophila disc large tumor suppressor, and zonula occludens-1 protein binding motif
LPS	Lipopolysaccharide
PBS	Phosphate Buffered Saline

Table of Contents

Chapter 1: Introduction

Lung anatomy

The lung is a vital organ that is required for respiration to oxygenate blood. Lungs bring oxygen-rich inspired air in close proximity to relatively deoxygenated venous blood in the pulmonary capillaries. The conducting zone of the respiratory tree is responsible for warming, humidifying, and filtering inspired air but does not participate in gas exchange. The conducting zone is made up of both large airways (trachea, and bronchi) and small airways (bronchioles). The respiratory zone is responsible for gas exchange and consists of respiratory bronchioles, alveolar ducts, and the alveoli.

Inspired air flows from the trachea to the left main and right main bronchus which are then subdivided into five lobar bronchi. Each lobar bronchus then divides into segmental bronchi, further branching into 20-25 more generations before terminating in a terminal bronchiole which marks the end of the conducting zone and beginning of the respiratory zone. The terminal bronchioles branch into several generations of the respiratory bronchioles. Each respiratory bronchiole can give rise to 2 to 11 alveolar ducts that each form 5 to 6 alveolar sacs, the fundamental and structural unit of the lung. Airway resistance is lowest in the alveoli due to the massive total cross-sectional area.

From a vasculature perspective, a main pulmonary artery supplies poorly oxygenated blood to each lung. This main pulmonary artery divides into a right and left main pulmonary artery, that further branches into lobar, segmental arteries, subsegmental pulmonary arteries, intralobular arteries, eventually forming arterioles that lead to pulmonary capillaries which surround the alveoli. Blood that has been oxygenated after passing near the alveoli is collected through venules that unite into larger vessels, eventually draining each lung through pulmonary veins to carry freshly oxygenated arterial blood to the left atrium heart to be delivered to the systemic vascular system.

The respiratory membrane consists of the alveolar and capillary walls, a thin structure through which gasses are transferred between the outside environment and the bloodstream. Gases first cross through the alveolar lining fluid that contains surfactant and is essential for maintaining lung function.

Subsequent layers of the respiratory membrane are the alveolar epithelia which consist of simple squamous epithelium and a basement membrane, a thin interstitial space, the capillary basement membrane, and the endothelial cell membrane. The entire respiratory membrane is only 0.2 - 0.6μm (Hall & Guyton, 2011).

The alveolus consists primarily of three cell types, type I pneumocytes, type II pneumocytes, and alveolar macrophages. Type I pneumocytes are thin, squamous cells that are optimal for gas diffusion and make up over 95% of alveolar surfaces (Weinberger et al., 2019). Type II pneumocytes are more numerous in the alveolus than type I pneumocytes but cover much less surface area as they are smaller cuboidal cells dispersed between type I cells. These cells serve as precursors to regenerate other type II pneumocytes or differentiate into type I pneumocytes. Type II pneumocytes are also responsible for secreting surfactant and tend to proliferate during lung damage. Pulmonary surfactant is primarily made up of phospholipids, surfactant proteins, and other neutral lipids and serve to increase pulmonary compliance, prevent atelectasis, and reduces surface tension (Nkadi et al., 2009). Alveolar macrophages are large phagocytic cells that phagocytose foreign materials and release cytokines and alveolar proteases to remove foreign particles or microorganisms from the respiratory surfaces.

The epithelial barrier and tight junctions

The alveolar epithelial barrier plays an essential function to protect the underlying tissues from the invasion of pathogens and regulate the paracellular flux of ions and solutes. These thin epithelial cells fit closely together to enable simple diffusion of ions and passive water flow between tissues. Alveolar epithelial cells are polarized, having an apical surface facing the luminal airway and a basal surface facing the interstitial tissue of the lung. The polarized nature of the epithelia permits electrochemical gradients to be created and to direct passive flow of water between tissues. Basolateral sodium, potassium ATPase pumps actively drive extracellular potassium from the interstitium into the cells while simultaneously pumping intracellular sodium out into the interstitium. This pump is paired with passive apical epithelial sodium channels to direct the flow of sodium from the luminal airway into the lung interstitium, setting

up an electrochemical gradient to direct the passive flow of water between tissues through aquaporins.

Different types of cell junctions bind epithelial cells together, enabling epithelia to maintain a paracellular barrier and control paracellular transport. Desmosomes provide structural support via interaction with intermediate filaments. Gap junctions permit electrical and chemical communication between cells. Adherens junctions form a belt-like structure to connect the actin cytoskeletons of adjacent cells. Lastly, tight junctions are the most apically located and regulate paracellular movement of solutes and water between epithelial layers. Adherens junctions and tight junctions both contribute to the apical junctional complex, a cell-to-cell adhesion system that maintains cell polarity and participates in signal transduction.

Tight junctions form a branching network of sealing protein complex strands to form selective channels for ions and water and control substance exchange, providing tissues both a physical as well as charge-, ion-, and size-selective barrier. Tight junction strands are 10 nm in diameter but vary in number and length (Schneeberger et al., 1978). Each strand is formed by a row of transmembrane proteins that are embedded in both plasma membranes of adjacent epithelia cells. The major transmembrane proteins associate with cytoplasmic proteins, such as ZO-1, to anchor the tight junction strand to the actin cytoskeletal network. The primary transmembrane proteins found in tight junctions are claudins, occludins, and junctional adhesion molecules, and the specific composition and dynamics of each tight junction regulate junctional barrier properties (Colegio et al., 2003; Sasaki et al., 2003).

Claudins are the predominant protein in tight junctions that directly regulate barrier permeability. This protein family is critical for paracellular barrier function and alone are sufficient to form tight junction strands (Gunzel & Yu, 2013). Unsurprisingly, claudin-null mice die shortly after birth (10h) due to hyperpermeability in the blood brain barrier (Nitta et al., 2003). Claudins are tetraspan transmembrane proteins with intracellular N- and C- termini, resulting in one intracellular loop and two extracellular loops (Hou et al., 2013; Hou & ScienceDirect, 2019). The carboxyl-terminal domain of claudins contain a structural PDZ (postsynaptic density protein (PSD95), Drosophila disc large tumor suppressor (DLG1), and zonula occludens-1 protein (ZO-1)) binding motif that plays a key role in anchoring transmembrane

claudins to intracellular ZO-1 and other scaffolding proteins (Kennedy, 1995).

One class of claudins, the sealing class, function to limit fluid flux and form charge-selective paracellular channels, often referred to as sealing claudins. Another class of claudins promote paracellular flux and are categorized as pore-forming claudins. The charge-selectivity and barrier functional properties of each type of claudins depend on the composition of its two extracellular loops.

The first and larger extracellular loop (EL-1) is primarily responsible for the paracellular selective permeability of tight junctions (Colegio et al., 2002). The EL-1 loop contains two cysteine residues that form a disulfide bond which stabilizes the EL-1 structure; loss of either of these cysteines prevent claudins from assembling into tight junctions (Wen et al., 2004). The second, smaller extracellular loop (EL-2) is responsible for claudin-to-claudin coordination by binding the claudin protein to a corresponding claudin in a neighboring cell. Claudin proteins can associate with the same claudin (homotypic) or a different claudin protein (heterotypic) on the same cell (cis-interaction) or with the claudin of a neighboring cell (trans-interaction). There are only specific interactions that can take place between different claudins which impact the permeability function. For example, claudins 2, 7, 10, 15, and 16 increase paracellular cation permeability (pore-forming) while claudins 4, 8, 11, 14, and 18 have a sealing function but not all of these claudins are expressed in the lung (Krause et al., 2008). Claudins 1, 2, 3, 4, 5, 7, 8, and 18 are expressed in alveolar epithelial cells (Daugherty et al., 2004; Kaarteenaho et al., 2010; Soini, 2011).

The three most predominantly expressed claudins in the alveolar epithelium are claudins 3, 4, and 18 (LaFemina et al., 2010). Claudin 4 belongs to the sealing class of claudins and generally functions as a paracellular sodium barrier (Colegio et al., 2003; Colegio et al., 2002; Van Itallie et al., 2001). Claudin 18 is highly expressed and specific to the alveolar epithelium as it is not found in the airways of the lung (Coyne et al., 2003).

The transepithelial permeability of the alveolar barrier can be increased by inflammatory stimuli by inducing junctional disassembly. Pathogenic bacteria will release pore-forming toxins, cytoskeleton-modifying proteins, and bacterial lipopolysaccharide to disrupt the endothelial barrier (Ivanov et al.,

2010). Additionally, mucosal immune cells induce inflammation by secreting proinflammatory cytokines which leads to sustained epithelial barrier disruption, increasing host exposure to further or additional insults (Ivanov et al., 2010).

Alcohol and acute respiratory distress syndrome

Acute respiratory distress syndrome (ARDS) is a severe and acute respiratory illness that allows fluid to build up in the alveoli, impairing oxygenation. Diffuse alveolar damage to the alveolar-capillary interface induces alveolar epithelial cells to release pro-inflammatory cytokines. These cytokines recruit and activate neutrophils to induce free radical-mediated and protease-mediated damage of type I and type II pneumocytes as well as capillary endothelial cells. The increase in vessel permeability due to membrane damage leads to leakage of a protein-rich fluid into the alveoli, causing widespread formation of intra-alveolar hyaline membranes. The dysregulated permeability and weakened fluid clearance allow fluid to filter from the pulmonary microvasculature faster than it can be removed from the airspace, leading to noncardiogenic pulmonary edema (Ware & Matthay, 2001). Additionally, the loss of surfactant contributes to further alveolar collapse.

In addition to alveolar epithelial injury, ARDS is associated with dysregulated lung inflammation. Activated and functionally distinct neutrophils accumulate in the lung and alveolar space that have enhanced chemotaxis, enhanced metabolic activity, delayed apoptosis, and a unique transcriptional profile (Juss et al., 2015; Juss et al., 2016; Zimmerman et al., 1983).

Clinically, ARDS is characterized by hypoxemia and cyanosis along with respiratory distress due to the thickened alveolar-capillary diffusion barrier and the increased surface tension, leading to alveolar air sac collapse. Consequences of this alveolar insult include impaired gas exchange, decreased lung compliance, and pulmonary hypertension. ARDS is commonly secondary to a variety of disease processes that predispose the lung to distress, including sepsis, pneumonia, trauma, aspiration, pancreatitis, shock, and hypersensitivity reactions. ARDS is a diagnosis of exclusion with several criteria, including bilateral lung opacities, respiratory failure within a week of the alveolar insult, a decreased ratio of the partial

pressure of oxygen in the arterial blood to the fraction of inspired oxygen, and symptoms of respiratory failure that are not due to heart failure or fluid overload (Meyer et al., 2021).

As recently as 2016, one study found the hospital mortality rate of ARDS remains as high as 35-45%, similar to the datasets that were used to validate the Berlin definition (Bellani et al., 2016; Force et al., 2012). The incidence of ARDS is likely even higher than what is currently reported, as the Berlin definition requires positive pressure ventilation. However, many patients with diffuse lung injury are supported with high-flow nasal cannula and without mechanical ventilation (Alqahtani et al., 2020; Force et al., 2012; Meyer et al., 2021).

Currently, the only treatment for ARDS is to address the underlying cause and mechanical ventilation support with positive end-expiratory pressure and low tidal volumes. Airspace flooding often destroys alveoli which need to be repaired to establish a functional barrier; however, recovery of the respiratory function is often complicated by damage and loss of type II pneumocytes, leading to interstitial fibrosis.

Chronic alcohol abuse has long been recognized as an independent risk factor that increases the incidence of developing ARDS by 3 to 4 fold (Moss et al., 1996; Moss & Burnham, 2003). The alcoholic lung has impaired alveolar barrier function due to an increase in paracellular leakage of fluid into the airspace, priming the lung for ARDS (Berkowitz et al., 2009; Burnham et al., 2009; Moss et al., 2003). Without additional insults, the alcoholic lung can compensate for the disturbed fluid imbalance by increasing compensatory fluid clearance mechanisms. However, when faced with an acute secondary insult or trauma, the compensatory mechanisms are quickly overwhelmed which can lead to alveolar flooding. Thus, longstanding alcohol abuse primes the lung to develop ARDS if exposed to an additional injury, such as sepsis, ventilator-induced injury, or pneumonia (Moss et al., 2003).

Alcohol-induced lung injury is primarily mediated through oxidative stress. The lungs have a robust antioxidant defense pathway due to their chronic exposure to environmental oxygen. Oxygen can be transformed through enzymatic and non-enzymatic processes into reactive oxygen species (ROS). Approximately 2% of inhaled oxygen generates these ROS, resulting in protein, lipid, and DNA damage; severe oxidative stress can lead to apoptosis or necrosis (Domej et al., 2014; Lennon et al., 1991). ROS

concentrations are reduced by antioxidant enzymes, such as superoxide dismutases and catalases, and direct antioxidants, such as vitamin E, glutathione, and ascorbate which are found both intracellularly and in the epithelial lining fluid (Domej et al., 2014; Rogers & Cismowski, 2018; Zhu et al., 1998). A

Chronic alcohol abuse decreases the level of the antioxidant glutathione in the fluid that lines the alveoli, rendering the lung more susceptible to oxidative damage. Patients with a history of chronic alcohol abuse have both decreased glutathione levels and increased levels of oxidized glutathione, indicating oxidative stress that correlated with higher levels of proteinaceous fluid in their lungs (Burnham et al., 2003; Guidot et al., 2000). Alcohol induces transforming growth factor B (TGF-β), a signaling pathway which decreases glutathione and increases the production of ROS (Arsalane et al., 1997; Jardine et al., 2002; Sturrock et al., 2006; Waghray et al., 2005). Additionally, one of the major by-products of alcohol, acetaldehyde, generates oxygen radicals and can cause lipid peroxidation (Brown et al., 2004; Lieber, 1993). Together, alcohol ingestion leaves the lung more vulnerable to a second oxidative stress and more susceptible to developing ARDS.

Scope of Dissertation

This dissertation addresses key questions regarding the molecular mechanisms that describe alcoholic lung disease, as well as poses potential new therapeutics to protect against the disease. In Chapter 2, we describe a novel application of Evans Blue dye to test lung barrier function as a large molecule permeability assay *in vivo*. We then use this assay in Chapter 3 to investigate whether chronic alcohol primes the lung for either alveolar or vascular barrier disruption when coupled with an endotoxemia acute lung injury. To further test whether the alcohol-mediated barrier disruption is sensitive to a non-inflammatory injury, we probe the integrity of the alveolar barrier to increased hydrostatic pressure in both alcohol and control animal models in Chapter 4.

After establishing the effect of chronic alcohol use on alveolar and endothelial permeability, we next wanted to examine two potential therapeutics that specifically target the alcohol-mediated changes in alveolar tight junctions. In Chapter 5, we evaluate the therapeutic potential of two peptide mimetics that

target tight junction proteins, either directly or indirectly, to mitigate the effect of alcohol-associated tight junction protein changes. Finally, in Chapter 6 we explore the potential of *Klebsiella pneumoniae*, an infectious model of pneumonia, as a 'second-hit' injury to alcoholic lung disease. We propose that this injury can potentially further characterize the molecular mechanisms of alcohol-mediated barrier dysfunction as well as the therapeutic value of the peptide mimetics previously characterized. Together, this dissertation aims to provide an *in vivo* murine model to characterize the detrimental effects of chronic alcohol abuse and test the potential of new therapeutic peptides to mitigate that alcohol-mediated damage.

Literature Cited

Alqahtani, J. S., Mendes, R. G., Aldhahir, A., Rowley, D., AlAhmari, M. D., Ntoumenopoulos, G., Alghamdi, S. M., Sreedharan, J. K., Aldabayan, Y. S., Oyelade, T., Alrajeh, A., Olivieri, C., AlQuaimi, M., Sullivan, J., Almeshari, M. A., & Esquinas, A. (2020). Global Current Practices of Ventilatory Support Management in COVID-19 Patients: An International Survey. *J Multidiscip Healthc*, *13*, 1635-1648. https://doi.org/10.2147/JMDH.S279031

Arsalane, K., Dubois, C. M., Muanza, T., Begin, R., Boudreau, F., Asselin, C., & Cantin, A. M. (1997). Transforming growth factor-beta1 is a potent inhibitor of glutathione synthesis in the lung epithelial cell line A549: transcriptional effect on the GSH rate-limiting enzyme gamma-glutamylcysteine synthetase. *Am J Respir Cell Mol Biol*, *17*(5), 599-607. https://doi.org/10.1165/ajrcmb.17.5.2833

Bellani, G., Laffey, J. G., Pham, T., Fan, E., Brochard, L., Esteban, A., Gattinoni, L., van Haren, F., Larsson, A., McAuley, D. F., Ranieri, M., Rubenfeld, G., Thompson, B. T., Wrigge, H., Slutsky, A. S., Pesenti, A., Investigators, L. S., & Group, E. T. (2016). Epidemiology, Patterns of Care, and Mortality for Patients With Acute Respiratory Distress Syndrome in Intensive Care Units in 50 Countries. *JAMA*, *315*(8), 788-800. https://doi.org/10.1001/jama.2016.0291

Berkowitz, D. M., Danai, P. A., Eaton, S., Moss, M., & Martin, G. S. (2009). Alcohol abuse enhances pulmonary edema in acute respiratory distress syndrome. *Alcohol Clin Exp Res*, *33*(10), 1690-1696. https://doi.org/10.1111/j.1530-0277.2009.01005.x

Brown, L. A., Harris, F. L., Ping, X. D., & Gauthier, T. W. (2004). Chronic ethanol ingestion and the risk of acute lung injury: a role for glutathione availability? *Alcohol*, *33*(3), 191-197. https://doi.org/10.1016/j.alcohol.2004.08.002

Burnham, E. L., Brown, L. A., Halls, L., & Moss, M. (2003). Effects of chronic alcohol abuse on alveolar epithelial barrier function and glutathione homeostasis. *Alcohol Clin Exp Res*, *27*(7), 1167-1172.

https://doi.org/10.1097/01.ALC.0000075821.34270.98

Burnham, E. L., Halkar, R., Burks, M., & Moss, M. (2009). The effects of alcohol abuse on pulmonary alveolar-capillary barrier function in humans. *Alcohol Alcohol*, *44*(1), 8-12. https://doi.org/10.1093/alcalc/agn051

Colegio, O. R., Van Itallie, C., Rahner, C., & Anderson, J. M. (2003). Claudin extracellular domains determine paracellular charge selectivity and resistance but not tight junction fibril architecture. *Am J Physiol Cell Physiol*, *284*(6), C1346-1354. https://doi.org/10.1152/ajpcell.00547.2002

Colegio, O. R., Van Itallie, C. M., McCrea, H. J., Rahner, C., & Anderson, J. M. (2002). Claudins create charge-selective channels in the paracellular pathway between epithelial cells. *Am J Physiol Cell Physiol*, *283*(1), C142-147. https://doi.org/10.1152/ajpcell.00038.2002

Coyne, C. B., Gambling, T. M., Boucher, R. C., Carson, J. L., & Johnson, L. G. (2003). Role of claudin interactions in airway tight junctional permeability. *Am J Physiol Lung Cell Mol Physiol*, *285*(5), L1166-1178. https://doi.org/10.1152/ajplung.00182.2003

Daugherty, B. L., Mateescu, M., Patel, A. S., Wade, K., Kimura, S., Gonzales, L. W., Guttentag, S., Ballard, P. L., & Koval, M. (2004). Developmental regulation of claudin localization by fetal alveolar epithelial cells. *Am J Physiol Lung Cell Mol Physiol*, *287*(6), L1266-1273. https://doi.org/10.1152/ajplung.00423.2003

Domej, W., Oettl, K., & Renner, W. (2014). Oxidative stress and free radicals in COPD--implications and relevance for treatment. *Int J Chron Obstruct Pulmon Dis*, *9*, 1207-1224. https://doi.org/10.2147/COPD.S51226

Force, A. D. T., Ranieri, V. M., Rubenfeld, G. D., Thompson, B. T., Ferguson, N. D., Caldwell, E., Fan, E., Camporota, L., & Slutsky, A. S. (2012). Acute respiratory distress syndrome: the Berlin Definition. *JAMA*, *307*(23), 2526-2533. https://doi.org/10.1001/jama.2012.5669

Guidot, D. M., Modelska, K., Lois, M., Jain, L., Moss, I. M., Pittet, J. F., & Brown, L. A. (2000). Ethanol ingestion via glutathione depletion impairs alveolar epithelial barrier function in rats. *Am J Physiol Lung Cell Mol Physiol*, *279*(1), L127-135.

https://doi.org/10.1152/ajplung.2000.279.1.L127

Gunzel, D., & Yu, A. S. (2013). Claudins and the modulation of tight junction permeability. *Physiol Rev*, *93*(2), 525-569. https://doi.org/10.1152/physrev.00019.2012

Hall, J. E., & Guyton, A. C. (2011). *Guyton and Hall textbook of medical physiology*. Saunders/Elsevier.

Hou, J., Rajagopal, M., & Yu, A. S. (2013). Claudins and the kidney. *Annu Rev Physiol*, *75*, 479-501. https://doi.org/10.1146/annurev-physiol-030212-183705

Hou, J., & ScienceDirect. (2019). *The paracellular channel : biology, physiology, and disease*. Academic Press.

Ivanov, A. I., Parkos, C. A., & Nusrat, A. (2010). Cytoskeletal regulation of epithelial barrier function during inflammation. *Am J Pathol*, *177*(2), 512-524. https://doi.org/10.2353/ajpath.2010.100168

Jardine, H., MacNee, W., Donaldson, K., & Rahman, I. (2002). Molecular mechanism of transforming growth factor (TGF)-beta1-induced glutathione depletion in alveolar epithelial cells. Involvement of AP-1/ARE and Fra-1. *J Biol Chem*, *277*(24), 21158-21166. https://doi.org/10.1074/jbc.M112145200

Juss, J., Herre, J., Begg, M., Bradley, G., Lennon, M., Amour, A., House, D., Hessel, E. M., Summers, C., Condliffe, A. M., & Chilvers, E. R. (2015). Genome-wide transcription profiling in neutrophils in acute respiratory distress syndrome. *Lancet*, *385 Suppl 1*, S55. https://doi.org/10.1016/S0140-6736(15)60370-1

Juss, J. K., House, D., Amour, A., Begg, M., Herre, J., Storisteanu, D. M., Hoenderdos, K., Bradley, G., Lennon, M., Summers, C., Hessel, E. M., Condliffe, A., & Chilvers, E. R. (2016). Acute Respiratory Distress Syndrome Neutrophils Have a Distinct Phenotype and Are Resistant to Phosphoinositide 3-Kinase Inhibition. *Am J Respir Crit Care Med*, *194*(8), 961-973. https://doi.org/10.1164/rccm.201509-1818OC

Kaarteenaho, R., Merikallio, H., Lehtonen, S., Harju, T., & Soini, Y. (2010). Divergent expression of claudin -1, -3, -4, -5 and -7 in developing human lung. *Respir Res*, *11*, 59. https://doi.org/10.1186/1465-9921-11-59

Kennedy, M. B. (1995). Origin of PDZ (DHR, GLGF) domains. *Trends Biochem Sci*, *20*(9), 350. https://doi.org/10.1016/s0968-0004(00)89074-x

Krause, G., Winkler, L., Mueller, S. L., Haseloff, R. F., Piontek, J., & Blasig, I. E. (2008). Structure and function of claudins. *Biochim Biophys Acta*, *1778*(3), 631-645. https://doi.org/10.1016/j.bbamem.2007.10.018

LaFemina, M. J., Rokkam, D., Chandrasena, A., Pan, J., Bajaj, A., Johnson, M., & Frank, J. A. (2010). Keratinocyte growth factor enhances barrier function without altering claudin expression in primary alveolar epithelial cells. *Am J Physiol Lung Cell Mol Physiol*, *299*(6), L724-734. https://doi.org/10.1152/ajplung.00233.2010

Lennon, S. V., Martin, S. J., & Cotter, T. G. (1991). Dose-dependent induction of apoptosis in human tumour cell lines by widely diverging stimuli. *Cell Prolif*, *24*(2), 203-214. https://doi.org/10.1111/j.1365-2184.1991.tb01150.x

Lieber, C. S. (1993). Biochemical factors in alcoholic liver disease. *Semin Liver Dis*, *13*(2), 136-153. https://doi.org/10.1055/s-2007-1007345

Meyer, N. J., Gattinoni, L., & Calfee, C. S. (2021). Acute respiratory distress syndrome. *Lancet*, *398*(10300), 622-637. https://doi.org/10.1016/S0140-6736(21)00439-6

Moss, M., Bucher, B., Moore, F. A., Moore, E. E., & Parsons, P. E. (1996). The role of chronic alcohol abuse in the development of acute respiratory distress syndrome in adults. *JAMA*, *275*(1), 50-54. https://www.ncbi.nlm.nih.gov/pubmed/8531287

Moss, M., & Burnham, E. L. (2003). Chronic alcohol abuse, acute respiratory distress syndrome, and multiple organ dysfunction. *Crit Care Med*, *31*(4 Suppl), S207-212. https://doi.org/10.1097/01.CCM.0000057845.77458.25

Moss, M., Parsons, P. E., Steinberg, K. P., Hudson, L. D., Guidot, D. M., Burnham, E. L., Eaton, S., & Cotsonis, G. A. (2003). Chronic alcohol abuse is associated with an increased incidence of acute respiratory distress syndrome and severity of multiple organ dysfunction in patients with septic shock. *Crit Care Med*, *31*(3), 869-877. https://doi.org/10.1097/01.CCM.0000055389.64497.11

Nitta, T., Hata, M., Gotoh, S., Seo, Y., Sasaki, H., Hashimoto, N., Furuse, M., & Tsukita, S. (2003). Size-selective loosening of the blood-brain barrier in claudin-5-deficient mice. *J Cell Biol*, *161*(3), 653-660. https://doi.org/10.1083/jcb.200302070

Nkadi, P. O., Merritt, T. A., & Pillers, D. A. (2009). An overview of pulmonary surfactant in the neonate: genetics, metabolism, and the role of surfactant in health and disease. *Mol Genet Metab*, *97*(2), 95-101. https://doi.org/10.1016/j.ymgme.2009.01.015

Rogers, L. K., & Cismowski, M. J. (2018). Oxidative Stress in the Lung - The Essential Paradox. *Curr Opin Toxicol*, *7*, 37-43. https://doi.org/10.1016/j.cotox.2017.09.001

Sasaki, H., Matsui, C., Furuse, K., Mimori-Kiyosue, Y., Furuse, M., & Tsukita, S. (2003). Dynamic behavior of paired claudin strands within apposing plasma membranes. *Proc Natl Acad Sci U S A*, *100*(7), 3971-3976. https://doi.org/10.1073/pnas.0630649100

Schneeberger, E. E., Walters, D. V., & Olver, R. E. (1978). Development of intercellular junctions in the pulmonary epithelium of the foetal lamb. *J Cell Sci*, *32*, 307-324. https://www.ncbi.nlm.nih.gov/pubmed/701398

Soini, Y. (2011). Claudins in lung diseases. *Respir Res*, *12*, 70. https://doi.org/10.1186/1465-9921-12-70

Sturrock, A., Cahill, B., Norman, K., Huecksteadt, T. P., Hill, K., Sanders, K., Karwande, S. V., Stringham, J. C., Bull, D. A., Gleich, M., Kennedy, T. P., & Hoidal, J. R. (2006). Transforming growth factor-beta1 induces Nox4 NAD(P)H oxidase and reactive oxygen species-dependent proliferation in human pulmonary artery smooth muscle cells. *Am J Physiol Lung Cell Mol Physiol*, *290*(4), L661-L673. https://doi.org/10.1152/ajplung.00269.2005

Van Itallie, C., Rahner, C., & Anderson, J. M. (2001). Regulated expression of claudin-4 decreases paracellular conductance through a selective decrease in sodium permeability. *J Clin Invest*, *107*(10), 1319-1327. https://doi.org/10.1172/JCI12464

Waghray, M., Cui, Z., Horowitz, J. C., Subramanian, I. M., Martinez, F. J., Toews, G. B., & Thannickal, V. J. (2005). Hydrogen peroxide is a diffusible paracrine signal for the induction of epithelial cell death by activated myofibroblasts. *FASEB J*, *19*(7), 854-856. https://doi.org/10.1096/fj.04-

2882fje

Ware, L. B., & Matthay, M. A. (2001). Alveolar fluid clearance is impaired in the majority of patients with acute lung injury and the acute respiratory distress syndrome. *Am J Respir Crit Care Med*, *163*(6), 1376-1383. https://doi.org/10.1164/ajrccm.163.6.2004035

Weinberger, S. E., Cockrill, B. A., Mandel, J., & ScienceDirect. (2019). *Principles of pulmonary medicine* (Seventh edition. ed.). Elsevier.

Wen, H., Watry, D. D., Marcondes, M. C., & Fox, H. S. (2004). Selective decrease in paracellular conductance of tight junctions: role of the first extracellular domain of claudin-5. *Mol Cell Biol*, *24*(19), 8408-8417. https://doi.org/10.1128/MCB.24.19.8408-8417.2004

Zhu, S., Manuel, M., Tanaka, S., Choe, N., Kagan, E., & Matalon, S. (1998). Contribution of reactive oxygen and nitrogen species to particulate-induced lung injury. *Environ Health Perspect*, *106 Suppl 5*, 1157-1163. https://doi.org/10.1289/ehp.98106s51157

Zimmerman, G. A., Renzetti, A. D., & Hill, H. R. (1983). Functional and metabolic activity of granulocytes from patients with adult respiratory distress syndrome. Evidence for activated neutrophils in the pulmonary circulation. *Am Rev Respir Dis*, *127*(3), 290-300. https://doi.org/10.1164/arrd.1983.127.3.290

Chapter 2: Measurement of Lung Vessel and Epithelial Permeability *in vivo* with Evans Blue

Prestina Smith, Lauren A. Jeffers, Michael Koval. Methods Mol Biol, 2021; 2367:137-148

DOI: 10.1007/7651_2020_345

Abstract

Lung fluid balance is maintained in part by the barriers formed by the pulmonary microvasculature and alveolar epithelium. Failure of either of these barriers leads to pulmonary edema, which limits lung function and exacerbates the severity of acute lung injury. Here we describe a method using Evans Blue dye to simultaneously measure the function of vascular and epithelial barriers of murine lungs in vivo.

Introduction

In order to efficiently mediate gas exchange, the lung needs to efficiently control fluid balance. Injury and inflammation impair the control of lung fluid, resulting in pulmonary edema which, when extensive, exacerbates lung injury and causes acute respiratory distress syndrome (ARDS) (Matthay & Zemans, 2011). Control of the lung air/liquid barrier is predominantly mediated by two distinct systems, the pulmonary microcirculation (Komarova et al., 2017; Mehta et al., 2004) and the alveolar epithelium (Koval, 2017), failure of which can lead to interstitial fluid accumulation (tissue edema) and airspace flooding, respectively (Figure 2.1). Tissue edema and airspace flooding both have the capacity to impair gas exchange and exacerbate injury. Understanding the relative contributions of the vascular endothelial and alveolar epithelial barriers in regulating lung fluid is critical to identifying effective therapeutic approaches to the treatment of ARDS.

It has long been appreciated that Evans Blue dye (T-1824) preferentially binds to serum albumin (Rawson, 1943), making it an effective marker for the ability of albumin to extravasate across

barriers and accumulate in tissues. Albumin is a 68 kDa, native serum protein that has been found to penetrate barriers and accumulate in airspaces in response to lung injury (e.g. (Bosmann et al., 2012)), which underscores its utility as a marker for lung barrier failure. Albumin permeability also is a particularly useful marker in that it can cross endothelial and epithelial barriers by both the paracellular route through tight junctions (Schlingmann et al., 2015) and the transcellular route through transcytosis (Martins et al., 2016; Sleep et al., 2013; Stewart et al., 2017).

In contrast to direct measurement of albumin in different lung compartments by ELISA or immunoblot, Evans Blue is easily measured by absorbance spectroscopy and is highly sensitive (Moitra et al., 2007). This is particularly critical for measurement of dye accumulation in the interstitium. Here we describe a protocol that enables the accumulation of Evans Blue in the airspace and interstitial compartments to be simultaneously determined, in order to measure the relative impact of injury on lung endothelial and epithelial barriers.

Materials

Evans Blue Injection

1. Dulbecco's Phosphate Buffered Saline (DPBS) without Ca^{2+}/Mg^{2+} (Corning/Mediatech #21–031-CV, Manassas, VA)
2. Evans Blue: Make a 0.5% solution in DPBS by adding 0.05 g of Evans Blue (MilliporeSigma E2129, St. Louis, MO) to 10 ml of DPBS (w/o Ca^{2+}/Mg^{2+}), then filter sterilize. Store at room temperature protected from light.
3. Sedative/Anesthetic cocktail (20% Ketamine + 5% xylazine solution): Add 1 ml 100 mg/ml ketamine (Mylan Institutional NDC 67457-108-10, Galway, Ireland). and 0.25 ml

20 mg/ml xylazine (Zoetis Inc NDC 59399-110-20, Kalamazoo, MI) to 3.75 ml DPBS without Ca^{2+}/Mg^{2+} to produce 5 ml total solution

4. Isoflurane (Piramal Enterprises Limited NDC 66794-017-25, Telangana, India)
5. 25G × 5/8 needles (BD PrecisionGlide #305122, Franklin Lakes, NJ) and 30G × 1 needles (BD PrecisionGlide #305128) (see Note 1).
6. 1 ml syringes (BD #309659)
7. Cotton Gauze Sponges, 5 × 5 cm (FisherBrand #22-362-178, Pittsburgh, PA)
8. Heat lamp
9. Small animal heating pad

Tissue Harvest

1. Animal surgical instruments: dissecting scissors, fine tip tweezers, smooth and rat tooth forceps, dissection board.
2. Portable balance to weigh animals (Mettler Toledo PL6000-S or equivalent)
3. Mouse trachea tube (DWK Kimble Kontes Brand Microflex Syringe Needles-Blunt, Fisher Scientific K868280–2001)
4. 5–0 Silk Suture (Ethicon #K870H, Somerville, NJ).
5. 21G × 1 ½ needles (BD PrecisionGlide #305167).
6. 10 ml syringe (BD #302995).

7. 1.5 ml conical microfuge tubes (Eppendorf, # 022364111, Enfield, CT). Each mouse requires 3 collection tubes each for blood/serum, bronchoalveolar lavage (BAL) fluid, and lung tissue.
8. Heparin (Aurobindo Pharma Limited NDC 63739-920-25, Memphis, TN) stock concentration 1000 USP: Used to coat needle and syringe for blood collection.
9. Formamide (Electron Microscopy Sciences #15745, Hatfield, PA). Add 250 µl per tube for extraction of lung tissue
10. DPBS with Ca^{2+}/Mg^{2+} (Corning/Mediatech #21–030-CV)
11. Lavage solution: DPBS with Ca^{2+}/Mg^{2+} containing 1:200 200mM phenylmethylsulfonyl fluoride (PMSF, MilliporeSigma, # P7626) and 1:500 1 M NaF (MilliporeSigma #S7920): Prepare 500 µl per mouse and keep lavage fluid on ice in an ice bucket (see Note 2)

Tissue Analysis

1. Heating block (Fisher Scientific Dry Bath Incubator #11–718 or equivalent)
2. Refrigerated microfuge (Eppendorf 5415 R or equivalent)
3. Microplate reader (Biotek Synergy H1 Multimode Plate Reader or equivalent)

Methods

Tail Vein Injection of Evans Blue

1. Prepare 0.5% Evans Blue solution.

2. Place mice in a cage under the heat lamp. Warm mice for 5 −10 min in order to dilate blood vessels (see Note 3).

3. Weigh each mouse and intraperitoneally (IP) inject 10 µl/g body weight + 10 µl ketamine/xylazine anesthetic cocktail. (see Note 4).

4. Place the mice back in the cage and allow anesthetic to take effect (see Note 5).

5. Place mouse on a platform so that the mouse is at a comfortable height and the tail hangs over the edge.

6. Rotate the tail to locate the lateral tail vein and potential injection site. Make sure the vein is facing upward (Figure 2.2).

7. Clean injection area with warm alcohol pad.

8. Fill syringe with 400 µl Evans Blue solution making sure to avoid air bubbles (see Note 6).

9. Hold the tail with the nondominant hand while stretching the tail so that the injection site is visible and the vein is in a straight line.

10. Insert 30G needle at a 10–15° angle, bevel up, into the injection site. Advance needle towards the head keeping the needle and syringe parallel to the tail. The needle should be visibly in the tail vein (Figure 2.2).

11. Slowly inject 200 µl of dye into the tail vein of the mouse. If you have correct placement of the needle the plunger will advance with ease (see Note 6).

12. Place mouse on heating pad and wait 1 h (see Note 7). Evans Blue will clearly dye the nose and footpads of treated mice (Figure 2.3).

Serum Collection

1. Rinse needle (21G) and 1 ml syringe with heparin in order to coat both needle and syringe (see Note 8)
2. Sacrifice the mouse using an approved injectable anesthetic overdose procedure. A 1 ml IP injection 1 ml of 20% Ketamine + 5% xylazine solution is sufficient (see Note 9).
3. Once unresponsive, pin mouse legs down on dissection board. Immobilize the head by placing a suture loop around the front incisors and pinning the loop down to the dissection board (see Note 10).
4. Wet the abdomen with water or ethanol to prevent fur from entering the abdominal cavity and contaminating tissue. Cut open the skin and peritoneum along the midline.
5. Cut though the ribcage and open chest cavity so that the bottom of the heart is exposed.
6. Puncture the left ventricle with the 21G needle attached to the heparinized 1 ml syringe. Slowly draw plunger back into syringe to start collecting blood. Collect a minimum of 250 µl blood/mouse.
7. Evacuate blood into collection tube and place on ice. (see Note 11)
8. Centrifuge blood 3,000 × g at 4°C for 15 min. Collect supernatants (serum) and transfer to a new tube. Freeze at −20°C (see Note 12).

BAL Fluid Collection

1. Cut away skin on the neck so that the area near the trachea is exposed. Carefully snip away thin tissue covering the trachea (see Note 13).
2. Turn the mouse so that the head is closer to you.
3. With the help of forceps, lay a string of surgical sutures behind the trachea.
4. Make a small nick at a 45° angle on the top surface of the trachea nearest the larynx (see Note 14).
5. Slide the 20G trachea tube into the nick and stop right above the ribcage. Ensure the surgical string is at least 2–3mm above the bottom tip of the trachea tube.
6. Secure the needle in place by tying a knot with the sutures around it.
7. Remove any air in the lungs by evacuating at least 1 ml of air from the lung using an empty 1 ml syringe.
8. Quickly replace the empty syringe with one filled with 500 µl of lavage fluid and slowly fill lungs with the fluid. Rinse the lungs twice with the same lavage fluid, then pull the plunger out to retrieve the final volume (see Note 15).
9. Collect the fluid in centrifuge tubes and place on ice.
10. Centrifuge BAL at 3,000 × g at 4°C for 15 min. Collect supernatants and transfer to a new tube. Freeze at −20°C (see Note 12).

Lung Tissue Collection

1. Rotate the mouse back to the original position with the feet closest to you.

2. Snip the aorta below the diaphragm so that blood can easily move from the perfused lungs (see Note 16).

3. Take a DPBS with Ca^{2+}/Mg^{2+}-filled 10 ml syringe attached to a 25G needle and insert the needle into the right ventricle, aiming in the direction of the pulmonary artery. Gently push the plunger of the syringe to perfuse the lungs with 5 ml of DPBS (see Note 17).

4. Carefully dissect out the lungs from the thoracic cavity by grabbing the trachea with forceps then snipping down behind the lungs while gently pulling the lungs away.

5. Once out, rinse the exterior of the lungs with DPBS with Ca^{2+}/Mg^{2} to remove any clotted exterior blood and cut away extra-pulmonary tissue (e.g., heart and vasculature) and remove cartilaginous tissue (trachea and large bronchi). Lungs with tissue accumulation of Evans Blue are visibly stained (Figure 2.3C – Figure 2.3E).

6. Place half the isolated lung tissue in a centrifuge tube containing 250 µl of formamide on ice. Weigh lung samples and record for later analysis (see Note 18).

7. Incubate at 55°C in a heating block for 48 h.

8. Centrifuge lung tissue at 3,000 × g at 4°C for 15 min. Collect supernatants and transfer to a new tube.

Evans Blue Measurement and Analysis

1. Aliquot 100 µl/well of samples from serum (diluted 1:10 in PBS), undiluted BAL Fluid, and lung tissue extract in a 96-well plate (see Note 19).

2. Measure absorbance of samples and standards at 620nm and 740nm using a microplate reader (see Note 20).

3. Correct the A_{620} readings for turbidity in BAL fluid and lung tissue using the correction factor $y = 1.193x + 0.007$ where x is A_{740} and A_{620} corrected = yA_{620} (Moitra et al., 2007). Use standards to get absolute Evans Blue concentrations in µg/ml.

4. Divide BAL fluid Evans Blue concentration by serum Evans Blue concentration to normalize and account for variability in the tail vein injections (see Note 21).

5. Divide lung tissue Evans Blue concentration by lung weights and then by serum Evans Blue concentration (see Note 22).

Notes

1. 30G needles are used for tail vein injection but 25G needles are used for sedation, since 30 G needles are too small to quickly sedate mice at the volumes required.

2. Pre-cooling lavage fluid on ice before BAL extraction significantly increases the yield and helps inhibit protease activity when harvesting BAL.

3. Make sure that the heat lamp is not too close to the cage by placing your hand near the bottom of the cage and holding for 30 s. The lamp should be no closer than 20–30 cm from the mice. If the heat is uncomfortable to you the lamp is too close and may cause the mice to overheat.

4. This anesthetic guideline is for mice weighing 25 – 35 g. For mice smaller than 25 g, use 10 µl/g body weight ketamine/xylazine. For mice larger than 35 g, use 10 µl/g body weight + 15 µl ketamine/xylazine. Alternatively, Evans Blue injection can be done on mice without anesthetic using a mouse restraint device (Red Tailveiner Restrainer Braintree Scientific Inc. #TV-RED 150-STD, Braintree, MA). Note that sedated and non-

sedated mice will give different Evans Blue permeability values due to differences in heart rate, breathing rate and stimulation of the sympathetic system.

5. Mice usually are non-responsive to a foot pinch after 5 min as an indication that they are anesthetized.

6. Although the syringe is filled with 400 µl Evans Blue solution, only 200 µl is administered. Having an excess of dye solution in the syringe enables the amount injected to be more accurately monitored, especially if the tail vein is initially missed. If it is difficult to advance the plunger the needle is not in the tail vein. The entire mouse should turn blue within 1 min, most notably in the pads of the feet, the nose, and the ears

7. The heating pad step is only required if anesthetic was used. The heat keeps mice warm as they recover to avoid a drop in body temperature due to the anesthetic. If mice were not anesthetized, place the mouse back into the cage for 1 h.

8. After 1 h mice are ready for tissue harvest. Harvest in the following order: 1) blood, 2) BAL fluid, 3) lung tissue.

9. Overdose with ketamine/xylazine is the preferred method of euthanization since CO_2 asphyxiation stops the heart from beating and reduces recovery of blood during collection. Harvest blood immediately after sacrifice for maximum collection. Do not use cervical dislocation, since this can tear the trachea rendering mice unable for BAL collection.

10. The head should be tilted back fully with the neck fully exposed.

11. It can be difficult to distinguish serum from red blood cells because they will be heavily dyed with Evans Blue. By collecting at least 200 µl of whole blood, the top 60 µl supernatant can be isolated without disrupting the cellular layer on the bottom.

12. Serum and centrifuged BAL fluid are stored frozen prior to analysis since the lung tissue requires 48 h processing time.

13. The trachea is beneath the salivary glands. Glands can be carefully cut away and gently pulled apart to uncover the trachea.

14. The nick should only cut the top surface of the trachea and should be just large enough to accommodate the 20G trachea tube. The cut should open less than half of the diameter of the trachea.

15. The lungs should clearly inflate with the addition of fluid. Typical fluid recovery is 300–350 µl of lavage fluid. This provides enough material for duplicate absorbance measurements and protein determination by the Bicinchoninic Acid (BCA) assay (Sigma-Aldrich #BCA1–1KT).

16. Snipping the aorta reduces the pressure needed when perfusing with PBS into the right ventricle, avoiding potential damage to the lung microvasculature.

17. Lungs should turn white (with patches of blue dye) in color with good perfusion. It is imperative that the lung is properly perfused so that dye from the blood will not interfere with the tissue analysis (Figure 2.3C – Figure 2.3E).

18. Before adding lung tissue, weigh the tubes containing formamide solution alone. This enables net lung weight to be calculated and used for data analysis. Be consistent in

analyzing the right or the left lung tissue/lobes. The remaining lung tissue can be snap frozen in liquid nitrogen and used for other analysis (e.g., immunoblot, Q-PCR).

19. Serum must be diluted 1:10 before analyzing to avoid crosstalk with other serum components. BAL and lung tissue extract should not be diluted. When possible, measure absorbance from duplicate or triplicate technical replicates.

20. Standards are made from serial dilutions of Evans Blue stock into DPBS with Ca^{2+}/Mg^{2+} (for serum and BAL fluid) or formamide (for lung tissue samples).

21. In this example (Figure 2.4), mice were given either a control or alcohol diet for 8 weeks and then challenged by either IT or IP lipopolysaccharide (LPS; endotoxin) as a sterile inflammatory challenge (Smith et al., 2019). Alcohol rendered the airspaces prone to flooding even in the absence of an additional insult. Interestingly, LPS decreased Evans Blue permeability into the airspaces, most likely due to an increase in Transforming Growth Factor (TGF)-alpha dependent stimulation of Epidermal Growth Factor (EGF) receptors (Koff et al., 2006). IT injury, but not IP injury, of alcohol-fed mice also resulted in failure of the endothelial barrier as indicated by the accumulation of Evans Blue in the interstitial space, consistent with increased severity of direct vs. indirect lung injury on lung fluid balance.

22. Assessing barrier function using Evans Blue dye tracks albumin, which is a 68 kDa protein. While this approach offers many advantages, it represents one parameter when considering the effects of injury on lung fluid balance. For instance, macromolecule permeability may not be impacted under conditions where fluid balance is altered by the effects of injury on ion homeostasis (Eaton et al., 2009).

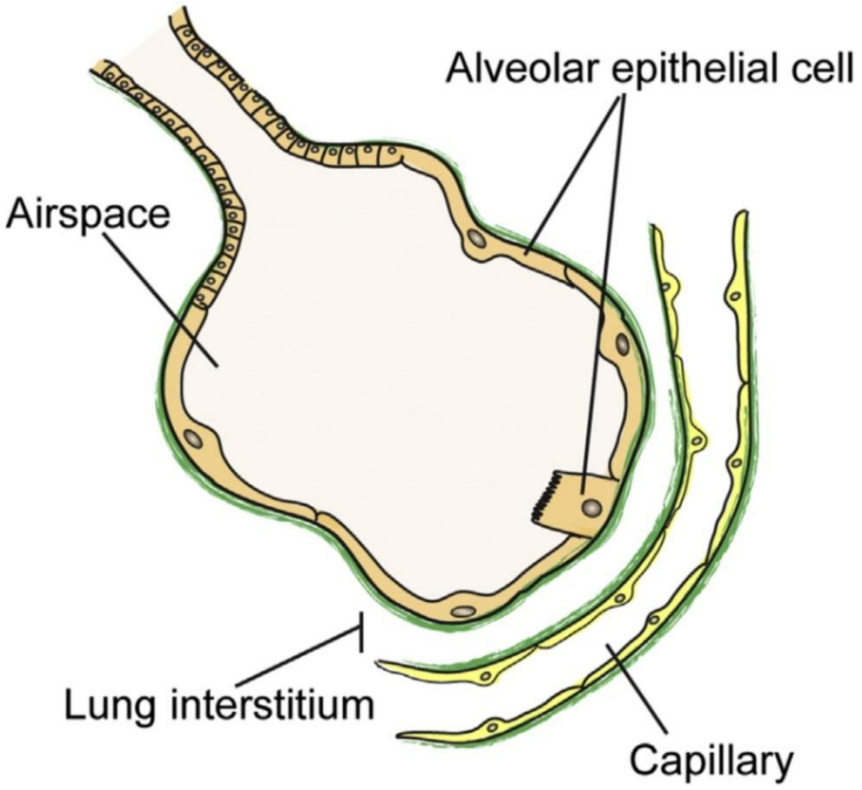

Figure 2.1. Diagram depicting a cross-section though a normal lung alveolus comprised of an epithelial sac surrounded by blood vessels.

Note that the transit of fluid-borne molecules from the vasculature must traverse across the vascular endothelial barrier though the interstitial tissue and across the alveolar epithelial barrier. Reproduced from (Smith et al., 2019)

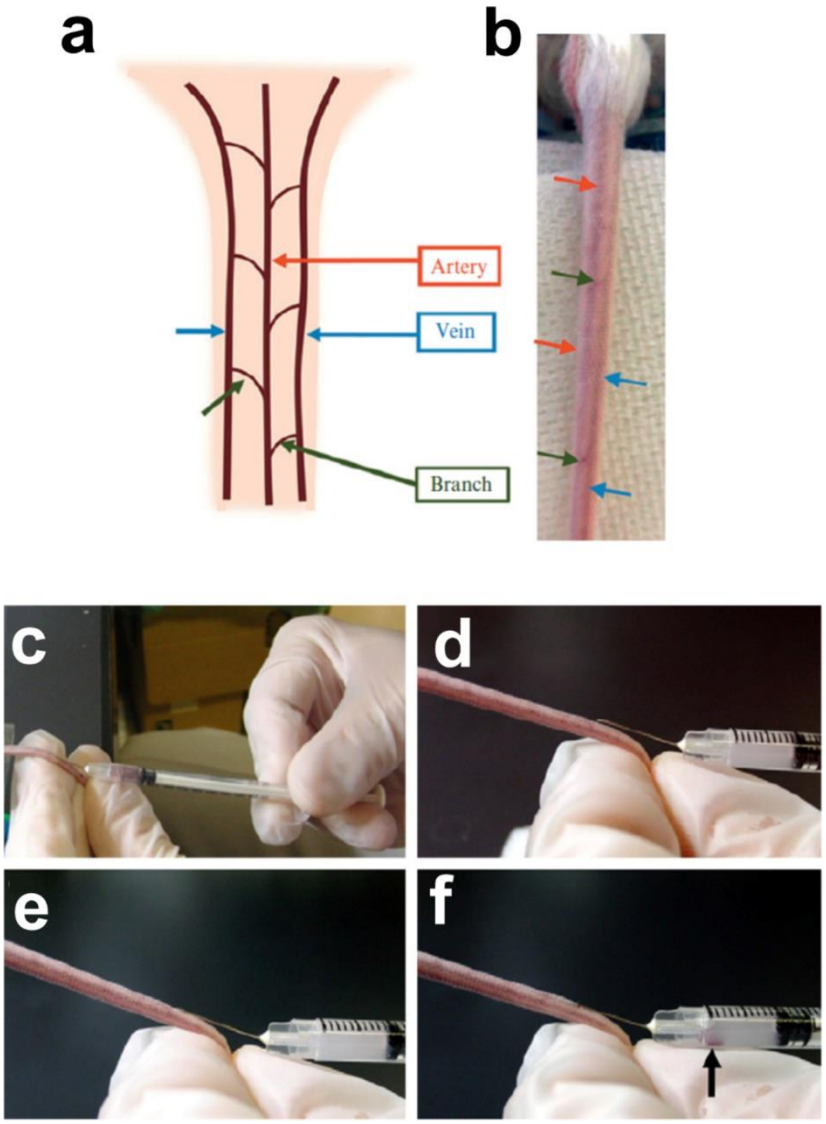

Figure 2.2. Tail vein injection.

(A,B) Diagram showing mouse tail vasculature. Branch vessels extend from the artery to the veins. Red arrows, artery; blue arrows, vein; green arrows, branch vessels. (C-F) Procedure for tail vein injection. (C) The outer tube is grasped by the first and second fingers. The third finger is placed under the inner cylinder. Place the needle on the surface of the tail in parallel (D) and insert it carefully (E). Once the needle tip is under the skin, pull back the syringe slightly during insertion to confirm that blood flows back to ensure that a vein is penetrated (F, arrow). Reproduced from (Hatakeyama et al., 2010) with permission.

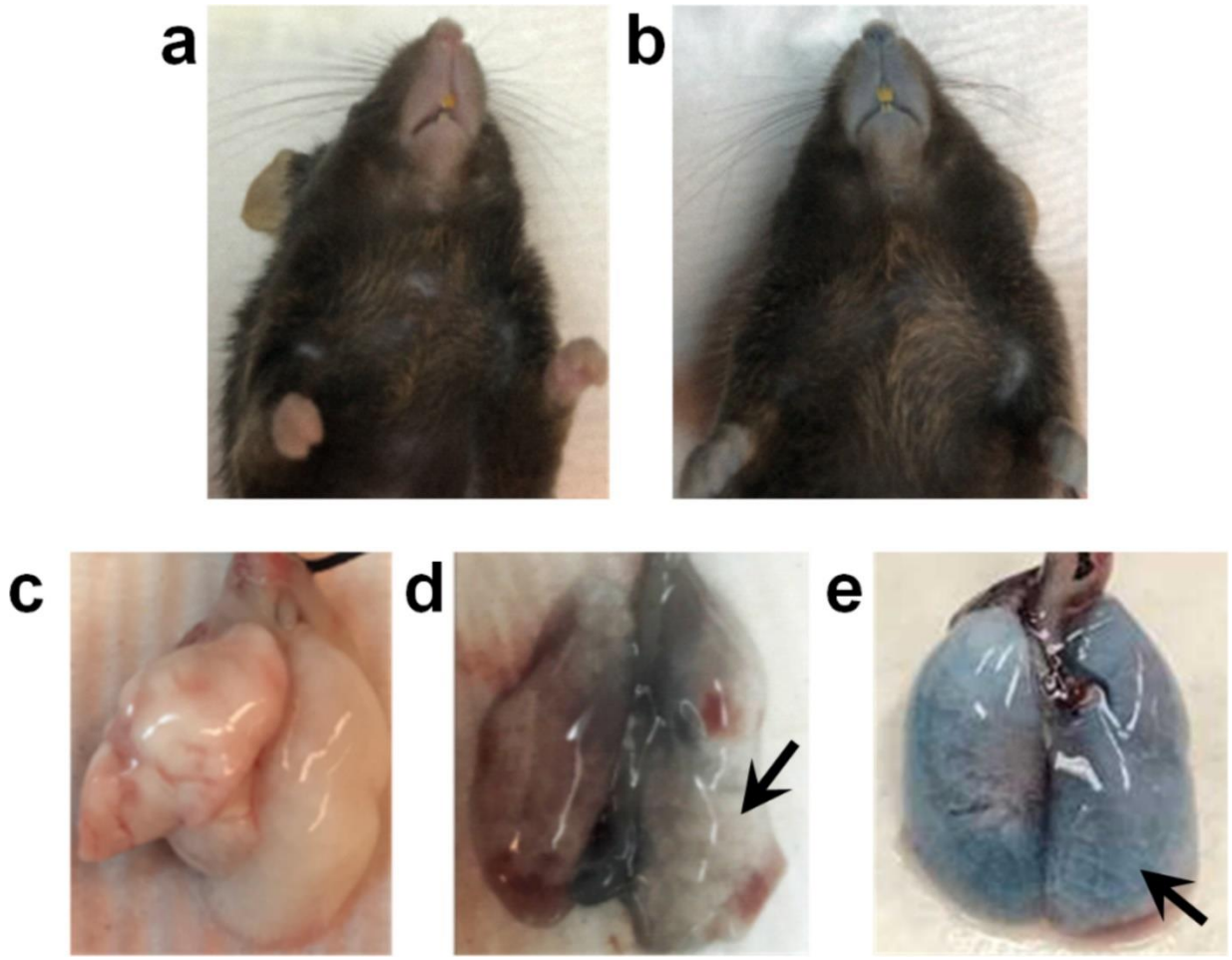

Figure 2.3. Appearance of Evans Blue in mice and murine lungs.

Mice that were either untreated (A) or intravenously injected with Evans Blue (B). Sixty minutes after injection, the treated mice show clear blue labeling of the nose and paws. (C-E). Representative images of lung tissue from mice that were either untreated (C), or after Evans Blue tail vein injection showing control (D) or alcohol fed and endotoxin treatment to induce acute lung injury (E). Uninjured mice show little tissue accumulation (arrow) of Evans Blue as compared with injured mice.

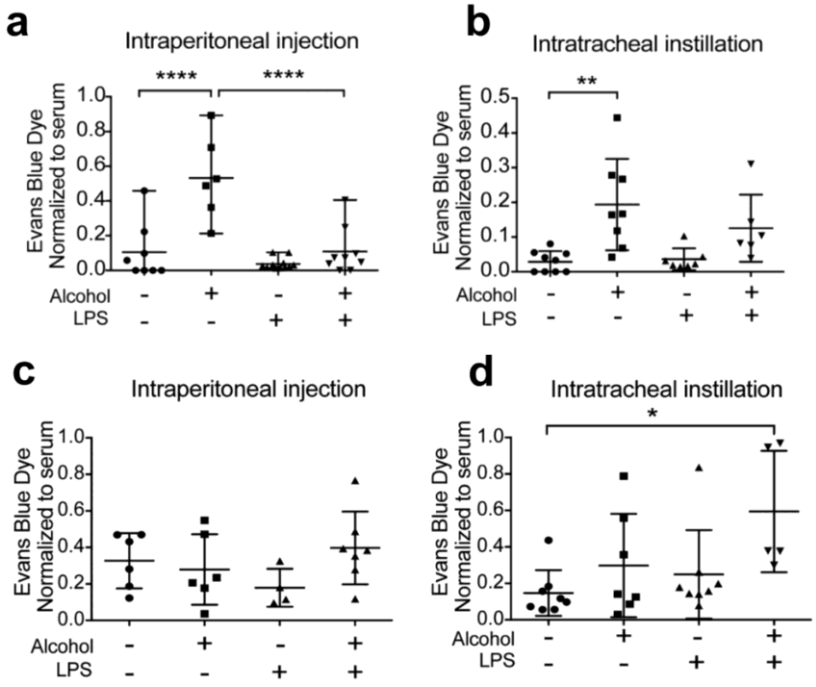

Figure 2.4. Effect of alcohol consumption and lipopolysaccharide on Evans Blue accumulation in lung airspaces and tissue.

Mice received an IP (A,C) or IT (B,D) treatment with either vehicle control or 5 mg/kg LPS in PBS. After 24 h the mice were administered Evans Blue by tail vein injection and allowed to recover for 2 h. Evans Blue dye was first collected by bronchoalveolar lavage (BAL) (A,B). Lung tissue was then harvested after BAL fluid collection and the right ventricle of the heart was perfused with PBS. Evans Blue dye was extracted from lung tissue by incubating in formamide at 55 °C for 48 h. Evans Blue concentration was analyzed via spectrophotometry (620 nm). Results were corrected for the presence of heme and normalized to Evans Blue serum levels and lung tissue weight. (A,B) Alcohol-feeding alone increased Evans blue levels in BAL fluid, suggesting that alcohol promotes alveolar epithelial barrier dysfunction (n = 6 – 9, ****$p < 0.0001$; **$p = 0.0021$). (C,D) Tissue Evans Blue dye content was only significantly increased in alcohol-fed mice that were given an IT administration of LPS. There was no significant change in any other groups. n = 4 – 8, * $p = 0.019$. Values reported as mean ± standard deviation. Reproduced from (Smith et al., 2019) with permission.

Literature Cited

Bosmann, M., Grailer, J. J., Zhu, K., Matthay, M. A., Sarma, J. V., Zetoune, F. S., & Ward, P. A. (2012). Anti-inflammatory effects of beta2 adrenergic receptor agonists in experimental acute lung injury. *FASEB J, 26*(5), 2137-2144. https://doi.org/10.1096/fj.11-201640

Eaton, D. C., Helms, M. N., Koval, M., Bao, H. F., & Jain, L. (2009). The contribution of epithelial sodium channels to alveolar function in health and disease. *Annu Rev Physiol, 71*, 403-423. https://doi.org/10.1146/annurev.physiol.010908.163250

Hatakeyama, S., Yamamoto, H., & Ohyama, C. (2010). Tumor formation assays. *Methods Enzymol, 479*, 397-411. https://doi.org/10.1016/S0076-6879(10)79023-6

Koff, J. L., Shao, M. X., Kim, S., Ueki, I. F., & Nadel, J. A. (2006). Pseudomonas lipopolysaccharide accelerates wound repair via activation of a novel epithelial cell signaling cascade. *J Immunol, 177*(12), 8693-8700. https://doi.org/10.4049/jimmunol.177.12.8693

Komarova, Y. A., Kruse, K., Mehta, D., & Malik, A. B. (2017). Protein Interactions at Endothelial Junctions and Signaling Mechanisms Regulating Endothelial Permeability. *Circ Res, 120*(1), 179-206. https://doi.org/10.1161/CIRCRESAHA.116.306534

Koval. (2017). *Junctional Interplay in Lung Epithelial Barrier Function* (S. V.K. & K. M., Eds.). Academic Press, Oxford.

Martins, J. P., Kennedy, P. J., Santos, H. A., Barrias, C., & Sarmento, B. (2016). A comprehensive review of the neonatal Fc receptor and its application in drug delivery. *Pharmacol Ther, 161*, 22-39. https://doi.org/10.1016/j.pharmthera.2016.03.007

Matthay, M. A., & Zemans, R. L. (2011). The acute respiratory distress syndrome: pathogenesis and treatment. *Annu Rev Pathol, 6*, 147-163. https://doi.org/10.1146/annurev-pathol-011110-130158

Mehta, D., Bhattacharya, J., Matthay, M. A., & Malik, A. B. (2004). Integrated control of lung fluid balance. *Am J Physiol Lung Cell Mol Physiol, 287*(6), L1081-1090. https://doi.org/10.1152/ajplung.00268.2004

Moitra, J., Sammani, S., & Garcia, J. G. (2007). Re-evaluation of Evans Blue dye as a marker of albumin clearance in murine models of acute lung injury. *Transl Res*, *150*(4), 253-265. https://doi.org/10.1016/j.trsl.2007.03.013

Rawson, R. A. (1943). The Binding of T-1824 and Structurally Related Diazo Dyes by the Plasma Proteins. *138*(5), 708-717. https://doi.org/10.1152/ajplegacy.1943.138.5.708

Schlingmann, B., Molina, S. A., & Koval, M. (2015). Claudins: Gatekeepers of lung epithelial function. *Semin Cell Dev Biol*, *42*, 47-57. https://doi.org/10.1016/j.semcdb.2015.04.009

Sleep, D., Cameron, J., & Evans, L. R. (2013). Albumin as a versatile platform for drug half-life extension. *Biochim Biophys Acta*, *1830*(12), 5526-5534. https://doi.org/10.1016/j.bbagen.2013.04.023

Smith, P., Jeffers, L. A., & Koval, M. (2019). Effects of different routes of endotoxin injury on barrier function in alcoholic lung syndrome. *Alcohol*, *80*, 81-89. https://doi.org/10.1016/j.alcohol.2018.08.007

Stewart, T., Koval, W. T., Molina, S. A., Bock, S. M., Lillard, J. W., Jr., Ross, R. F., Desai, T. A., & Koval, M. (2017). Calibrated flux measurements reveal a nanostructure-stimulated transcytotic pathway. *Exp Cell Res*, *355*(2), 153-161. https://doi.org/10.1016/j.yexcr.2017.03.065

Chapter 3: Effects of Different Routes of Endotoxin Injury on Barrier Function in Alcoholic Lung Syndrome

Prestina Smith, Lauren A. Jeffers, Michael Koval. Alcohol, 2019 Nov;80:81-89.

DOI: https://doi.org/10.1016/j.alcohol.2018.08.007

Abstract

In the lung, chronic alcohol consumption is a risk factor for acute respiratory distress syndrome (ARDS), a disorder that can be fatal due to airspace flooding. The severity of pulmonary edema is controlled by multiple barriers, and in particular the alveolar epithelial barrier and pulmonary microvasculature. However, to date, the effects of chronic alcohol ingestion on both of these barriers in the lung has not been directly and simultaneously measured. In addition, the effects of alcohol on systemic, indirect lung injury versus direct injury have not been compared. In this study, we used tissue morphometry and Evans Blue permeability assays to assess the effects of alcohol and endotoxemia injury on pulmonary barrier function comparing intraperitoneal (IP) administration of lipopolysaccharide (LPS) to intratracheal (IT) administration. Consistent with previous reports, we found that in alcohol-fed mice, the alveolar barrier was impaired, allowing Evans Blue to permeate into the airspaces. Moreover, IT administered LPS caused a significant breach of both the alveolar epithelial and vascular barriers in alcohol-fed mice, whereas the endothelial barrier was less affected in response to IP administered LPS. The alveolar barrier of control mice remained intact for both IP and IT administered LPS. However, both injuries caused significant interstitial edema, independently of whether the mice were fed alcohol or not. These data suggest that in order to properly target pulmonary edema due to alcoholic lung syndrome, both the alveolar and endothelial barriers need to be considered as well as the nature of the "second hit" that initiates ARDS.

Introduction

Alcohol abuse disorder is highly prevalent, affecting over 15 million adults in the United States and 208 million worldwide (Adams, 2015). Alcohol abuse is also one of the leading causes of global mortality; in 2014, 5.9% of all deaths were attributable to alcohol consumption (*Global status report on alcohol and health 2014*, 2014). Alcohol abuse contributes to an array of health complications as chronic alcohol consumption affects multiple organs and is a risk factor for developing cardiovascular disease, cancer, diabetes and chronic lung disease (*Facts About Alcohol*, 2018).

Chronic alcohol consumption alone leads an inconspicuous pulmonary pathology. Instead of causing overt, inflammatory lung damage, alcohol exacerbates the severity of lung injury due to an additional insult, a so-called second hit, by conditions such as pneumonia or sepsis. Chronic alcohol abuse increases the incidence of acute respiratory distress syndrome (ARDS) by 3–4 fold, making it a major risk factor for the condition (Kershaw & Guidot, 2008). ARDS is a type of acute lung injury that is marked by significant pulmonary edema, which impairs normal gas exchange in the lung. At advanced stages, flooding of the airspace further impairs gas exchange, and can increase patient mortality as a result of barotrauma due to the need for more aggressive ventilation. Although there have been advances in understanding the pathogenesis of ARDS, there are currently no effective pharmacological treatments, which makes ARDS a prime field of study for research (Pham & Rubenfeld, 2017; Ware & Matthay, 2000).

Two hit mouse models are commonly used to study the pathological progression of ARDS. Here, we used administration of a bacterial endotoxin as the second insult in an alcohol-primed lung. Bacterial endotoxins (lipopolysaccharide; LPS) elicit an immune response and are commonly used to induce injury in animal models (Copeland et al., 2005; Knapp, 2009). LPS injury models present mild injury and can be introduced via multiple routes. Intraperitoneal (IP) injection of LPS more closely mimics a systemic injury in which multiple organ systems are affected. By contrast, intubation-mediated intratracheal (IT) instillation of LPS serves as a direct insult that initially impacts the lung epithelium.

In this study, we investigated the effects of two different endotoxin-mediated lung injury mouse models after chronic alcohol consumption and compared how they affect pulmonary edema in the interstitial and alveolar compartments. Both IP and IT LPS treatment caused tissue edema in both control and alcohol-fed mice, however, only alcohol-fed mice had a significant breach in alveolar epithelial barrier function in response to either LPS treatment. Moreover, the pulmonary capillary barrier became further compromised in alcohol-fed mice challenged with IT LPS. These data are discussed in the context of the way alcohol impacts multiple pulmonary barriers and how that has the potential to increase susceptibility to poor outcomes in ARDS.

Materials and Methods

Mice

Experiments were performed in accordance with the National Institutes of Health Guidelines for the Use of Laboratory Animals guidelines and were approved by the Institutional Animal Care and Use Committee at Emory University School of Medicine. Isogenetic eight-week-old male C57BL/6 wild-type mice were used for all experiments (Jackson Laboratory, Bar Harbor, ME; Charles River, Wilmington, MA). Animals were housed with a maximum of five animals per cage. All animals were kept under constant temperature at 21 °C and under 12 h light-dark cycle with ad libitum access to regular chow diet. In the alcohol group, ethanol was administered by increasing ethanol concentration from 0% to 20% in 5% increments over a two-week period, and then mice were maintained at 20% ethanol for an additional six weeks. For instillation experiments, mice were anesthetized via IP injection of xylazine (10 mg/kg) and ketamine (100 mg/kg). Mice were suspended by their incisors on a rodent tilting work stand (Hallowell, Pittsfield, MA) for orotracheal instillation as previously described (Lawrenz et al., 2014).

Lipopolysaccharide (LPS) administration

Alcohol- and water-fed mice were injected with 5 mg/kg E. coli 055:B5 LPS purchased from Sigma (L2637). Mice were randomly assigned to receive either IP injection (250 µl) or IT instillation (50 µl). For control treatments, mice received a 250 µl IP injection of PBS or were IT instilled with 50 µl PBS. Mouse

weight was measured before PBS or LPS injection and 24 h later. Results are reported as percent change in weight ± standard deviation.

Lung permeability as measured by Evans Blue extravasation

Mice were anesthetized via IP injection of xylazine (10 mg/kg) and ketamine (100 mg/kg). Proper depth of anesthesia was verified by monitoring of respiratory rate and monitoring when mice showed no limb withdrawal response to foot compression. Mice were placed on a heating pad and the tail was sterilized with an alcohol wipe. Using a syringe with a 30 gauge needle, 200 µl of 0.5% Evans Blue in PBS was injected into the tail vein. The mice were allowed to recover on a heating pad for 1 h and then sacrificed while still under anesthesia. 250 µl of blood was collected by cardiac puncture and centrifuged at 1500 × g for 15 min to collect serum. Bronchoalveolar lung lavage (BAL) fluid was collected by flushing the lungs twice via a tracheal tube with 500 µl of PBS with protease inhibitors. After BAL collection, lungs were perfused through the right ventricle with 5 ml PBS, harvested, and processed for further analysis ex vivo.

To extract Evans Blue from lung tissue, tissue was weighed and then incubated in 250 µl formamide at 55 °C for 48 h. Evans Blue in serum, lung tissue and BAL fluid was analyzed by spectrophotometry (620 nm) (Radu & Chernoff, 2013). Evans Blue readings were corrected for contaminating heme in BAL fluid and lung tissue by analyzing samples at 740 nm and using the correction factor $y = 1.193x + 0.007$ as previously described (Moitra et al., 2007) and normalized to corresponding serum Evans Blue levels.

Lung histology

For histological sectioning, the superior and inferior lobe of the left lung was harvested after the BAL fluid was collected and a cardiac perfusion of PBS was performed. The left lung was placed into 4% paraformaldehyde at a depth sufficient to fill the airspace with fixative, incubated for at least 24 h at room temperature (RT) for fixation and then embedded in paraffin. Four 5 µm sections were cut at 50 µm intervals throughout the tissue and mounted on glass slides. Sections were deparaffinized and stained with hematoxylin and eosin (H&E). Sectioning and staining of samples were performed by the Winship

Pathology Core Laboratory, Emory University. To assess septal thickness, five H&E photomicrographs (40x) per sample were randomly captured from the central and peripheral regions of the superior, middle, and inferior sections. The widths of twenty randomly selected septa per image were measured using ImageJ, for a total of 100 measurements per mouse.

Total lung protein

Recovered bronchoalveolar lavage (BAL) fluid was kept on ice and centrifuged at 1500 × g for 15 min. Supernatant was collected and stored at −20 °C. Total BAL fluid protein was measured using the Pierce BCA Protein Assay Kit (Thermo Fisher Scientific).

Protein expression and myeloperoxidase analysis

Lung tissue was snap-frozen in liquid nitrogen at the time of sacrifice. Tissue was later weighed, thawed on ice, and added to 5 ml/mg tissue of lysis buffer (50 mM Tris HCl; 10 mM EDTA; 100 mM NaCl; 0.5% Triton X-100) with protease inhibitors, homogenized with a Dounce homogenizer, incubated for 30 min on ice, and sonicated 4 × 3 s. Homogenates were centrifuged at 10,000 × g for 10 min. Supernatants were collected, and total protein concentration was assessed using the Pierce BCA Protein Assay kit (ThermoFisher Scientific). Lung tissue lysates were used for either ELISA or immunoblot analysis. Myeloperoxidase (MPO) was quantified using a mouse MPO ELISA kit (Abcam, Ab155458). 40 µl of each sample was diluted into the kit buffer, aliquoted into a 96 well anti-MPO plate and incubated overnight at 4 °C. After washing, biotinylated anti-mouse MPO was incubated in the well for 1 h at RT to allow for MPO detection. Unbound antibody was removed by washing and an HRP-streptavidin solution was added to the wells for 45 min at RT. Wells were washed four times and a TMB substrate solution was added to the wells and incubated for 30 min at RT to allow the color to develop in proportion to the amount of bound MPO. A stop solution was added and the intensity of the color was measured at 450 nm. For immunoblot analysis, protein was diluted with 6x Laemlli buffer with DTT and heated for 10 min at 60 °C. Protein was separated via electrophoresis on a 4–20% SDS-PAGE stain-free gel (BioRad, Hercules, CA) and transferred to a PVDF membrane using the Transblot Turbo (BioRad) at

25 V for 7 min. Membranes were blocked in Odyssey Blocking Buffer (LI-COR, Lincoln, NE) for 1 h at RT. Membranes were then incubated overnight with 1:1000 dilution rabbit anti-CD11b (Abcam, ab133357) or 1:10,000 dilution mouse anti-beta actin (Thermo Fisher, MA5-15739) as a loading control. Membranes were washed in TBS + 0.5% Triton X-100. The blots were incubated for one hour with 1:10,000 dilution goat anti-rabbit IgG IRDye 800CW (LI-COR, 92632211) and 1:10,000 Goat anti-mouse IgG IRDye 680RD (LI-COR, 92668070) and then imaged and quantified using an Odyssey Classic imager (LI-COR) and band densitometry normalized to actin using Fiji.

Statistical Analysis

Comparisons between groups were performed by one-way ANOVA with Tukey's multiple comparisons test using GraphPad Prism software. Data are represented as mean ± standard deviation and the statistical significance level was set at 0.05.

Results

LPS insult and chronic alcohol ingestion altered body weight

In order to evaluate the systemic effects of chronic alcohol consumption in mice, we measured the total body weight of adult wild-type male C57BL/6 mice that consumed 20% alcohol in their drinking water for 8 weeks along with ad libitum access to normal chow. In this experimental model, mice fed alcohol weighed an average of 3 g more than their water fed controls (Figure 3.1A). Next, we investigated the effects of LPS on body weight. To this end, we introduced LPS via two methods: indirect lung injury by IP LPS injection and direct lung injury by IT LPS instillation. Mice were weighed before and 24 h after LPS treatment. We found that both IP and IT administration of LPS reduced body weight by 10% (Figure 3.1B,C) consistent with a previous study examining the effects of LPS injury on weight (Wang et al., 2016). The decreased body weight with LPS is likely due to the bacterial endotoxin inducing inflammation-induced anorexia, a protective sickness response behavior that causes a loss of appetite and reduced food intake (Konsman et al., 2002; van Niekerk et al., 2016). Note also that mice that received either an injection of PBS or LPS were anesthetized for the instillation procedure, while mice given an IP

injection were not. Thus, the 3% loss of body weight after PBS IT instillation compared to 0.5% weight loss after PBS IP injection was likely from decreased water and food intake due to minor trauma associated with the IT instillation procedure.

Alcohol alone promoted the appearance of airspace protein that is further exacerbated by direct LPS injury

We next measured the extent of acute lung injury in our two-hit model. First, differences between indirect and direct lung injury on lung airspace protein content after chronic alcohol consumption were determined. Total protein was measured in bronchoalveolar lavage (BAL) fluid from control or alcohol-fed mice that received either an IP or IT administration of LPS. Total BAL protein was increased in alcohol-fed mice regardless of whether they received an LPS challenge. However, for water-fed mice, there was significantly less BAL protein, and administration of IP LPS alone did not induce significant BAL protein accumulation (Figure 3.2A). By contrast, IT instillation of LPS significantly increased BAL protein in both alcohol-fed and control mice consistent with an increased severity of a direct insult on the lung epithelium. Taken together, these results suggest that alcohol alone is sufficient to increase BAL protein content which was further exacerbated by direct lung injury (Figure 3.2B).

To determine whether LPS-induced BAL protein reflects an increase in inflammation, we performed an immunoblot analysis of total lung tissue lysates following BAL harvest for interstitial expression of a broad-spectrum marker for leukocytes, CD11b (Figure 3.3A, B). We found no significant difference in CD11b expression in IP LPS challenged mice, even when examining alcohol-fed mice (Figure 3.3C). However, in mice that received IT LPS instillation (Figure 3.3D), there was a significant increase in CD11b for both alcohol-fed and control mice.

To further investigate inflammation in response to alcohol and LPS, we examined the extent of neutrophil infiltration into the lung tissue by measuring myeloperoxidase (MPO) content in total lung homogenates using ELISA. Consistent with measurements of total lung CD11b, we found no significant difference in total lung MPO for mice challenged with IP LPS regardless of whether they were on a

control or alcohol diet (Figure 3.3E). In contrast, we found that for direct lung injury using IT LPS, there was a significant increase in MPO (Figure 3.3F). These results suggest that direct IT injury induced an inflammatory response that did not occur in response to IP LPS challenge, further supporting a model of enhanced inflammation in alcohol-fed mice subjected to direct lung injury.

Alcohol and LPS independently induced interstitial edema

To further evaluate the extent of acute lung injury in alcohol-fed mice after LPS challenge, we measured histological changes using H & E stained paraffin-embedded lung sections from control and LPS injured mice and quantified alveolar septal thickness (Figure 3.4A). Alcohol alone increased alveolar septal thickness as compared with control animals, and both IP and IT administered LPS increased septal thickness to a comparable width, regardless of whether the mice had been fed alcohol (Figure 3.4B,C). 3These results suggest that alcohol and LPS drove fluid accumulation into the lung interstitium, resulting in tissue edema.

Direct LPS challenge in alcohol-fed mice increased lung permeability

An Evans Blue dye assay was performed to quantify the extent of permeability in lung tissue and airspaces. Evans Blue dye complexes with albumin, a 68 kDa protein that under normal physiological conditions has limited permeability across the vascular endothelial and alveolar epithelial barriers. Alcohol alone and an IP injection of LPS had no effect on Evans Blue accumulation in the lung (Figure 3.5A).

Although most of our endpoints were 24 h post LPS injury, there is the potential for the severity of IP LPS to peak at an earlier time point than 24 h (Mitchell et al., 2015). Given this, we examined interstitial Evans Blue content in injured alcohol fed mice 3 h after IP LPS. We found that at 3 h, there was 0.54 ± 0.16 ng/μl Evans Blue per g tissue normalized to serum ($n = 3$) which was comparable to the value obtained for tissue isolated 24 h post injury (0.40 ± 0.20, $n = 7$), suggesting that we did not miss an earlier peak effect of IP LPS on interstitial permeability.

In contrast to IP injured mice, IT instillation of LPS in alcohol-fed mice resulted in increased

Evans Blue in lung tissue (Figure 3.5B). The increased presence of Evans Blue dye in the interstitial compartment suggests there was an increase in vascular permeability to macromolecules in response to the combination of chronic alcohol ingestion and IT LPS (Radu & Chernoff, 2013).

Next, alveolar epithelial barrier dysfunction was determined by measuring Evans Blue present in BAL isolated from injured and non-injured mice. Alcohol alone was sufficient to increase Evans Blue in the airspace (Figure 3.6). Surprisingly, when introduced by IP administration, LPS significantly diminished the increase in Evans Blue present in BAL at 24 h following injury. This was also the case 3 h after IP LPS, where BAL Evans Blue 0.062 ± 0.022 (n = 3) (ng/µl) normalized to serum, which was comparable to the value obtained for BAL isolated 24 h post IP injury (0.11 ± 0.13, n = 7). These data suggest a possible protective effect on alveolar barrier function may have occurred as a result of systemic endotoxemia induced by IP LPS. By contrast, this was not the case for alcohol-fed mice treated with IT LPS, where the Evans Blue content of BAL was comparable in both saline and LPS instilled mice. Taken together, these data are consistent with direct LPS injury to the alveolar epithelium having a greater effect on alveolar barrier function than systemic endotoxemia, particularly in the context of chronic alcohol ingestion.

Discussion

In this study, we performed a direct comparison of the effects of mild endotoxemia administered either directly (IT) or indirectly (IP) on lung permeability in mice exposed to dietary alcohol. By separately analyzing the interstitial and airspace compartments we were able to distinguish edema present in different compartments. Most notably, water-fed, injured mice were able to maintain a tight alveolar barrier, even though there was tissue edema in response to injury (Figure 3.6). Taken together, these results suggest that alcohol-dependent changes in lung permeability differ, depending on whether the second hit is administered by direct versus indirect injury.

Previous studies have demonstrated that chronic alcohol ingestion impairs lung barrier and immune function(Mehta et al., 2013; Price et al., 2017; Schlingmann et al., 2016; Simet et al., 2012;

Yeligar et al., 2016), resulting in increased susceptibility to ARDS. Here we used an Evans Blue permeability assay to confirm that, in response to alcohol alone, there is an increase in macromolecule permeability from the circulation into the airspaces (Figure 3.6, Figure 3.7B). Consistent with increased Evans Blue in BAL, there also was an increase in total BAL protein in response to alcohol. In addition, alcohol induced an increase in tissue edema, which has the potential to further prime the lung for injury. Despite these changes in pulmonary barrier function, at baseline there was not a significant change in immune cell recruitment, based on CD11b levels or MPO (Patarroyo et al., 1990), in support of the hypothesis that the effects of chronic alcohol alone on lung permeability did not involve inflammation (Ward et al., 2015).

Systemic administration of LPS by IP injection had a mild effect on lung permeability in control fed mice, where tissue edema increased, but the alveolar barrier remained intact. IP administered LPS did not have an additive effect on lung tissue edema in alcohol-fed mice. Interestingly, systemic administration of LPS caused a significant decrease in Evans Blue permeability into the airspaces of alcohol-fed mice (Figure 3.6A). Although this seems counterintuitive, it is not without precedent, since low dose treatment of airway epithelial cells with LPS enhances wound repair via Transforming Growth Factor (TGF)-alpha dependent stimulation of Epidermal Growth Factor (EGF) receptors (Koff et al., 2006), and EGF has previously been demonstrated to enhance alveolar epithelial and intestinal barrier function (Borok et al., 1996; Chen et al., 2005; Klingensmith et al., 2017). Moreover, mice have relatively mild lung edema and lung inflammation in response to systemic sepsis induced by cecal ligation and puncture (CLP) regardless of whether they were administered dietary alcohol (Yoseph et al., 2013). These data support the hypothesis that alveolar barrier function may be preserved by paracrine signaling molecules stimulated by CLP-induced sepsis; studies are currently underway to determine whether this is the case and to determine whether TGF-alpha has a protective effect in vivo.

By contrast with IP administration, IT administration induced a lung pro-inflammatory response in both control and alcohol-fed mice as evidenced by increased BAL protein content, lung-associated CD11b and MPO (Figure 3.2, Figure 3.3). However, as compared with alcohol-fed mice, control mice did

not show an increase in BAL Evans Blue content (Figure 3.6B), suggesting that part of the increase in BAL protein induced by IT LPS was due to factors beyond alveolar permeability, including secretion of surfactant and pro-inflammatory cytokines as previously demonstrated (Fehrenbach et al., 1998). Overall tissue edema was comparable for both water and alcohol-fed mice injured by IT LPS, but alcohol-fed mice also showed a significant increase in tissue associated Evans Blue (Figure 3.4B), suggesting that in addition to an effect on the alveolar epithelial barrier, there was an added breach of the pulmonary microvascular barrier. The finding that alcohol can impair the pulmonary vascular barrier is consistent with previous reports demonstrating increased leakage of the blood brain barrier in response to alcohol (Haorah et al., 2007; Singh et al., 2007).

This study provides evidence that in alcoholic lung syndrome, both tissue edema and airspace edema are likely to be important drivers with the potential to predispose the lung to ARDS. This is particularly relevant to direct lung injury, since the relatively mild insult of IT LPS increased permeability of the vascular barrier as well as the alveolar barrier in mice fed alcohol (Figure 3.6, Figure 3.7D). The effect of direct injury on both pulmonary barriers is likely to be further exacerbated when the injury is more severe, such as bacterial or viral pneumonia that are commonly found in critical care patients. Current work is underway to determine whether protecting the alveolar epithelial barrier is sufficient to protect the lung from a second hit in alcoholic lung syndrome or whether it is necessary to target both the alveolar epithelial and pulmonary microvascular barriers to attenuate the severity of ARDS. If both barriers need to be targeted, determining whether both the epithelial and endothelial lung barriers have a common molecular mechanism would be of interest as a method to enable simultaneous and efficient targeting of them both to protect the alcoholic lung from ARDS.

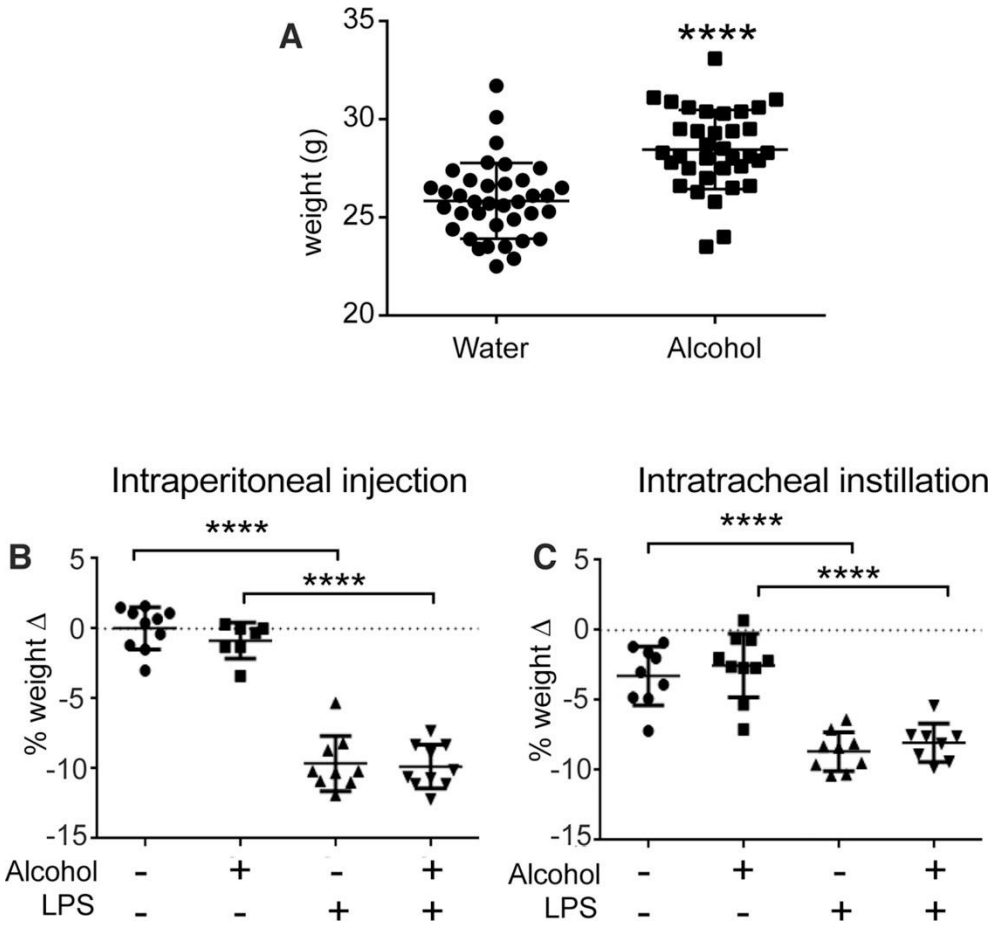

Figure 3.1. Effect of alcohol consumption and lipopolysaccharide on mouse weight.

(A) After 8 weeks, alcohol-fed mice weighed on average 3 g more than water-fed mice (n = 10–26. ****p < 0.0001). (B,C) Mice received an IP injection (B) or IT instillation (C) of either vehicle control or 5 mg/kg LPS in PBS. Mice were weighed before LPS treatment and then at 24 h after injury. Injured mice showed an equivalent loss of ~8–10% of body weight, regardless of type of LPS injury or whether they were on a water or alcohol diet. Mice given PBS vehicle IT also showed a modest decrease in weight (~3%) suggesting a mild injury response. Values represent percent change in weight, reported as mean ± standard deviation (n = 7–10 mice per group, ****p < 0.0001 relative to control).

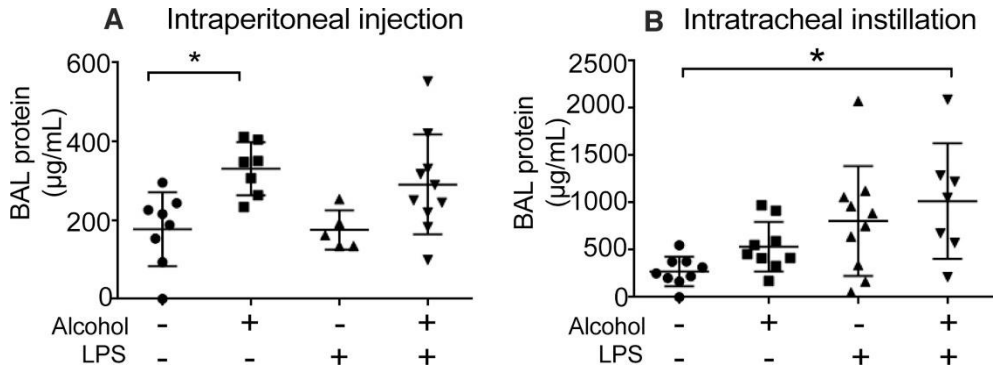

Figure 3.2. Alcohol increased lung airspace protein content.

Mice received an IP (A) or IT (B) treatment with either vehicle control or 5 mg/kg LPS in PBS. Total protein concentration in BAL fluid was measured using the BCA assay. (A) Alcohol-fed mice had increased total lavage protein compared to water-fed mice (n = 5–10, *p = 0.024). IP injection had no significant effect on total BAL protein. (B) In mice that were given an IT LPS, both alcohol and LPS independently increased total lavage protein concentration (n = 5–10, *p = 0.011). Values reported as mean ± standard deviation.

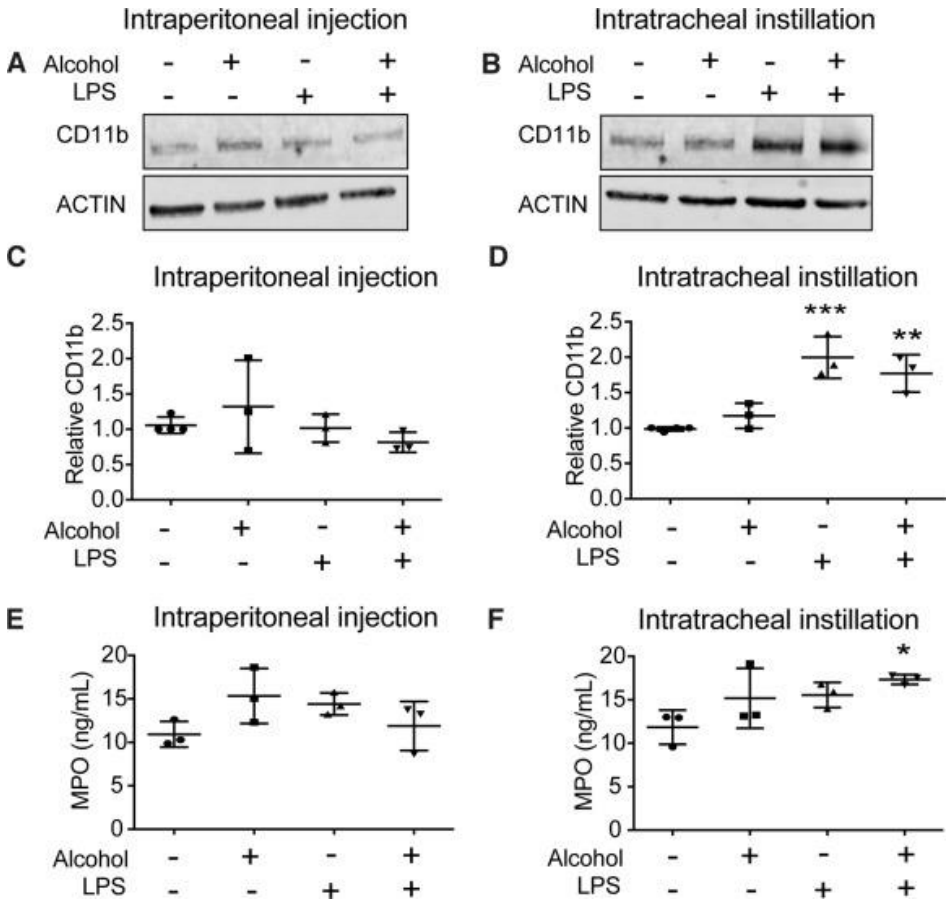

Figure 3.3. Alcohol and intratracheal lipopolysaccharide induced an inflammatory response in lung tissue.

Lungs from treated mice post-lavage were processed and the leukocyte marker CD11b protein expression was measured by immunoblot and normalized to actin in mice that received either an IP (A,C) or IT (B,D) treatment with either vehicle control or LPS. (A, C) There was no significant change in CD11b levels in alcohol or water-fed mice given IP LPS. (B,D) By contrast, CD11b showed significant increases in response to IT LPS both for control and alcohol fed mice (n = 3–4, ***p = 0.0006) (water fed IT LPS vs control); **p = 0.033 (alcohol fed IT LPS vs. alcohol control). (E,F) Lung neutrophil content was measured by the abundance of myeloperoxidase (MPO) by ELISA in mice that received either IP (E) or IT (F) LPS. Alcohol-fed mice with IT LPS injury showed significantly more MPO than water fed controls, suggesting increased neutrophil infiltrate (n = 3–4, *p = 0.05). Symbols represent samples from distinct animal replicates, values reported as mean ± standard deviation.

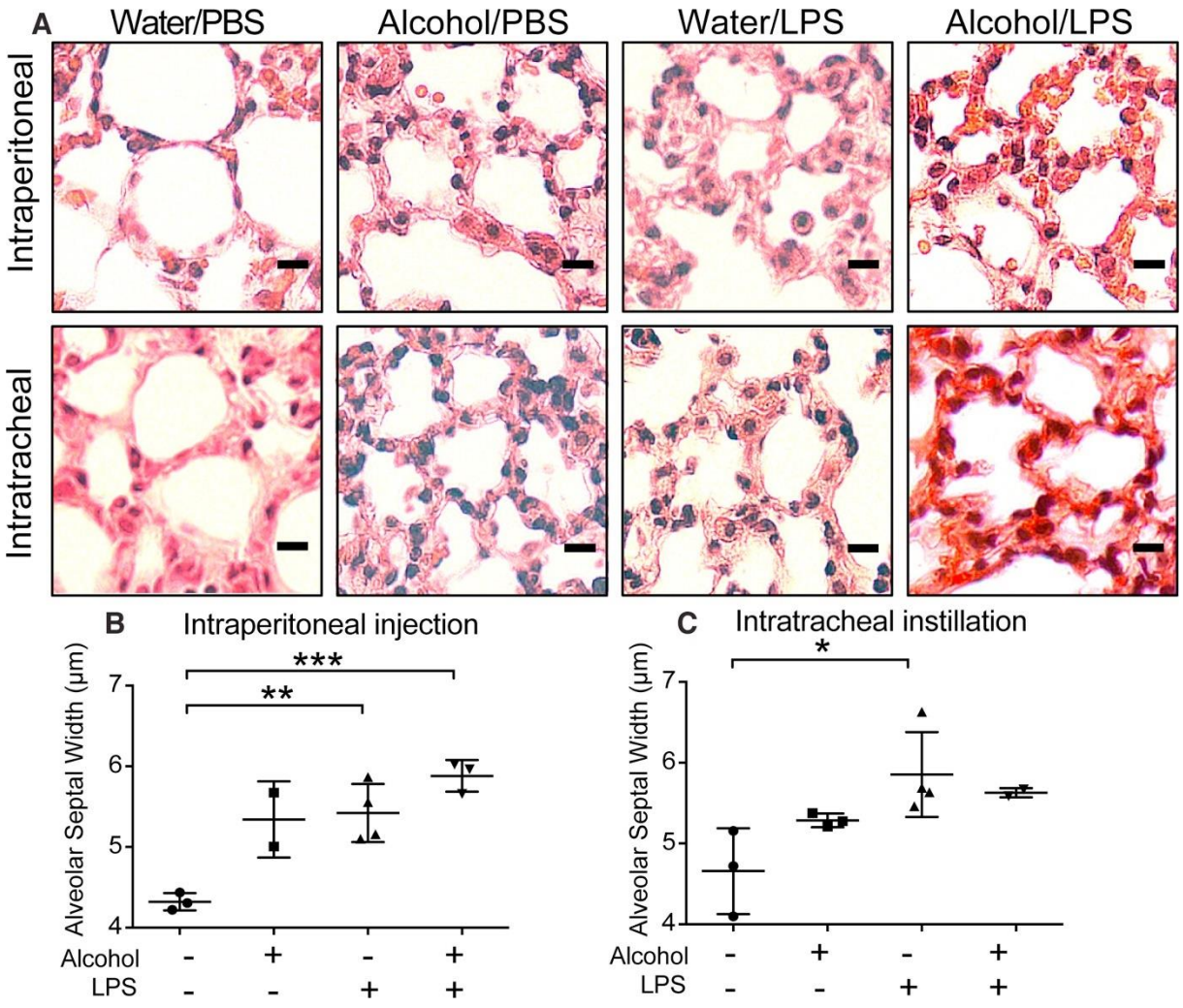

Figure 3.4. Alcohol consumption and lipopolysaccharide independently increased alveolar septal thickness.

Mice received an IP or IT treatment with either vehicle control or 5 mg/kg LPS in PBS. (A) H&E staining of the lungs of control or experimental mice. Photomicrographs are representative samples from one of 2–5 independent mice. Bar = 10 μm. (B, C) Alveolar septal thickness was measured in mice 24 h after IP (B) or IT(C) treatment with LPS. Alcohol and LPS injury increased alveolar septal width in IP treated mice (**p = 0.0057; ***p = 0.0009) as well as in IT LPS treated mice (*p = 0.024). Results represent twenty measurements per field of view from 5 fields per lung, for a total of 100 measurements per mouse. n = 2–5 mice per group. Values reported as mean ± standard deviation.

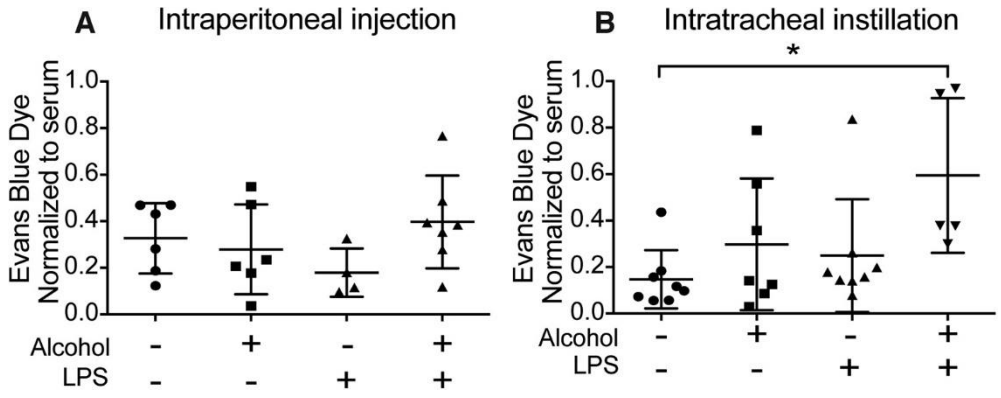

Figure 3.5. Effect of alcohol consumption and lipopolysaccharide on Evans Blue accumulation in lung tissue.

Mice received an IP (A) or IT (B) treatment with either vehicle control or 5 mg/kg LPS in PBS. After 24 h, the mice were then administered Evans Blue by tail vein injection and allowed to recover for 2 h. Lung tissue was harvested after BAL fluid collection and the right ventricle of the heart was perfused with PBS. Evans Blue dye was extracted from lung tissue by incubating in formamide at 55 °C for 48 h and analyzed via spectrophotometry (620 nm). Results were corrected for the presence of heme and normalized to Evans Blue serum levels and lung tissue weight. Tissue Evans Blue dye content was only significantly increased in alcohol-fed mice that were given an IT administration of LPS. There was no significant change in any other groups. n = 4–8, *p = 0.019. Values reported as mean ± standard deviation.

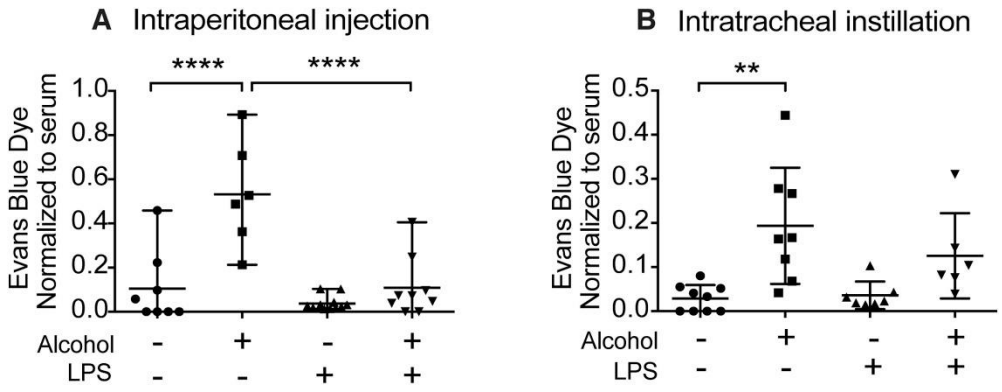

Figure 3.6. Effect of alcohol consumption and LPS on Evans Blue in airspaces.

Mice received an IP (A) or IT (B) treatment with either vehicle control or 5 mg/kg LPS in PBS. After 24 h the mice were administered Evans Blue by tail vein injection and allowed to recover for 2 h. Evans Blue dye in bronchoalveolar lavage (BAL) fluid was measured via spectrophotometry (620 nm). Results were corrected for the presence of heme and normalized to Evans Blue serum levels. In contrast to tissue data (Figure 3.5), alcohol-feeding alone increased Evans blue levels in BAL fluid, suggesting that alcohol promotes alveolar epithelial barrier dysfunction (n = 6–9, ****$p < 0.0001$; **$p = 0.0021$). Values reported as mean ± standard deviation.

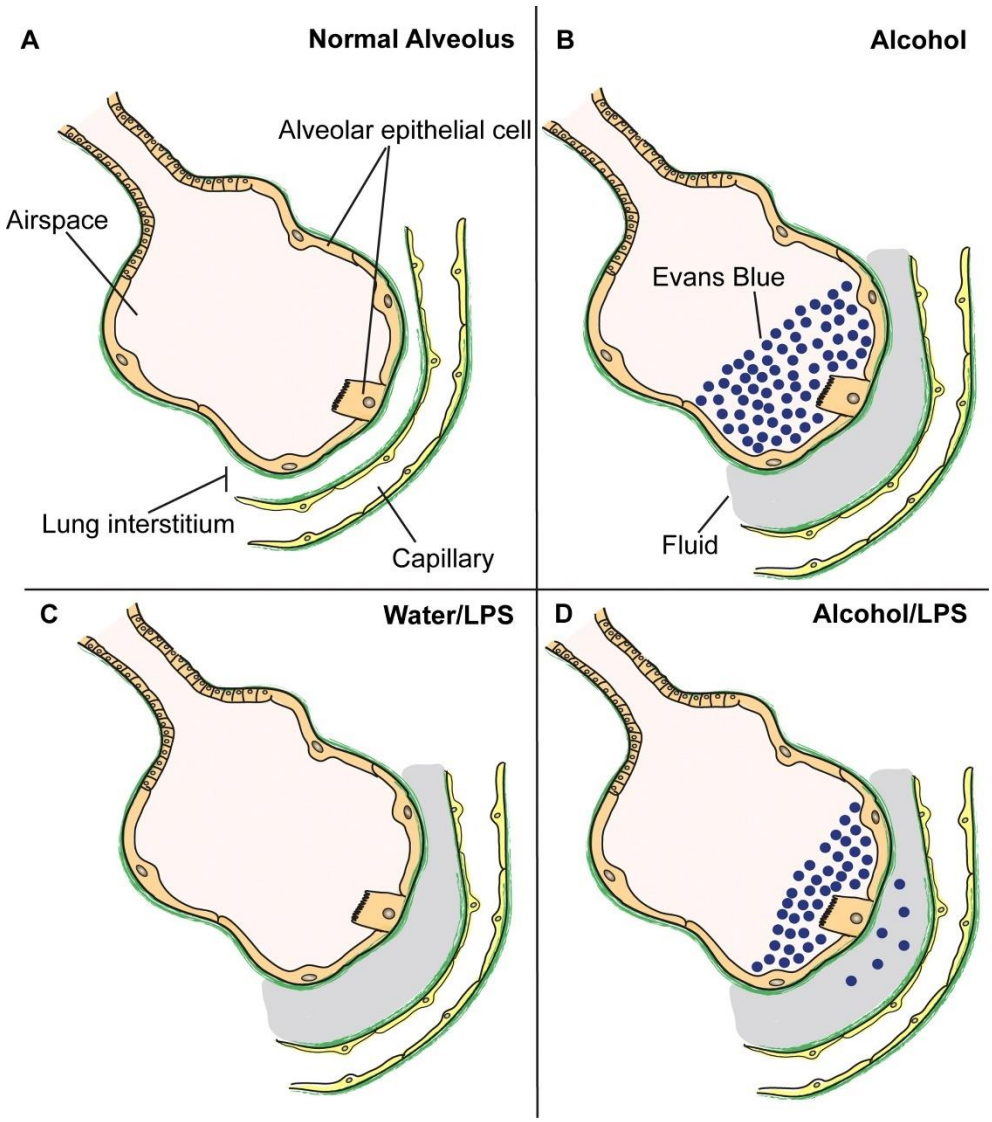

Figure 3.7. Model of lung permeability after alcohol and intratracheal lipopolysaccharide.

A) Cartoon of a cross section through a normal lung alveolus comprised of an epithelial sac surrounded by blood vessels. Alcohol and LPS independently lead to fluid accumulation in the lung interstitium (B–D). Alcohol also promoted the accumulation of Evans Blue into BAL, consistent with a defect in alveolar barrier function (B,D). Treatment of alcohol-fed mice with IT LPS also stimulated an increase in interstitial Evans Blue, suggesting an additional deficit in vascular barrier function (D).

Literature Cited

Adams, e. a. (2015). National Survey on Drug Use and Health. In.

Borok, Z., Hami, A., Danto, S. I., Lubman, R. L., Kim, K. J., & Crandall, E. D. (1996). Effects of EGF on alveolar epithelial junctional permeability and active sodium transport. *Am J Physiol*, *270*(4 Pt 1), L559-565. https://doi.org/10.1152/ajplung.1996.270.4.L559

Chen, S. P., Zhou, B., Willis, B. C., Sandoval, A. J., Liebler, J. M., Kim, K. J., Ann, D. K., Crandall, E. D., & Borok, Z. (2005). Effects of transdifferentiation and EGF on claudin isoform expression in alveolar epithelial cells. *J Appl Physiol (1985)*, *98*(1), 322-328. https://doi.org/10.1152/japplphysiol.00681.2004

Copeland, S., Warren, H. S., Lowry, S. F., Calvano, S. E., Remick, D., Inflammation, & the Host Response to Injury, I. (2005). Acute inflammatory response to endotoxin in mice and humans. *Clin Diagn Lab Immunol*, *12*(1), 60-67. https://doi.org/10.1128/CDLI.12.1.60-67.2005

Facts About Alcohol. (2018). National Council on Alcoholism and Drug Dependence. Retrieved June 18, 2018 from

Fehrenbach, H., Brasch, F., Uhlig, S., Weisser, M., Stamme, C., Wendel, A., & Richter, J. (1998). Early alterations in intracellular and alveolar surfactant of the rat lung in response to endotoxin. *Am J Respir Crit Care Med*, *157*(5 Pt 1), 1630-1639. https://doi.org/10.1164/ajrccm.157.5.9611070

Global status report on alcohol and health 2014. (2014).

Haorah, J., Knipe, B., Gorantla, S., Zheng, J., & Persidsky, Y. (2007). Alcohol-induced blood-brain barrier dysfunction is mediated via inositol 1,4,5-triphosphate receptor (IP3R)-gated intracellular calcium release. *J Neurochem*, *100*(2), 324-336. https://doi.org/10.1111/j.1471-4159.2006.04245.x

Kershaw, C. D., & Guidot, D. M. (2008). Alcoholic lung disease. *Alcohol Res Health*, *31*(1), 66-75. https://www.ncbi.nlm.nih.gov/pubmed/23584753

Klingensmith, N. J., Yoseph, B. P., Liang, Z., Lyons, J. D., Burd, E. M., Margoles, L. M., Koval, M., Ford, M. L., & Coopersmith, C. M. (2017). Epidermal Growth Factor Improves Intestinal Integrity and Survival in Murine Sepsis Following Chronic Alcohol Ingestion. *Shock*, *47*(2), 184-192. https://doi.org/10.1097/SHK.0000000000000709

Knapp, S. (2009). LPS and bacterial lung inflammation models. *Asthma and respiratory diseases*, *6*(4), 113-118. https://doi.org/10.1016/j.ddmod.2009.08.003

Koff, J. L., Shao, M. X., Kim, S., Ueki, I. F., & Nadel, J. A. (2006). Pseudomonas lipopolysaccharide accelerates wound repair via activation of a novel epithelial cell signaling cascade. *J Immunol*, *177*(12), 8693-8700. https://doi.org/10.4049/jimmunol.177.12.8693

Konsman, J. P., Parnet, P., & Dantzer, R. (2002). Cytokine-induced sickness behaviour: mechanisms and implications. *Trends Neurosci*, *25*(3), 154-159. https://doi.org/10.1016/s0166-2236(00)02088-9

Lawrenz, M. B., Fodah, R. A., Gutierrez, M. G., & Warawa, J. (2014). Intubation-mediated intratracheal (IMIT) instillation: a noninvasive, lung-specific delivery system. *J Vis Exp*(93), e52261. https://doi.org/10.3791/52261

Mehta, A. J., Yeligar, S. M., Elon, L., Brown, L. A., & Guidot, D. M. (2013). Alcoholism causes alveolar macrophage zinc deficiency and immune dysfunction. *Am J Respir Crit Care Med*, *188*(6), 716-723. https://doi.org/10.1164/rccm.201301-0061OC

Mitchell, L. A., Ward, C., Kwon, M., Mitchell, P. O., Quintero, D. A., Nusrat, A., Parkos, C. A., & Koval, M. (2015). Junctional adhesion molecule A promotes epithelial tight junction assembly to augment lung barrier function. *Am J Pathol*, *185*(2), 372-386. https://doi.org/10.1016/j.ajpath.2014.10.010

Moitra, J., Sammani, S., & Garcia, J. G. (2007). Re-evaluation of Evans Blue dye as a marker of albumin clearance in murine models of acute lung injury. *Transl Res*, *150*(4), 253-265. https://doi.org/10.1016/j.trsl.2007.03.013

Patarroyo, M., Prieto, J., Rincon, J., Timonen, T., Lundberg, C., Lindbom, L., Asjo, B., & Gahmberg, C. G. (1990). Leukocyte-cell adhesion: a molecular process fundamental in leukocyte physiology.

Immunol Rev, *114*, 67-108. https://doi.org/10.1111/j.1600-065x.1990.tb00562.x

Pham, T., & Rubenfeld, G. D. (2017). Fifty Years of Research in ARDS. The Epidemiology of Acute Respiratory Distress Syndrome. A 50th Birthday Review. *Am J Respir Crit Care Med*, *195*(7), 860-870. https://doi.org/10.1164/rccm.201609-1773CP

Price, M. E., Pavlik, J. A., Liu, M., Ding, S. J., Wyatt, T. A., & Sisson, J. H. (2017). Alcohol drives S-nitrosylation and redox activation of protein phosphatase 1, causing bovine airway cilia dysfunction. *Am J Physiol Lung Cell Mol Physiol*, *312*(3), L432-L439. https://doi.org/10.1152/ajplung.00513.2016

Radu, M., & Chernoff, J. (2013). An in vivo assay to test blood vessel permeability. *J Vis Exp*(73), e50062. https://doi.org/10.3791/50062

Schlingmann, B., Overgaard, C. E., Molina, S. A., Lynn, K. S., Mitchell, L. A., Dorsainvil White, S., Mattheyses, A. L., Guidot, D. M., Capaldo, C. T., & Koval, M. (2016). Regulation of claudin/zonula occludens-1 complexes by hetero-claudin interactions. *Nat Commun*, *7*, 12276. https://doi.org/10.1038/ncomms12276

Simet, S. M., Wyatt, T. A., DeVasure, J., Yanov, D., Allen-Gipson, D., & Sisson, J. H. (2012). Alcohol increases the permeability of airway epithelial tight junctions in Beas-2B and NHBE cells. *Alcohol Clin Exp Res*, *36*(3), 432-442. https://doi.org/10.1111/j.1530-0277.2011.01640.x

Singh, A. K., Jiang, Y., Gupta, S., & Benlhabib, E. (2007). Effects of chronic ethanol drinking on the blood brain barrier and ensuing neuronal toxicity in alcohol-preferring rats subjected to intraperitoneal LPS injection. *Alcohol Alcohol*, *42*(5), 385-399. https://doi.org/10.1093/alcalc/agl120

van Niekerk, G., Isaacs, A. W., Nell, T., & Engelbrecht, A. M. (2016). Sickness-Associated Anorexia: Mother Nature's Idea of Immunonutrition? *Mediators Inflamm*, *2016*, 8071539. https://doi.org/10.1155/2016/8071539

Wang, Z., Li, W., Chen, J., Shi, H., Zhao, M., You, H., Rao, C., Zhan, Y., Yang, Y., & Xie, P. (2016). Proteomic analysis reveals energy metabolic dysfunction and neurogenesis in the prefrontal

cortex of a lipopolysaccharide-induced mouse model of depression. *Mol Med Rep*, *13*(2), 1813-1820. https://doi.org/10.3892/mmr.2015.4741

Ward, C., Schlingmann, B., Stecenko, A. A., Guidot, D. M., & Koval, M. (2015). NF-kappaB inhibitors impair lung epithelial tight junctions in the absence of inflammation. *Tissue Barriers*, *3*(1-2), e982424. https://doi.org/10.4161/21688370.2014.982424

Ware, L. B., & Matthay, M. A. (2000). The acute respiratory distress syndrome. *N Engl J Med*, *342*(18), 1334-1349. https://doi.org/10.1056/NEJM200005043421806

Yeligar, S. M., Mehta, A. J., Harris, F. L., Brown, L. A., & Hart, C. M. (2016). Peroxisome Proliferator-Activated Receptor gamma Regulates Chronic Alcohol-Induced Alveolar Macrophage Dysfunction. *Am J Respir Cell Mol Biol*, *55*(1), 35-46. https://doi.org/10.1165/rcmb.2015-0077OC

Yoseph, B. P., Breed, E., Overgaard, C. E., Ward, C. J., Liang, Z., Wagener, M. E., Lexcen, D. R., Lusczek, E. R., Beilman, G. J., Burd, E. M., Farris, A. B., Guidot, D. M., Koval, M., Ford, M. L., & Coopersmith, C. M. (2013). Chronic alcohol ingestion increases mortality and organ injury in a murine model of septic peritonitis. *PLoS One*, *8*(5), e62792. https://doi.org/10.1371/journal.pone.0062792

Chapter 4: Effects of Interstitial Fluid pressure on Alveolar Barrier Function

Introduction

Due to generally low alveolar epithelial permeability, most fluid that is filtered into the interstitium from the pulmonary vasculature is reabsorbed back into the circulation. Additionally, several other processes promote reabsorption of interstitial fluid, including the protein osmotic gradient between the pulmonary capillaries and interstitium, lymphatic flow, a hydrostatic pressure gradient from peripheral to central vessels, and pleural and mediastinal sinks (Erdmann et al., 1975; Hastings et al., 2004; Matthay & Wiener-Kronish, 1990; Meyer et al., 2021; Staub, 1974).

Chronic alcohol abuse has been identified as a major risk factor for developing alveolar flooding (Kershaw & Guidot, 2008). The healthy lung can generally tolerate moderate increases in the pressure of fluid from the surrounding interstitium without causing alveolar flooding, however whether the alcoholic lung is more sensitive to develop alveolar leak due to increased interstitial fluid pressure is not known. Additionally, patients with chronic alcohol abuse at baseline and with a diagnosis of ARDS have greater extravascular water levels which can contribute to increased interstitial water pressure surrounding the alveoli (Berkowitz et al., 2009).

Microvascular stresses can be a potent cofactor in the development of pulmonary edema. Increased cardiac output can increase the pre-alveolar microvasculature pressure, leading to increased vascular pressure across the lung (Marini et al., 2003). There are several examples of how increasing transmural pulmonary vasculature pressure, without corresponding inflammation, can small vascular tears (Marini et al., 2003). Mitral stenosis increases pulmonary venous and capillary pressure leading to acute edema, hemoptysis, and hemosiderin-laden macrophages, indicating involvement of the pulmonary, not bronchial, circulation. In conditions of extreme exertions, high blood flow throughout the lung can cause post-exertional hemorrhage (Broccard et al., 2001; Hopkins et al., 1997).

Since a clinical study has demonstrated that there is no correlation between albumin levels in alcoholic ICU patients and extravascular lung water levels (Berkowitz et al., 2009), we wanted to measure

the mechanical effects of increased pressure on the molecular integrity of lung barrier function. We specifically wanted to investigate if alcohol lowers the fluid interstitial pressure threshold which causes alveolar flooding.

Additionally, the protein osmotic gradient between the interstitium and pulmonary microvasculature can be lost when the endothelial vascular barrier becomes highly permeable to protein and solutes, such as during acute lung injury, which will promote an interstitium that can become flooded (Meyer et al., 2021). These small increases in pulmonary microvascular permeability can increase interstitial edema. Additional studies will need to be performed to test the impact of how a 'second-hit' lung injury, such as pneumonia, affects the sensitivity of the normal and alcoholic lung to develop pulmonary edema. Here, we hypothesized that the alcoholic lung is more sensitive than a normal lung to develop pulmonary edema and lung injury with increasing lung interstitial pressures at baseline and in response to bacterial pneumonia.

Materials and Methods

Mice

Experiments were performed in accordance with the National Institutes of Health Guidelines for the Use of Laboratory Animals guidelines and were approved by the Institutional Animal Care and Use Committee at Emory University School of Medicine. Isogenetic twelve-week-old male C57BL/6 wild-type mice were used for all experiments (Jackson Laboratory, Bar Harbor, ME). Animals were housed with a maximum of five animals per cage. All animals were kept under constant temperature at 21 °C and under 12 h light-dark cycle with ad libitum access to regular chow diet. In the alcohol group, ethanol was administered by increasing ethanol concentration from 0% to 20% in 5% increments over a two-week period, and then mice were maintained at 20% ethanol for an additional 8 weeks. For instillation experiments, mice were anesthetized via IP injection of xylazine (10 mg/kg) and ketamine (100 mg/kg). Mice were suspended by their incisors on a rodent tilting work stand (Hallowell, Pittsfield, MA) for orotracheal instillation as previously described (Lawrenz et al., 2014). Mice were weighed while awake

and prior to receiving a sedative for all weight measurements.

Lung permeability as measured by Evans Blue extravasation

24 h after intraperitoneal or intravascular treatment, mice were either re-anesthetized or placed in a mouse restrainer (Braintree Scientific, Inc., Braintree, MA) for the conscious procedure for an Evans Blue permeability assay. Mice were placed on a heating pad or kept in the mouse restrainer and the tail was sterilized with an alcohol wipe. 200 µl of 0.5% Evans Blue in PBS was injected into the tail vein with a 30-gauge needle. The mice were allowed to recover on a heating pad for 1 h and then sacrificed while still under anesthesia. 250 µl of blood was collected by cardiac puncture and centrifuged at 1500 × g for 15 min to collect serum. Bronchoalveolar lung lavage (BAL) fluid was collected by flushing the lungs twice via a tracheal tube with 500 µl of ice-cold PBS with protease inhibitors and centrifuged at 1500 x g for 15 minutes to collect cell-free BAL fluid.

Evans Blue in the serum and BAL fluid was analyzed by spectrophotometry (620 nm) (Radu & Chernoff, 2013). Evans Blue readings were corrected for contaminating heme analyzing samples at 740 nm and using the correction factor y = 1.193x +0.007 as previously described (Moitra et al., 2007) and reported as Evans Blue in the BAL and/or normalized to corresponding serum Evans Blue levels.

Wet to Dry Analysis

Both left and right lungs were excised 4 h or 24 h after intravascular PBS treatment and immediately weighed (lung wet weight). Lungs were dried in a convection oven at 65˚C for 60 h and re-weighed (lung dry weight). Wet to dry ratio was calculated as lung wet weight divided by lung dry weight.

Total lung protein

Recovered bronchoalveolar lavage (BAL) fluid was kept on ice and centrifuged at 1500 × g for 15 min. Supernatant was collected and stored at −20 °C. Total BAL fluid protein was measured using the Pierce BCA Protein Assay Kit (Thermo Fisher Scientific).

Statistical Analysis

Comparisons between two groups was performed by unpaired, two-tailed t-test while comparisons between multiple groups were performed by one-way ANOVA with Tukey's multiple comparisons test using GraphPad Prism software. Data are represented as mean ± standard error of the mean and the statistical significance level was set at 0.05.

Results

Intraperitoneal fluid in anesthetized and conscious mice has a minimal impact on alveolar leak

We have previously demonstrated that the Evans Blue permeability assay can be used to measure alveolar lung vessel and epithelial permeability *in vivo* (Smith et al., 2019, 2021). We found that dietary alcohol increases lung permeability and disrupts the alveolar epithelial barrier as measured by Evans Blue present in the recovered bronchoalveolar lavage (BAL) fluid when coupled with an additional insult (Smith et al., 2019). Animals from control experiments in this previous work suggested that increasing fluid volume in anesthetized mice may cause an increase in alveolar leak as measured by increased leak of Evans Blue dye the bronchoalveolar lavage fluid. We hypothesized that this alveolar barrier dysfunction was potentially due to increased hydrostatic pressure as the second insult when coupled with alcohol.

In this study, water-fed or alcohol-fed mice received an intraperitoneal injection of 0 µl or 250 µl PBS, anesthetized with xylazine and ketamine, and given a tail vein injection of Evans Blue 24 h later. Evans Blue levels were measured in the BAL and were normalized to Evans Blue serum levels to normalize input (Figure 4.1A). There was no effect of additional intraperitoneal fluid on alveolar leak in water-fed mice, although there was a statistically insignificant but trending increase in Evans Blue in the lavage in alcohol-fed mice.

We next wanted to test if the rate of blood circulation would accentuate the effect of increased intravascular fluid on alveolar leak. Anesthetized mice have been shown to have as lower heart rate and respiratory rate than awake mice (Erhardt et al., 1984; Ho et al., 2011; Uechi et al., 1998). Mice received

an intraperitoneal fluid injection of 0 µl or 250 µl PBS followed by a tail vein injection of Evans Blue 24 h later while conscious and restrained in a mouse restrainer (Braintree Scientific, Inc., Braintree, MA). Interestingly, the effect of intraperitoneal fluid in alcohol-fed mice was dampened relative to its effect in sedated mice (Figure 4.1A, B). This may have been due to increased extravasation of Evans Blue dye into non-pulmonary tissues from increased vascular systemic circulation.

Intravascular fluid does not affect alveolar leak of protein

As a small bolus of intraperitoneal fluid did not provoke a corresponding increase in alveolar leak, we next wanted to test if increasing hydrostatic pressure directly into the circulatory system to increase hydrostatic pressure would cause a dose-dependent increase in alveolar leak. We additionally wanted to measure if an epithelium that was already at maximum capacity for maintaining fluid balance, the alcoholic lung, would be able to sustain increased fluid pressure without causing measurable alveolar leak. Mice were anesthetized and received either 250, 500 or 750 µl via tail vein injection of PBS to induce increasing levels of hydrostatic pressure. BAL was then collected 24 h later and total protein levels were measured. The range of protein concentrations was consistent with other models of non-inflammatory BAL protein concentration (Smith et al., 2019). Increasing volumes of fluid did not induce significant changes in BAL protein accumulation in either water-fed or alcohol-fed mice (Figure 4.2).

Increasing vascular pressure with fluid does not increase alveolar leak or cause pulmonary edema

Previously we have demonstrated that the Evans Blue permeability assay can be used to measure alveolar lung vessel and epithelial permeability *in vivo* (Smith et al., 2019, 2021). Direct, intratracheal injury with either saline or LPS increases lung permeability and disrupts the alveolar epithelial barrier in alcohol-fed mice as measured by Evans Blue present in the recovered bronchoalveolar lavage (BAL) fluid (Smith et al., 2019). To determine if increased hydrostatic pressure administered by injection of intravascular fluid, water-fed and alcohol-fed mice received a 250 – 750 µl bolus of PBS via tail vein injection and then 200 µl of Evans Blue dye 24 h later. As expected, Evans Blue recovered in the serum

decreased with increasing volumes of intravascular PBS in a dose-dependent manner in both alcohol-fed and water-fed mice (Figure 4.3). Evans Blue levels were measured in the BAL (Figure 4.4A) and were normalized to Evans Blue serum levels to normalize input (Figure 4.4B). There was no effect of increased hydrostatic pressure on alveolar leak in either water-fed or alcohol-fed groups. We speculate that after 24 h, both groups of mice excreted the excessive volume and returned to steady state fluid homeostasis in the alveolar epithelium.

Since an increase in alveolar leak as measured by Evans Blue in the BAL was not detected at the tested ranges of fluid (250 – 750 µl), we wanted to measure if we were inducing any measurable pulmonary edema within this time frame. Lung wet:dry weight ratios are commonly used as an estimate for pulmonary edema (Du et al., 2018; Jang et al., 2019; Miserocchi et al., 1993). Water-fed and alcohol-fed mice were given an intravascular bolus of PBS (0, 500, or 1000 µl), then lungs were extracted either 4 h or 24 h after. Neither water-fed (Figure 4.5A) or alcohol-fed mice (Figure 4.5B) had any difference in wet:dry lung weight ratios after 4 h or 24 h after any volume of intravascular fluid as compared to baseline. This suggests that these intravascular volumes did not induce pulmonary edema within the tested time frame, which may explain the lack of alveolar leak as measured by Evans Blue in the BAL.

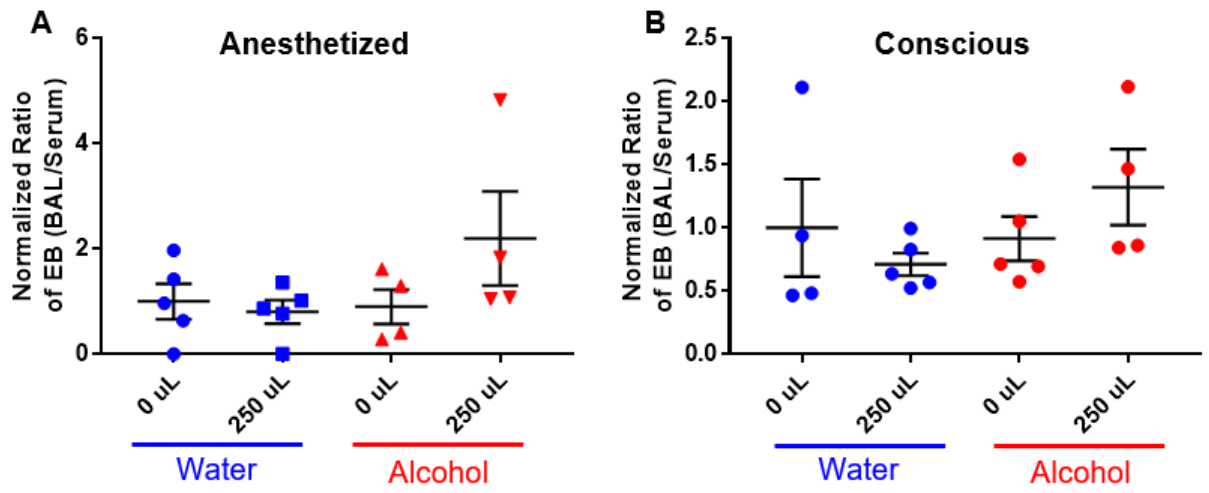

Figure 4.1 Anesthesia is essential for Evans Blue assays of lung permeability.

Mice received an intraperitoneal treatment of 0µl or 250µL of PBS. After 24 h, the mice were then administered Evans Blue by tail vein injection while anesthetized with ketamine/xylazine (A) or kept conscious while in an IACUC-approved mouse restrainer (B) and allowed to recover for 1 h before BAL and blood were collected. Results were corrected for the presence of heme and normalized to Evans Blue serum levels. IP injection had no significant effect on alveolar leak of Evans Blue into BAL in either anesthetized or conscious mice. n = 4-5. Values reported as mean ± standard error of the mean. Values reported as mean ± standard error of the mean.

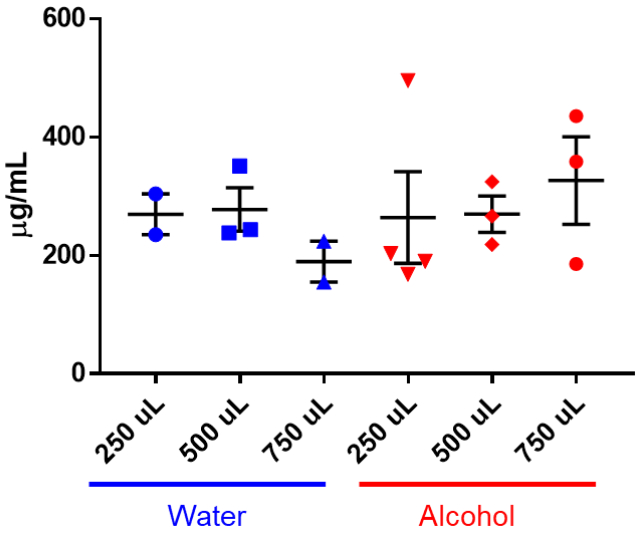

Figure 4.2. No effect of increased intravascular fluid on total protein levels in bronchoalveolar lavage fluid.

Mice received an intravascular treatment of 250 – 750 µL of PBS. BAL was collected 24 h later. Total protein concentration in BAL fluid was measured using the BCA assay. There was no difference in total BAL protein between control-fed and alcohol-fed mice at any IP fluid volume. n = 2-4. Values reported as mean ± standard error of the mean.

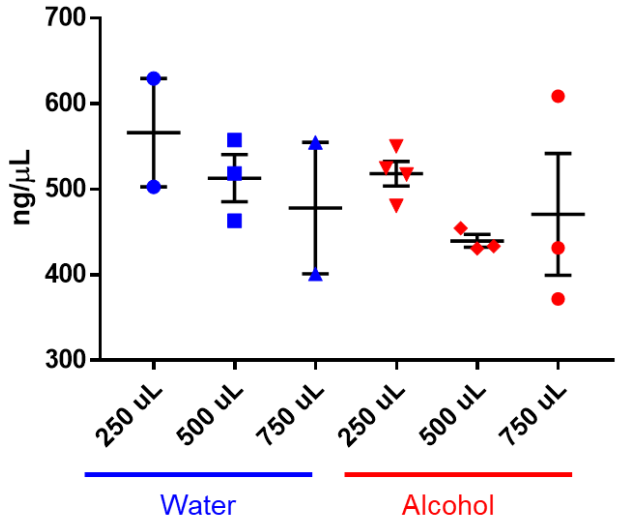

Figure 4.3. Intravascular fluid dilutes Evans Blue in mouse serum in volume-dependent manner.

Mice received an intravascular treatment of 250 - 750µL of PBS. After 24 h, the mice were then administered Evans Blue by tail vein injection while anesthetized and allowed to recover for 1 h before blood was collected. Results were corrected for the presence of heme. Increasing volumes of IP fluid diluted Evans Blue in serum in volume-dependent manner. n = 2-4. Values reported as mean ± standard error of the mean.

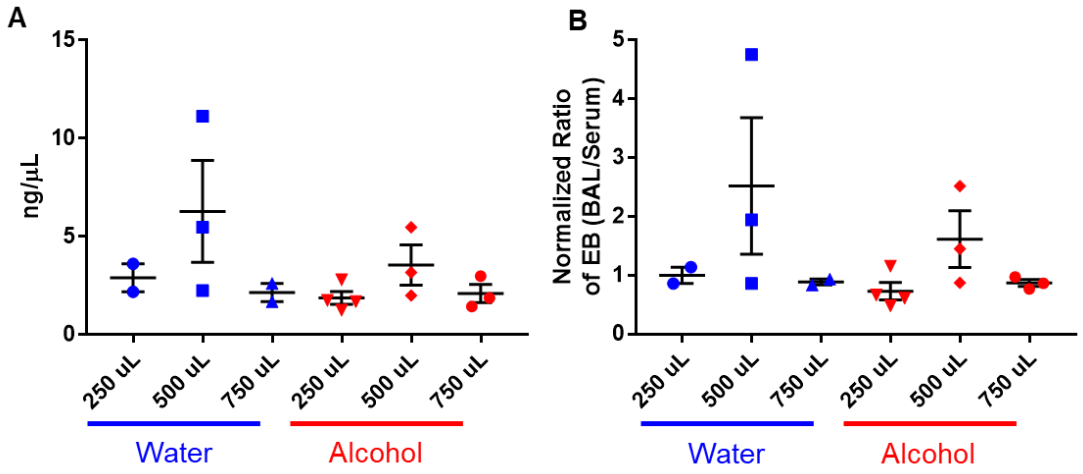

Figure 4.4. No effect of increased intravascular fluid on alveolar leak at baseline.

Mice received an intravascular treatment of 250 – 750µL of PBS. After 24 h, the mice were then administered Evans Blue by tail vein injection while anesthetized and allowed to recover for 1 h before BAL and blood were collected. Results were corrected for the presence of heme and are represented as BAL (A) or BAL normalized to Evans Blue serum levels (B). Increasing intravascular fluid had no effect on alveolar leak in control-fed or alcohol-fed mice. n = 2-4. Values reported as mean ± standard error of the mean.

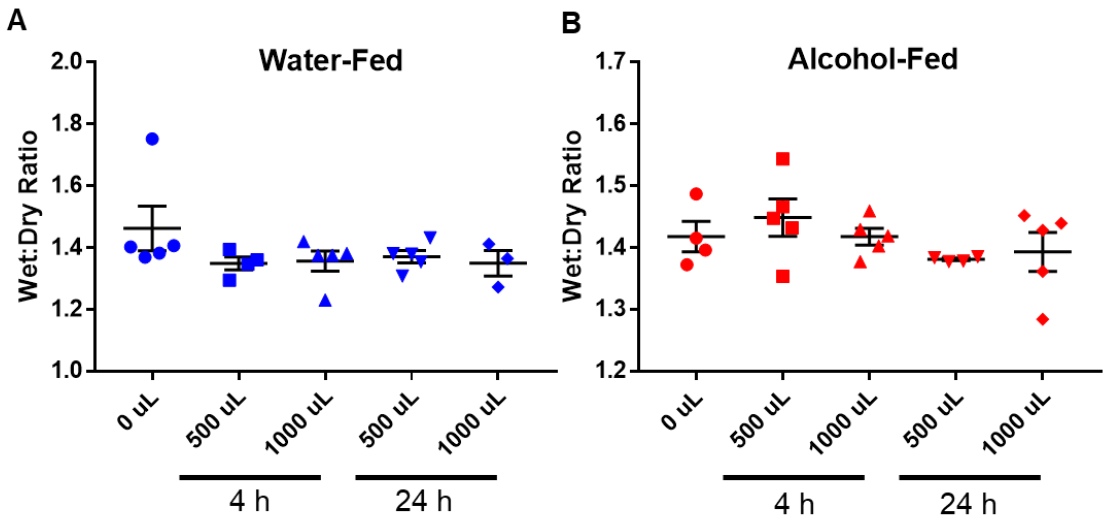

Figure 4.5. No pulmonary edema observed in mice given intravascular bolus of fluid.

Water-fed (A) or alcohol-fed (B) mice received an intravascular treatment of 0µL, 500µL or 1mL of PBS. After 4 or 24 h, both lungs were collected and weighed upon excision (lung wet weight). Lungs were dried in an oven at 65˚ for 60 h and then weighed (lung dry weight). Wet to dry ratio was calculated as lung wet weight divided by lung dry weight. n = 3-5. Values reported as mean ± standard error of the mean.

Literature Cited

Berkowitz, D. M., Danai, P. A., Eaton, S., Moss, M., & Martin, G. S. (2009). Alcohol abuse enhances pulmonary edema in acute respiratory distress syndrome. *Alcohol Clin Exp Res*, *33*(10), 1690-1696. https://doi.org/10.1111/j.1530-0277.2009.01005.x

Broccard, A. F., Liaudet, L., Aubert, J. D., Schnyder, P., & Schaller, M. D. (2001). Negative pressure post-tracheal extubation alveolar hemorrhage. *Anesth Analg*, *92*(1), 273-275. https://doi.org/10.1097/00000539-200101000-00055

Du, Z. A., Sun, M. N., & Hu, Z. S. (2018). Saikosaponin a Ameliorates LPS-Induced Acute Lung Injury in Mice. *Inflammation*, *41*(1), 193-198. https://doi.org/10.1007/s10753-017-0677-3

Erdmann, A. J., 3rd, Vaughan, T. R., Jr., Brigham, K. L., Woolverton, W. C., & Staub, N. C. (1975). Effect of increased vascular pressure on lung fluid balance in unanesthetized sheep. *Circ Res*, *37*(3), 271-284. https://doi.org/10.1161/01.res.37.3.271

Erhardt, W., Hebestedt, A., Aschenbrenner, G., Pichotka, B., & Blumel, G. (1984). A comparative study with various anesthetics in mice (pentobarbitone, ketamine-xylazine, carfentanyl-etomidate). *Res Exp Med (Berl)*, *184*(3), 159-169. https://doi.org/10.1007/BF01852390

Hastings, R. H., Folkesson, H. G., & Matthay, M. A. (2004). Mechanisms of alveolar protein clearance in the intact lung. *Am J Physiol Lung Cell Mol Physiol*, *286*(4), L679-689. https://doi.org/10.1152/ajplung.00205.2003

Ho, D., Zhao, X., Gao, S., Hong, C., Vatner, D. E., & Vatner, S. F. (2011). Heart Rate and Electrocardiography Monitoring in Mice. *Curr Protoc Mouse Biol*, *1*, 123-139. https://doi.org/10.1002/9780470942390.mo100159

Hopkins, S. R., Schoene, R. B., Henderson, W. R., Spragg, R. G., Martin, T. R., & West, J. B. (1997). Intense exercise impairs the integrity of the pulmonary blood-gas barrier in elite athletes. *Am J Respir Crit Care Med*, *155*(3), 1090-1094. https://doi.org/10.1164/ajrccm.155.3.9116992

Jang, E. A., Kim, J. Y., Tin, T. D., Song, J. A., Lee, S. H., & Kwak, S. H. (2019). The effects of BMS-

470539 on lipopolysaccharide-induced acute lung injury. *Acute Crit Care*, *34*(2), 133-140. https://doi.org/10.4266/acc.2019.00507

Kershaw, C. D., & Guidot, D. M. (2008). Alcoholic lung disease. *Alcohol Res Health*, *31*(1), 66-75. https://www.ncbi.nlm.nih.gov/pubmed/23584753

Lawrenz, M. B., Fodah, R. A., Gutierrez, M. G., & Warawa, J. (2014). Intubation-mediated intratracheal (IMIT) instillation: a noninvasive, lung-specific delivery system. *J Vis Exp*(93), e52261. https://doi.org/10.3791/52261

Marini, J. J., Hotchkiss, J. R., & Broccard, A. F. (2003). Bench-to-bedside review: microvascular and airspace linkage in ventilator-induced lung injury. *Crit Care*, *7*(6), 435-444. https://doi.org/10.1186/cc2392

Matthay, M. A., & Wiener-Kronish, J. P. (1990). Intact epithelial barrier function is critical for the resolution of alveolar edema in humans. *Am Rev Respir Dis*, *142*(6 Pt 1), 1250-1257. https://doi.org/10.1164/ajrccm/142.6_Pt_1.1250

Meyer, N. J., Gattinoni, L., & Calfee, C. S. (2021). Acute respiratory distress syndrome. *Lancet*, *398*(10300), 622-637. https://doi.org/10.1016/S0140-6736(21)00439-6

Miserocchi, G., Negrini, D., Del Fabbro, M., & Venturoli, D. (1993). Pulmonary interstitial pressure in intact in situ lung: transition to interstitial edema. *J Appl Physiol (1985)*, *74*(3), 1171-1177. https://doi.org/10.1152/jappl.1993.74.3.1171

Moitra, J., Sammani, S., & Garcia, J. G. (2007). Re-evaluation of Evans Blue dye as a marker of albumin clearance in murine models of acute lung injury. *Transl Res*, *150*(4), 253-265. https://doi.org/10.1016/j.trsl.2007.03.013

Radu, M., & Chernoff, J. (2013). An in vivo assay to test blood vessel permeability. *J Vis Exp*(73), e50062. https://doi.org/10.3791/50062

Smith, P., Jeffers, L. A., & Koval, M. (2019). Effects of different routes of endotoxin injury on barrier function in alcoholic lung syndrome. *Alcohol*, *80*, 81-89. https://doi.org/10.1016/j.alcohol.2018.08.007

Smith, P., Jeffers, L. A., & Koval, M. (2021). Measurement of Lung Vessel and Epithelial Permeability In Vivo with Evans Blue. *Methods Mol Biol*, *2367*, 137-148. https://doi.org/10.1007/7651_2020_345

Staub, N. C. (1974). Pulmonary edema. *Physiol Rev*, *54*(3), 678-811. https://doi.org/10.1152/physrev.1974.54.3.678

Uechi, M., Asai, K., Osaka, M., Smith, A., Sato, N., Wagner, T. E., Ishikawa, Y., Hayakawa, H., Vatner, D. E., Shannon, R. P., Homcy, C. J., & Vatner, S. F. (1998). Depressed heart rate variability and arterial baroreflex in conscious transgenic mice with overexpression of cardiac Gsalpha. *Circ Res*, *82*(4), 416-423. https://doi.org/10.1161/01.res.82.4.416

Chapter 5: Therapeutic Drug candidates to Improve Alcohol-mediated Barrier Dysfunction

Introduction

Chronic alcohol abuse has been shown to change the composition of tight junctions and decrease alveolar barrier function, predisposing the lung to develop ARDS (Schlingmann et al., 2016). Currently, there is no therapy targeted to mitigate the effects of alcoholic lung syndrome nor its underlying pathophysiology.

As described in the Introduction, alveolar barrier function critically depends on the physiologic barrier formed by the alveolar epithelia cells that separate the inspired air in the alveolus from the fluid-filled tissues. Tight junction protein complexes form a sealing barrier that regulates paracellular fluid diffusion. Disruption of this barrier results in pulmonary edema and respiratory failure, predisposing the lung to develop ARDS. Thus, targeting tight junctions offers a unique therapeutic opportunity to treat the alcohol damaged lung.

Interaction between Connexin 43 and ZO-1

Both the epithelial and endothelial tissue depend on a functional barrier to regulate fluid homeostasis. Various cellular complexes, including tight junctions, adherens junctions, gap junctions, and the actin cytoskeletal network function together to modulate barrier function (Garcia, 2009; Giepmans, 2004; Herve et al., 2007). Connexins, also known as gap junction proteins, are a family of integral membrane proteins that assemble to form channels between adjacent cells and allow intercellular communication by permitting bidirectional cytosolic exchange of ions, metabolites, and second messengers (Aasen et al., 2019; Laird, 2006). The gap junction protein subunit Cx43 is the most studied and ubiquitously expressed isoform and is involved in regulating barrier function and permeability by influencing junction assembly, cell polarity, cytoskeletal dynamics, and cell to cell contacts (Francis et al., 2011; Kameritsch et al., 2012; Leithe et al., 2018; Matsuuchi & Naus, 2013; Olk et al., 2009; Oyamada et al., 2013).

Cx43 is a 43 kDa, 382 amino acid long polypeptide that contains four conserved alpha-helical transmembrane domains, one intracellular and two extracellular loops, and cytoplasmic carboxyl- and amino-terminal tails. As the connexin proteins are a relatively conserved gene and protein family, the major difference between the different connexin proteins is the length and sequence of the C-terminal tail (CT). The CT of Cx43 is approximately 150 amino acids long, accounting for 39% of the entire protein (Ambrosi et al., 2016; Axelsen et al., 2013). The CT is largely disordered and has a rich composition of prolines and serines that are largely absent from the intracellular domains and loops, making Cx43 a potential target for protein interactions and kinases (Leithe et al., 2018). Protein interactions with CT enable Cx43 to control cell growth, differentiation, and migration, functions that are independent of its role in intercellular communication (Leithe et al., 2018).

At the terminal-most portion of its CT, Cx43 contains a four amino acid PDZ2-binding ligand (aspartic acid (D), leucine (L), glutamic acid (E), isoleucine (I)) that is capable of binding to the second PDZ domain of ZO-1 (Giepmans & Moolenaar, 1998; Toyofuku et al., 1998). A high-affinity interaction exists between Cx43 and ZO-1 as the hydrophobic side chains of Cx43 insert into the hydrophobic groove in the PDZ2 domain of ZO-1 (Chen et al., 2008). In addition to its contributions to its channel properties, the CT of Cx43 is essential to barrier function, as mice that lack Cx43 CT exhibit high postnatal lethality due to epithelial barrier dysfunction, despite the truncated Cx43 protein forming functional open gap junctional channels (Maass et al., 2004).

ZO-1 belongs to a family of multidomain scaffolding proteins that organize the protein components of the tight junction and link them to the cortical actin cytoskeleton (Fanning & Anderson, 2009). Of the three isoforms that have been discovered, ZO-1 is the most studied and well characterized. ZO-1 is a 220 kDa protein and can bind a large variety of binding partners due to its diverse and numerously available domains and motifs (Belardi et al., 2020). The N-terminus of ZO-1 contains three PDZ domains, an SH3 and GUK domain and a Unique-5 and -6 motifs, while the C-terminus contains an actin-binding domain allowing ZO-1 to tether its binding partners to the cytoskeletal network. ZO-1 is described a “tension transducer” and can exhibit either an open or closed conformation which regulates access to its central

most binding regions (Spadaro et al., 2017). During actomyosin tension, tension is created between membrane-anchored proteins bound to ZO-1's N-terminus and actin-binding proteins and the actomyosin apparatus bound to the ZO-1's C-terminus (Haas et al., 2020; Spadaro et al., 2017; Strauss & Gourdie, 2020).

ZO-1 plays a role in the dynamic remodeling of Cx43 gap junctions, constrains the growth rate of gap junctions after they are formed, negatively regulates the rate at which undocked Cx43 connexons incorporate into gap junction plaques, and may be involved in modulating Cx43 gap junction endocytosis (Bruce et al., 2008; Hunter et al., 2005; Rhett et al., 2011). Interestingly, Cx43 CT is also capable of binding to ZO-2; it binds to ZO-1 in quiescent cells and to ZO-2 during cell cycle progression (Singh et al., 2005).

Cx43 and ZO-1 interaction is negatively regulated by phosphorylation of Ser373 on Cx43 (Chen et al., 2008). Phosphorylation of Ser373 alters Cx43 conformation, leading to an uncoupling of the CT from ZO-1. Akt-mediated phosphorylation of the same residue interrupted the *in vivo* interaction between Cx43 and ZO-1, which was associated with enlarged gap junctions and increased gap junction intercellular communication. Additionally, this Akt-dependent phosphorylation of Ser373 is increased during both cardiac ischemia and in the epidermal wound response (Dunn & Lampe, 2014).

Blockage of the PDZ-mediated interaction between ZO-1 and Cx43 led to a reduction of peripherally associated ZO-1 and increase in the aggregate size of gap junctions (Hunter et al., 2005). C-terminal tagging of Cx43 with GFP was shown to interfere with the regulatory mechanism that controlled gap junction size as well as disrupt binding of Cx43 to ZO-1 (Giepmans & Moolenaar, 1998; Giepmans et al., 2001; Hunter et al., 2005).

Alpha Carboxyl-Terminal Mimetic Peptide (αCT1)

Alpha carboxyl terminus 1 (αCT1) is a 25-amino acid peptide that contains an antennapedia cell internalization sequence linked to the 9 CT-most amino acids of Cx43 (RPRPDDLEI) (Hunter et al., 2005). The binding characteristic between the terminal-most portion of Cx43's CT and the PDZ2 domain

of ZO-1 was confirmed with the use of αCT1 (Jiang et al., 2019). The peptide was originally developed as a membrane-permeable peptide inhibitor to probe the organization and size of gap junctions by inhibiting the interaction of and colocalization of ZO-1 with Cx43. Once intracellular, αCT1 competes for binding to ZO-1 and reduces ZO-1 availability for interaction with the PDZ-binding domain of endogenous Cx43 (Hunter et al., 2005). This interaction was found to be specific for the PDZ2 domain of ZO-1, not the PDZ1 domain, and required the free C-terminal isoleucine.

There are two potentially independent molecular mechanisms for αCT1 peptide actions. The first involves the inhibition of Cx43 and ZO-1 interaction by competing for binding to the PDZ2 domain of ZO-1. A second, ZO-1-independent mechanism, may involve the PKC-mediated phosphorylation of Cx43 Ser368, a phosphorylation event that had no impact on the interaction between Cx43 and ZO-1 (O'Quinn et al., 2011). This phosphorylation status is retained at intercalated disks during early ischemia and is likely associated with cardioprotection induced by ischemic preconditioning (Ek-Vitorin et al., 2006).

Previous therapeutic uses of αCT1

The αCT1 peptide has been used extensively for various novel therapeutic purposes in the fields of tissue engineering and regenerative medicine. αCT1 modulated the wound-healing response to silicone implants by attenuating neutrophil infiltration, increasing vascularity of the capsule tissue, reducing type 1 collagen deposition around the implant, and reducing the continued presence of contractile myofibroblasts (Soder et al., 2009). In this study, pluronic gel was used as it has mild surfactant properties that aid in peptide dispersion. The peptide was also found to provide cardioprotection from ischemia-reperfusion injury when infused after the ischemic injury and may be used as a novel therapy for patients who experienced an acute myocardial infarction (Jiang et al., 2019).

Pre-treatment of αCT1 was successfully used *in vivo* to reduce choroidal neovascularization and fluid leakage following laser-photocoagulation, ameliorating retinal pigment epithelial damage and providing potential therapeutic value in age-related macular degeneration-like pathologies (Obert et al., 2017).

Additionally, αCT1 was found to reduce Cx43 gap junction remodeling in injury border zone tissues

after cryoinfarction of the left ventricle in mice, which was associated with a decreased propensity of the injured hearts to develop inducible arrhythmias and sustained improvements in ventricular contractile performance over an 8-week study (O'Quinn et al., 2011; Ongstad et al., 2013). Last, αCT1 promoted healing in diabetic foot ulcers and venous leg ulcers, two types of chronic and slow-healing skin wounds in phase 2 clinical testing (Ghatnekar et al., 2015; Grek et al., 2017; Grek et al., 2015). The peptide mimetic recently completed a phase 3 clinical trial for chronic skin wounds (Multicenter Study of the Efficacy and Safety of Granexin Gel in the Treatment of Diabetic Foot Ulcer [GAIT1]) (ClinicalTrials.gov). The αCT1 peptide also improved scar visual appearance by decreasing directionality of fibroblast movement and generated a 3D collagen matrix postwounding, similar to unwounded skin (Grek et al., 2017; Montgomery et al., 2021).

Therapeutic potential for αCT1 to treat alcoholic lung syndrome

The primary mechanism of action of αCT1 is to bind to ZO-1 and release it from intracellular Cx43, freeing ZO-1 to potentially associate with claudins and stabilize ZO-1 at the plasma membrane to prevent tight junction degradation in response to injury (Strauss et al., 2021). The resulting association stabilizes both gap junctions and tight junctions, which permits increased cellular communication, dampened inflammatory responses, reduced neutrophil infiltration, and reduced fibroblast proliferation. Given the therapeutical potential of αCT1 to improve microvascular dysfunction and edema, we wanted to test the therapeutic opportunity of the αCT1 peptide to treat alcohol-mediated lung dysfunction.

Role of Claudin 5 in alcoholic lung disease

It has been well established that claudin tight junction proteins are essential to the regulation of tight junction permeability (Gunzel & Fromm, 2012; Gunzel & Yu, 2013). In a model of alveolar epithelial cells derived from alcohol-fed rats, we have previously shown that alcohol decreases alveolar epithelial barrier function and is associated with a change in the composition of tight junction proteins (Schlingmann et al., 2016). Interestingly, in response to alcohol exposure, levels of claudin 4 protein decreased by nearly 6-fold, while levels of claudin 5 increased by over 3-fold. These data were consistent

with previous studies of freshly isolated type II cells and alveolar epithelial cells cultured on tissue culture plastic (Fernandez et al., 2007). Claudin 5 increased paracellular leak in a dose-dependent manner as measured by a decrease in transepithelial resistance and increases paracellular flux (Schlingmann et al., 2016; Wang et al., 2003). This effect was also reversable using both shRNA and an inhibitor, the claudin 5 mimetic peptide (C5).

Claudin 5 peptide mimetic (C5)

The DFYNP sequence is a short amino acid sequence found on the second extracellular loop (EL2) of claudins and is conserved on claudins 3, 4, 7, and 8. Treatment of mammary epithelial cells showed mis-localization of claudins 3 and 4 away from tight junctions in response to the linear DFYNP peptide, suggesting targeting this area on EL2 has the potential to disrupt endogenous claudin localization and activity (Baumgartner et al., 2011).

The DFYNP sequence is shared by several claudins that are present and contribute to lung barrier function, including claudins 3 and 4. The C5 peptide (Ac-EFYDP-NH_2) is specific to claudin 5 and has two amino acid substitutions as compared to the DFYNP sequence. C5 that has been used previously to target and disrupt claudin 5 activity (Schlingmann et al., 2016). While this sequence is specific to both claudin 1 and claudin 5, claudin 1 expression is unaffected by the peptide (Nasako et al., 2020; Schlingmann et al., 2016). In addition to being specific to claudin 5, the aspartic acid (D) residue of the original DFYNP peptide is not required from the peptide interaction with claudin proteins (Baumgartner et al., 2011). The EFYDP sequence found in the C5 peptide is unlikely to cross-react with other non-homologous claudins.

We have previously demonstrated that claudin 5 has significant deleterious effects on alveolar barrier function and that C5 increased barrier function in alcohol-exposed alveolar epithelial cells (Schlingmann et al., 2016). Therefore, claudin 5 represents a novel and potential pharmacologic target to restore alveolar barrier function and fluid clearance *in vivo* and prevent acute respiratory distress syndrome in the most vulnerable patients.

Materials and Methods

Mice

Experiments were performed in accordance with the National Institutes of Health Guidelines for the Use of Laboratory Animals guidelines and were approved by the Institutional Animal Care and Use Committee at Emory University School of Medicine. Isogenetic twelve-week-old male C57BL/6 wild-type mice were used for all experiments (Jackson Laboratory, Bar Harbor, ME). Animals were housed with a maximum of five animals per cage. All animals were kept under constant temperature at 21 °C and under 12 h light-dark cycle with ad libitum access to regular chow diet. In the alcohol group, ethanol was administered by increasing ethanol concentration from 0% to 20% in 5% increments over a two week period, and then mice were maintained at 20% ethanol for an additional 16 weeks. For instillation experiments, mice were anesthetized via IP injection of xylazine (10 mg/kg) and ketamine (100 mg/kg). Mice were suspended by their incisors on a rodent tilting work stand (Hallowell, Pittsfield, MA) for orotracheal instillation as previously described (Lawrenz et al., 2014). Mice were weighed while awake and prior to receiving a sedative for all weight measurements.

Lipopolysaccharide (LPS) administration

Alcohol- and water-fed mice were injected with 5 mg/kg E. coli 055:B5 LPS purchased from Sigma (L2637). Anesthetized mice received an intratracheal instillation (50 µl) of LPS. Results are reported as percent change in weight ± standard error of the mean.

Nebulized treatment with αCT1 or C5

To antagonize Cx43 interaction with ZO-1, a 25-amino acid peptide that contains a 16 amino acid antennapedia cell internalization sequence (RQPKIWFPNRRKPWKK) linked to the Cx43 CT amino acids 374-382 (RPRPDDLEI) that encompass the ZO-1 PDZ2 binding domain (Hunter et al., 2005). A control peptide for αCT1was generated by reversing the Cx43 amino acid sequence (IELDDPRPR). Both peptides were dissolved in PBS and diluted with PBS for nebulization.

To antagonize claudin 5, a short D-peptide (Ac-EFYDP-NH_2) analogous to the claudin-3/4 peptide

that was previously described (Baumgartner et al., 2011), synthesized by LifeTein (Sumerset, NJ), and named C5 (Schlingmann et al., 2016). A control peptide for C5 experiments was synthesized (Ac-LYQY-NH_2). Cysteine residues are added to both ends of the peptide to stabilize the peptide. D-amino acids were used to generate the C5 peptide as D-amino acids were found to be significantly more stable to proteolysis than the L-amino acid form in the DFYNP sequence (Baumgartner et al., 2011). Both C5 and control peptides were dissolved in 30% DMSO in water prior to dilution in PBS for nebulization.

One hour after mice received an intratracheal treatment of LPS, mice were randomly assigned to receive either the therapeutic drug or its corresponding peptide. αCT1 and its control peptide were nebulized in 1 mL of PBS for a final exposure dose of 5 mg/kg. C5 and its control peptide were nebulized in 1 mL of PBS for a final exposure of either 5 mg/kg or 50 mg/kg as indicated. Anesthetized mice were placed in a mouse restraining tube and peptide was nebulized over room air to deliver the full 1 mL in 10 minutes (AeronebLab Aerogen, Galway, Ireland). Mice were allowed to fully recover and wake on a heating pad before returning for overnight observation.

Lung permeability as measured by Evans Blue extravasation

Approximately 24 h after nebulization with a therapeutic peptide or its control, mice were re-weighed and anesthetized for an Evans Blue permeability assay. Mice were placed on a heating pad and the tail was sterilized with an alcohol wipe. 200 µl of 0.5% Evans Blue in PBS was injected into the tail vein with a 30-gauge needle. The mice were allowed to recover on a heating pad for 1 h and then sacrificed while still under anesthesia. 250 µl of blood was collected by cardiac puncture and centrifuged at 1500 × g for 15 min to collect serum. Bronchoalveolar lung lavage (BAL) fluid was collected by flushing the lungs twice via a tracheal tube with 500 µl of ice-cold PBS with protease inhibitors and centrifuged at 1500 x g for 15 minutes to collect cell-free BAL fluid.

Evans Blue in the serum and BAL fluid was analyzed by spectrophotometry (620 nm) (Radu & Chernoff, 2013). Evans Blue readings were corrected for contaminating heme analyzing samples at 740 nm and using the correction factor $y = 1.193x + 0.007$ as previously described (Moitra et al., 2007) and

reported as Evans Blue in the BAL and/or normalized to corresponding serum Evans Blue levels.

Immunoblot of Claudin 5 and Actin

Lung tissue was snap-frozen in liquid nitrogen at the time of sacrifice. Tissue was later weighed, thawed on ice, and added to 5 ml/mg tissue of lysis buffer (50 mM Tris HCl; 10 mM EDTA; 100 mM NaCl; 0.5% Triton X-100) with protease inhibitors, homogenized with a Dounce homogenizer, incubated for 30 min on ice, and sonicated 4 × 3 s. Homogenates were centrifuged at 10,000 × g for 10 min. Supernatants were collected, and total protein concentration was assessed using the Pierce BCA Protein Assay kit (ThermoFisher Scientific). Protein was diluted with 6x Laemlli buffer with DTT and heated for 10 min at 60 °C. Protein was separated via electrophoresis on a 4–20% SDS-PAGE stain-free gel (BioRad, Hercules, CA) and transferred to a PVDF membrane using the Transblot Turbo (BioRad) at 25V for 7 min. Membranes were blocked in Odyssey Blocking Buffer (LI-COR, Lincoln, NE) for 1 h at RT. Membranes were then incubated overnight with 1:250 dilution mouse anti-claudin 5 (Thermo-Fisher, 35-2500) or 1:10,000 dilution rabbit anti-beta actin (Millipore Sigma, A2103) as a loading control. Membranes were washed in TBS + 0.5% Triton X-100. The blots were incubated for one hour with 1:10,000 dilution goat anti-rabbit IgG IRDye 680RD (LI-COR, 925-68071) and 1:10,000 Goat anti-mouse IgG IRDye 800CW (LI-COR, 926-32210) and then imaged and quantified using an Odyssey Classic imager (LI-COR) and band densitometry normalized to actin using Fiji.

Statistical Analysis

Comparisons between two groups was performed by unpaired, two-tailed t-test while comparisons between multiple groups were performed by one-way ANOVA with Tukey's multiple comparisons test using GraphPad Prism software. Data are represented as mean ± standard error of the mean and the statistical significance level was set at 0.05.

Results

Claudin 5 expression is increased after chronic exposure to alcohol

Alcohol was previously shown to upregulate claudin 5 expression in alveolar epithelial cells derived from alcohol-fed rats (Schlingmann et al., 2016). To determine alcohol had the same effect in mice and establish the murine model for additional therapeutic models for alcoholic lung disease, expression of claudin 5 was measured by immunoblot from whole lungs derived from alcohol-fed or water-fed control mice (Figure 5.1). Relative protein expression of claudin 5 levels was increased by over 60 % (1.665 ± .1301, n = 12) in alcohol-fed mice relative to control (1 ± .1301, n = 13). While this finding was conducted in whole lungs, the effect of alcohol on claudin 5 is likely to be significantly greater if the alveolar epithelial cells were isolated from the non-epithelial tissue in this model. It is likely the magnitude of the effect was dampened given the steady state high expression of claudin 5 in endothelial cells (Kaarteenaho et al., 2010; Kakogiannos et al., 2020).

C5 peptide did not impact total blood volume

We have previously demonstrated the restorative properties of the C5 peptide on alveolar barrier function in alcohol-exposed primary alveolar epithelial cells (Schlingmann et al., 2016). Since dietary alcohol increased levels of claudin 5 protein *in vivo* (Figure 5.1) and caused alveolar barrier dysfunction (Smith et al., 2019), I performed an Evans Blue permeability assay to test if C5 had therapeutical potential to reverse alcohol-induced barrier dysfunction. Wild-type C57BL/6 mice consumed 20% ethanol for 16 weeks with *ad labitum* access to normal lab chow and were compared to age-matched, littermate water-fed control mice. All mice received an instillation treatment of LPS and were subsequently exposed 1 hour later to either a control peptide or C5 at 5 mg/kg (Figure 5.2A) or 50 mg/kg (Figure 5.2B) via nebulization for 10 minutes. An Evans Blue permeability assay was conducted 24 h later by tail vein injection while anesthetized (Smith et al., 2019, 2021). All four groups of mice had similar concentrations of Evans Blue dye in their serum, suggesting C5 does not have an acute effect on blood volume.

C5 peptide did not improve alcohol-induced alveolar leak

We have previously demonstrated that the Evans Blue permeability assay can be used to measure alveolar epithelial permeability *in vivo* (Smith et al., 2019). To determine if C5 was able to mitigate the

effect of alcohol-induced epithelial barrier dysregulation after a direct LPS injury, I conducted an Evans Blue permeability assay on water-fed or alcohol-fed mice that received an intratracheal treatment of LPS followed by either nebulized C5 (5 mg/kg) or control peptide. Evans Blue levels were measured in the BAL (Figure 5.3A) and were normalized to Evans Blue serum levels to normalize input (Figure 5.3B). The experiment was repeated at a higher concentration of C5, 50 mg/kg, and produced similar results (Figure 5.4). Evans Blue was higher in alcohol-fed mice relative to water control in both control peptide and C5 peptide groups, at both concentrations, although this was not statistically significant likely due to low sample size. A predictive power analysis recommends 8-10 mice per experimental group based on previous data (Smith et al., 2019). It is possible that the C5 peptide was too hydrophilic to penetrate the surfactant layer that covers the apical surface of the alveoli.

αCT1 does not impact weight loss or total blood volume

We have previously shown that lipopolysaccharide (LPS) administered by intratracheal instillation resulted in a reduced body weight of 5-10%, which is consistent with previous studies that measured the effects of LPS on body weight (Smith et al., 2019; Wang et al., 2016). This weight loss was attributed to the bacterial endotoxin inducing a protective sickness response behavior, inflammation-induced anorexia, that causes a loss of appetite and reduce food intake (Konsman et al., 2002; van Niekerk et al., 2016). To evaluate the systemic effect of αCT1 on inflammation-induced weight loss, wild-type C57BL/6 mice consumed 20% ethanol for 16 weeks with *ad labitum* access to normal lab chow and were compared to age-matched, littermate water-fed control mice. All mice received an instillation treatment of LPS and were subsequently exposed 1 hour later to either 5mg/kg αCT1 or a control peptide via nebulization for 10 minutes. All four groups of mice lost approximately 5 – 10% of their original pre-weight (Figure 5.5). There was no difference in weight loss between control peptide and αCT1 in either water-fed or alcohol-fed mice, although αCT1-treated alcohol-fed mice lost less weight than control peptide-treated water-fed mice. Taken together, αCT1 does not seem to have systemic effect on inflammation-induced weight loss.

Evans Blue dye has long been used in biomedicine to estimate blood volume and vascular

permeability (Evans & Schulemann, 1914; Lawrence & Walters, 1959; Persson & Ullberg, 1979; Radu & Chernoff, 2013; Yao et al., 2018). In order to measure if αCT1 affected total mouse blood volume, water-fed or alcohol-fed were given an intratracheal instillation of LPS followed by either αCT1 or control peptide nebulization. Approximately 24 h after peptide treatment, mice were administered Evans Blue dye by tail vein injection while anesthetized to conduct an Evans Blue permeability assay as previously described (Smith et al., 2019). Blood was collected 1 h later and it was found that all four groups of mice had similar concentrations of Evans Blue dye in their serum (Figure 5.6). This suggests that αCT1 does not have an acute effect on total blood volume.

αCT1 improved alcohol-induced alveolar leak

We have previously demonstrated that the Evans Blue permeability assay can be used to measure alveolar lung vessel and epithelial permeability *in vivo* (Smith et al., 2019, 2021). We have shown that a direct, intratracheal injury with either saline or LPS increases lung permeability and disrupts the alveolar epithelial barrier in alcohol-fed mice as measured by Evans Blue present in the recovered bronchoalveolar lavage (BAL) fluid (Smith et al., 2019). As previously discussed, αCT1 has significant therapeutic potential to improve both epithelial and endothelial barrier function. We wanted to determine if αCT1 was able to mitigate the effect of alcohol-induced epithelial barrier dysregulation after a direct LPS injury as measured by an Evans Blue permeability assay. In this study, water-fed or alcohol-fed mice received an intratracheal treatment of LPS followed by either nebulized αCT1 or control peptide and then an Evans Blue tail vein injection 24 h later. Evans Blue levels were measured in the BAL (Figure 5.7A) and were normalized to Evans Blue serum levels to normalize input (Figure 5.7B).

Not surprisingly, alcohol-fed mice had a 2-fold increase in Evans Blue relative to water-fed mice when both groups were nebulized with the control peptide (Figure 5.7B). This is consistent with our previous findings of the negative effect of alcohol on lung barrier function (Schlingmann et al., 2016; Smith et al., 2019). Interestingly, αCT1 reduced the amount of alveolar leak, as measured by Evans Blue, by over 80% in alcohol-fed mice, restoring the levels to near baseline levels. The αCT1 peptide had no

effect on water-fed mice which was expected as these mice had an intact, functional barrier despite exposure to LPS.

Discussion

In the present study, two therapeutic peptides were evaluated to mitigate alcohol-mediated barrier dysfunction following a 'second-hit' endotoxin injury. Both peptides target the Claudin-18/ZO-1/actin cytoskeletal association and interaction to restore normal paracellular permeability. The C5 peptide targets and disrupts the second extracellular loop of claudin 5 and inhibits heterotypic cis-interactions of claudin 5 with claudin 18. The αCT1 peptide targeting the C-terminus of Cx43 and inhibits ZO-1/Cx43 interaction and stabilizes the ZO-1 structure to more freely associate with claudin 18 by inhibiting connexin-claudin steric hindrance at the ZO-1 PDZ binding domains. Here, C5 did not reverse the alveolar leak in alcohol-fed mice at the two tested concentrations, 5 mg/kg and 50 mg/kg. However, the αCT1 peptide showed therapeutic value in alcohol-fed mice by improving alveolar barrier leak as measured by an Evans Blue permeability assay.

The composition and dynamics of tight junction proteins found in the apical junctional complex play a large role in mediating paracellular flux of solutes and ions. Evidence suggests that the claudin family of proteins are the major determinants of paracellular permeability (Gunzel & Yu, 2013). The specific composition of claudins located in the tight junctions largely determines their permeability properties (Schneeberger & Lynch, 2004). Claudin 5 is normally lowly expressed in alveolar epithelial cells but is upregulated in response to dietary alcohol (Schlingmann et al., 2016). Additionally, claudin 5 was shown to be both necessary and sufficient to diminish alveolar barrier dysfunction in alcohol-exposed alveolar epithelial cells (Schlingmann et al., 2016). Here, we found that dietary alcohol significantly increased the expression of claudin in total lung lysates of mice (Figure 5.1). Claudin 5 is expressed ubiquitously in endothelial tight junctions, including the pulmonary microvasculature (Chen et al., 2014; Morita et al., 1999; Zhou et al., 2018). Therefore, it is likely the endogenous levels of claudin 5 in the pulmonary microvasculature of both water-fed and alcohol-fed dampened the measurable impact of alcohol and relative increase of claudin 5 in the pulmonary epithelia. To determine the effect of alcohol on epithelial tight junctions in the lung, type I and type II pneumocytes should be isolated and examined

for claudin 5 protein levels following chronic alcohol exposure (Chen et al., 2004; Sinha & Lowell, 2016).

The C5 peptide has been used previously to restore alcohol-mediated barrier dysfunction *in vitro* by increasing transepithelial resistance and decreasing flux of calcein and Texas Red dextran across the alveolar epithelial monolayer in cells derived from alcohol-fed rats (Schlingmann et al., 2016). Here, we used an Evans Blue permeability assay to measure barrier function in alcohol-fed mice. Interestingly, the C5 peptide delivered via nebulization 1 hr following LPS treatment did not rescue the effects of alcohol at either of the tested concentrations (Figure 5.3, Figure 5.4). Future work should focus on optimizing C5 delivery parameters, including peptide concentration and delivery method and time following acute lung injury. Additionally, the five amino acid peptide may need to include a hydrophobic segment to permit penetration of the hydrophobic surfactant proteins that line the apical surface of the epithelial cells (Wustneck et al., 2005).

We also tested αCT1 peptide to restore paracellular permeability following chronic alcohol treatment. αCT1 co-localizes with ZO-1 and upregulated cell-cell border localization of ZO-1 in cultured endothelial cells (Strauss et al., 2021). The αCT1 peptide has previously been extensively used in tissue for various novel therapeutic purposes in the fields of tissue engineering and regenerative medicine (Ghatnekar et al., 2015; Grek et al., 2017; Grek et al., 2015; Jiang et al., 2019; Montgomery et al., 2021; O'Quinn et al., 2011; Obert et al., 2017; Ongstad et al., 2013; Soder et al., 2009). Here, we determined that nebulized αCT1 treatment following intratracheal endotoxin injury rescued alcohol-mediated barrier dysfunction by decreasing the extravasation of Evans Blue into the alveolar air space. There was no difference in weight or serum concentration of Evans Blue dye following nebulized treatment of αCT1, suggesting little to no systemic side effects on systemic vascular permeability. These data suggest αCT1 has significant potential therapeutic value in the prevention and treatment of pathologic increases in alveolar epithelial permeability, such as with pulmonary edema.

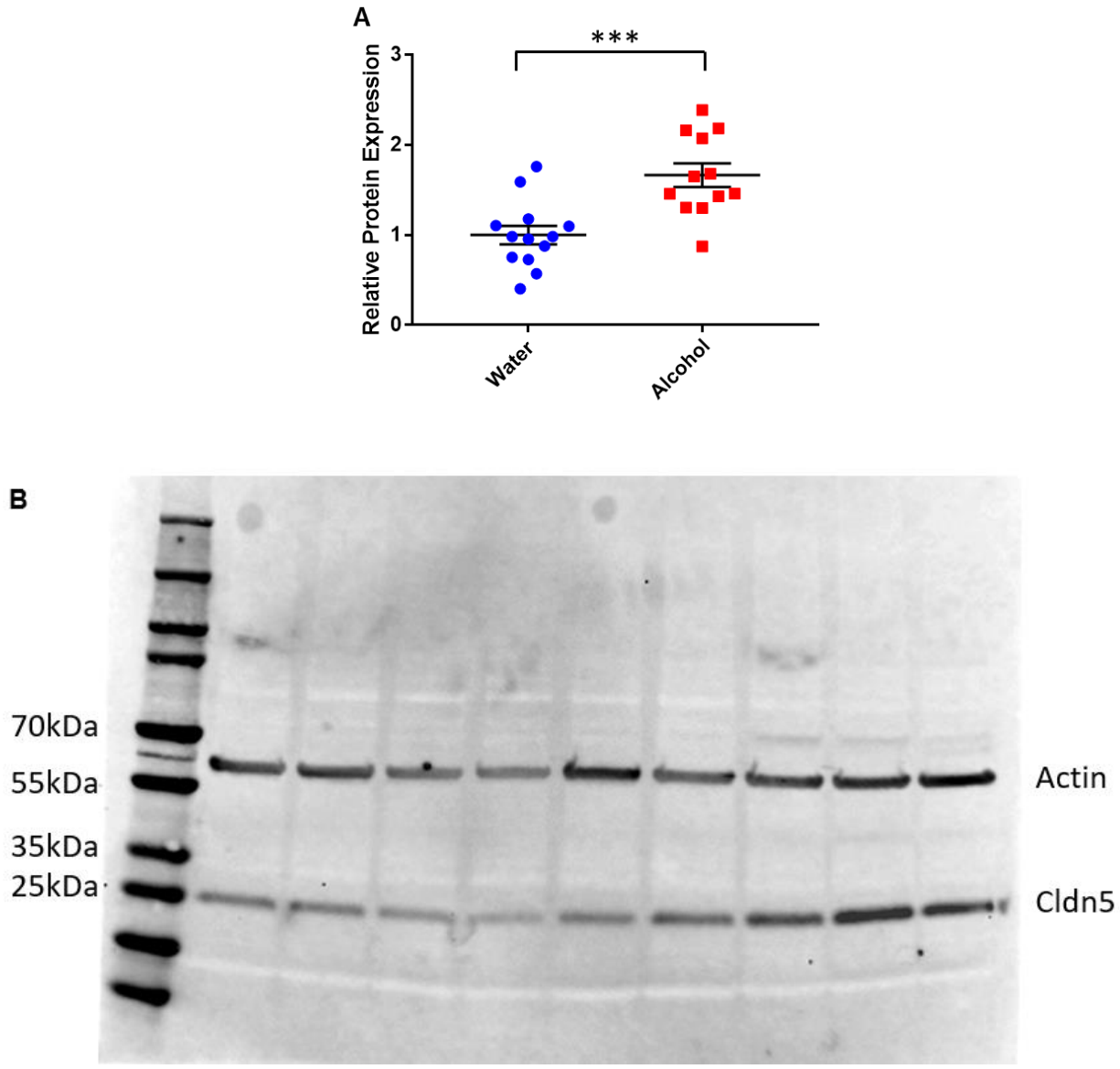

Figure 5.1. Dietary alcohol increases the expression of claudin 5.

Lungs from alcohol-fed or water-fed mice were collected and processed for protein extraction. (A) Claudin 5 (Cldn5) was measured by immunoblot and normalized to actin. (B) A representative immunoblot. n = 12-13. ***p = 0.0005. Values reported as mean ± standard error of the mean.

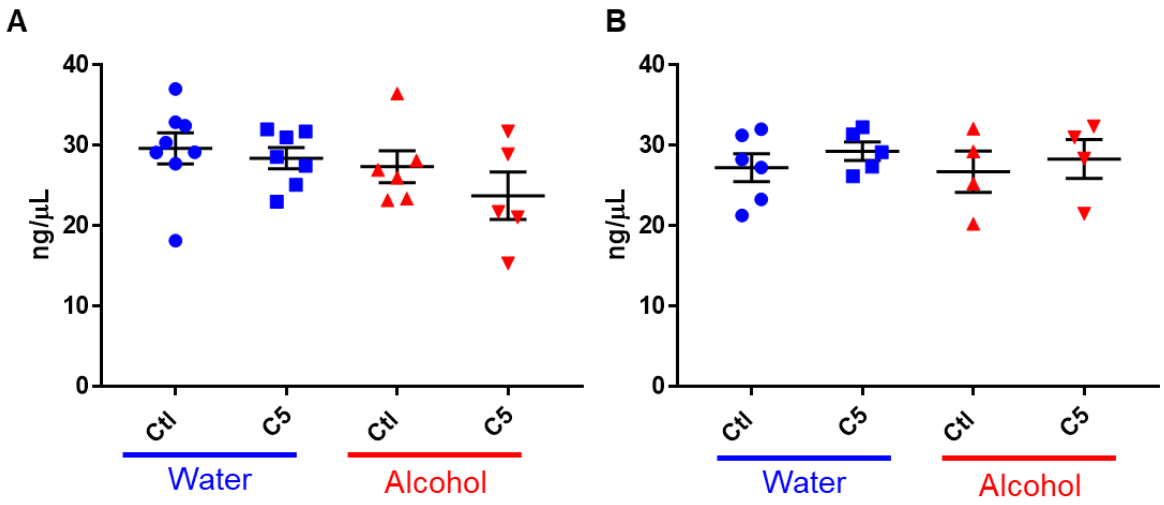

Figure 5.2. No difference in serum concentration of Evans Blue dye with C5 treatment.

Mice received an IT treatment of LPS at 5mg/kg. After 1 h, mice were nebulized with control or C5 peptide at 5 mg/kg (A) or 50 mg/kg (B) for 10 mins. 24 h later the mice were administered Evans Blue by tail vein injection while anesthetized and allowed to recover for 1 h before blood was collected. Results were corrected for the presence of heme. There was no difference in Evans Blue serum levels between control peptide and C5 in either water-fed or alcohol-fed mice. n = 4-8. Values reported as mean ± standard error of the mean.

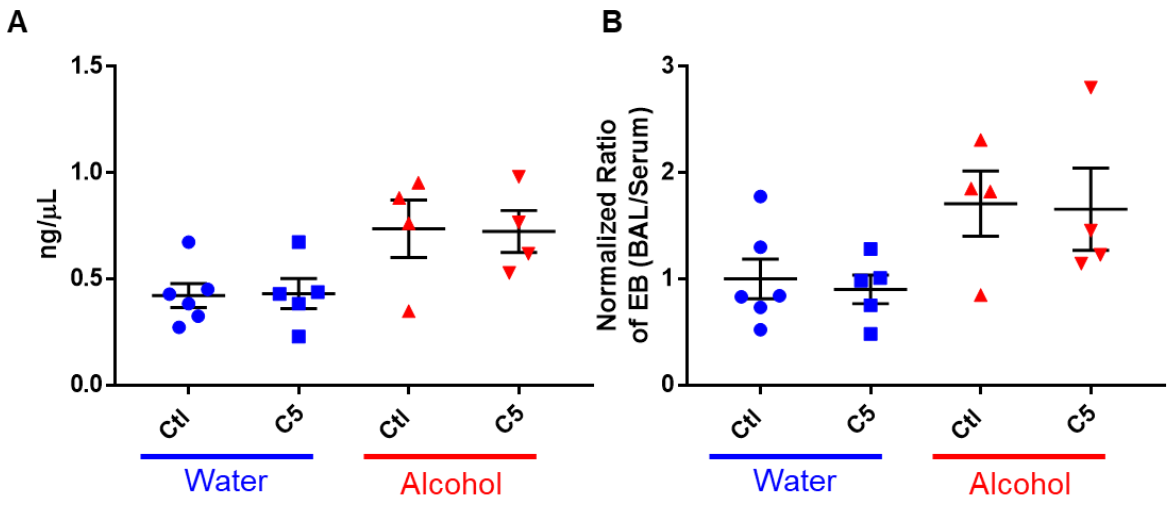

Figure 5.3. C5 (5 mg/kg) did not reverse alveolar leak of Evans Blue dye in alcohol-fed mice.

Mice received an IT treatment of LPS at 5 mg/kg. After 1 h, mice were nebulized with control or C5 peptide at 5 mg/kg for 10 mins. 24 h later the mice were administered Evans Blue by tail vein injection while anesthetized and allowed to recover for 1 h before BAL and blood were collected. Results were corrected for the presence of heme and are represented as BAL (A) or BAL normalized to Evans Blue serum levels (B). n = 5-8. Values reported as mean ± standard error of the mean.

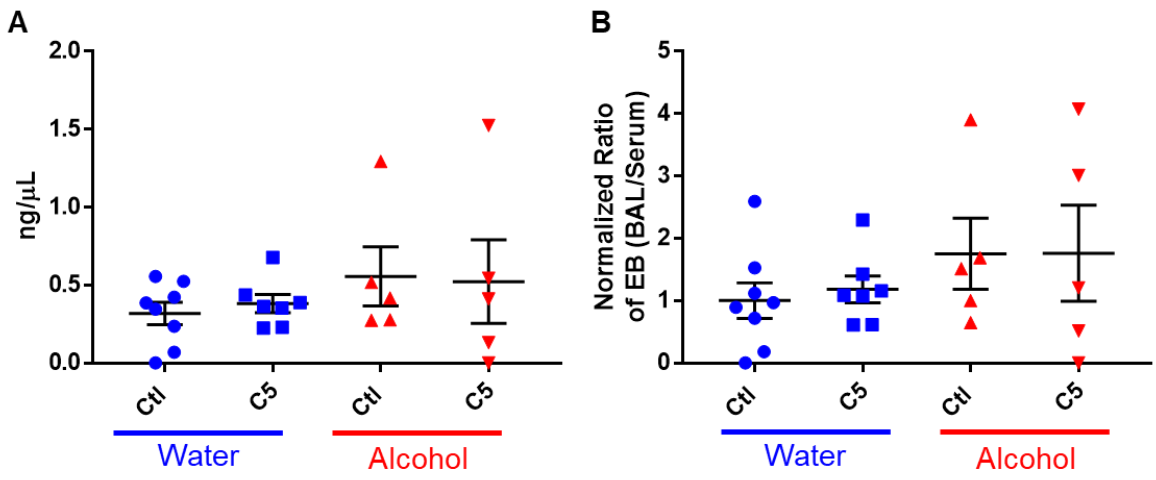

Figure 5.4. C5 (50 mg/kg) did not reverse alveolar leak of Evans Blue dye in alcohol-fed mice.

Mice received an IT treatment of LPS at 5 mg/kg. After 1 h, mice were nebulized with control or C5 peptide at 50 mg/kg for 10 mins. 24 h later the mice were administered Evans Blue by tail vein injection while anesthetized and allowed to recover for 1 h before BAL and blood were collected. Results were corrected for the presence of heme and are represented as BAL (A) or BAL normalized to Evans Blue serum levels (B). n = 4-6. Values reported as mean ± standard error of the mean.

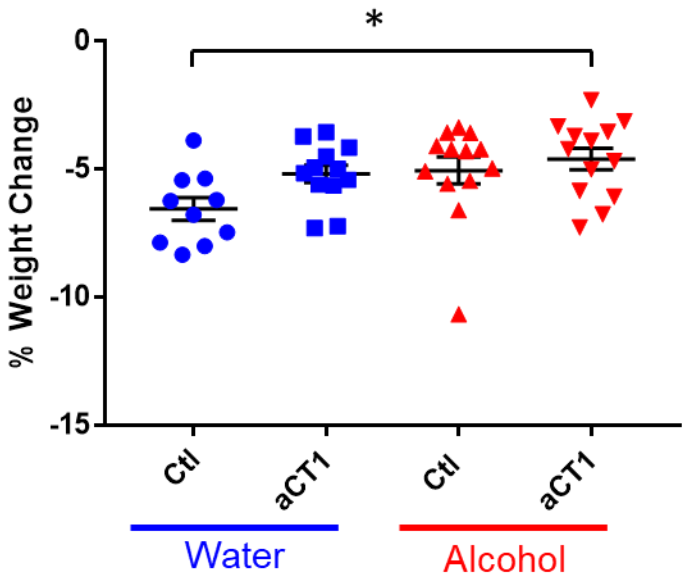

Figure 5.5. αCT1 has no significant impact on intratracheal lipopolysaccharide-mediated weight loss.

Mice were weighed (pre-weight) and then received an IT treatment of LPS at 5mg/kg. Control peptide or αCT1 was nebulized 1 h later at 5mg/kg for 10 mins. Mice were re-weighed 24 h later (post-weight). Data represent % weight change from pre-weight. There was no difference in weight loss between control peptide and αCT1 in either water-fed or alcohol-fed mice. n = 10-13, *p = 0.022. Values reported as mean ± standard error of the mean.

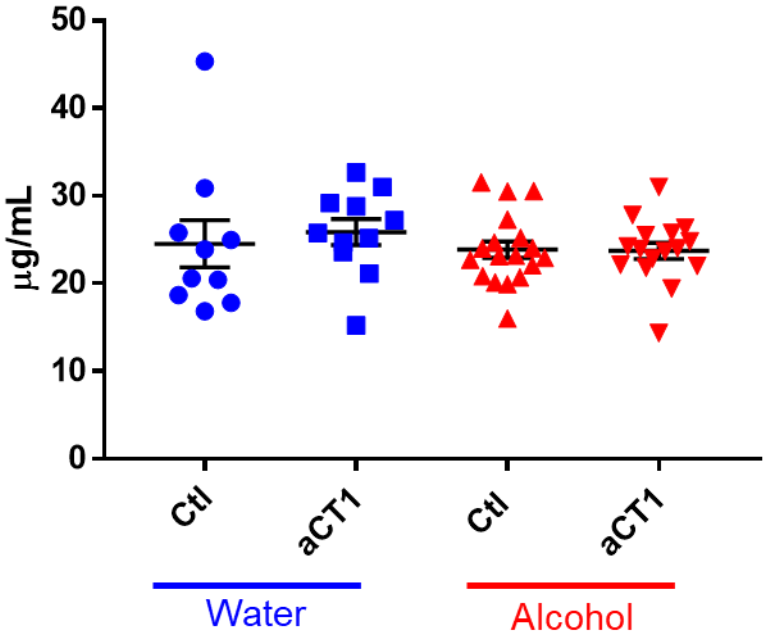

Figure 5.6. No difference in serum concentration of Evans Blue dye with αCT1 treatment.

Mice received an IT treatment of LPS at 5mg/kg. After 1 h, mice were nebulized with control or αCT1 peptide at 5mg/kg for 10 mins. 24 h later the mice were administered Evans Blue by tail vein injection while anesthetized and allowed to recover for 1 h before blood was collected. Results were corrected for the presence of heme. There was no difference in Evans Blue serum levels between control peptide and αCT1 in either water-fed or alcohol-fed mice. n = 10-18. Values reported as mean ± standard error of the mean.

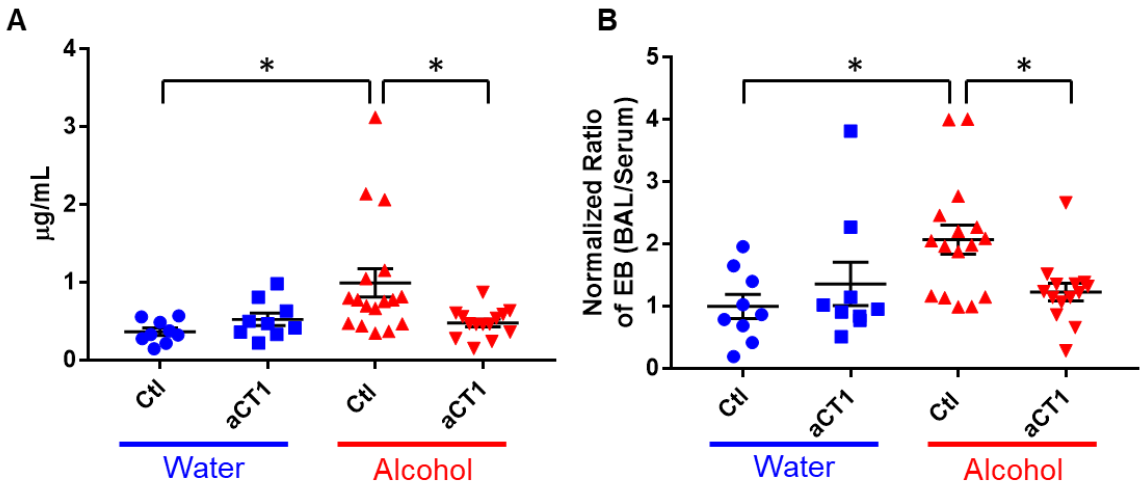

Figure 5.7. αCT1 reverses alveolar leak of Evans Blue dye in alcohol-fed mice.

Mice received an IT treatment of LPS at 5mg/kg. After 1 h, mice were nebulized with control or αCT1 peptide at 5mg/kg for 10 mins. 24 h later the mice were administered Evans Blue by tail vein injection while anesthetized and allowed to recover for 1 h before BAL and blood were collected. Results were corrected for the presence of heme and are represented as BAL (A) or BAL normalized to Evans Blue serum levels (B). Alcohol-fed mice had increased alveolar leak compared to water-fed mice, and this increase was reversed to baseline levels after treatment with αCT1. n = 9-17. *$p < 0.05$. Values reported as mean ± standard error of the mean.

Literature Cited

Aasen, T., Leithe, E., Graham, S. V., Kameritsch, P., Mayan, M. D., Mesnil, M., Pogoda, K., & Tabernero, A. (2019). Connexins in cancer: bridging the gap to the clinic. *Oncogene*, *38*(23), 4429-4451. https://doi.org/10.1038/s41388-019-0741-6

Ambrosi, C., Ren, C., Spagnol, G., Cavin, G., Cone, A., Grintsevich, E. E., Sosinsky, G. E., & Sorgen, P. L. (2016). Connexin43 Forms Supramolecular Complexes through Non-Overlapping Binding Sites for Drebrin, Tubulin, and ZO-1. *PLoS One*, *11*(6), e0157073. https://doi.org/10.1371/journal.pone.0157073

Axelsen, L. N., Calloe, K., Holstein-Rathlou, N. H., & Nielsen, M. S. (2013). Managing the complexity of communication: regulation of gap junctions by post-translational modification. *Front Pharmacol*, *4*, 130. https://doi.org/10.3389/fphar.2013.00130

Baumgartner, H. K., Beeman, N., Hodges, R. S., & Neville, M. C. (2011). A D-peptide analog of the second extracellular loop of claudin-3 and -4 leads to mislocalized claudin and cellular apoptosis in mammary epithelial cells. *Chem Biol Drug Des*, *77*(2), 124-136. https://doi.org/10.1111/j.1747-0285.2010.01061.x

Belardi, B., Hamkins-Indik, T., Harris, A. R., Kim, J., Xu, K., & Fletcher, D. A. (2020). A Weak Link with Actin Organizes Tight Junctions to Control Epithelial Permeability. *Dev Cell*, *54*(6), 792-804 e797. https://doi.org/10.1016/j.devcel.2020.07.022

Bruce, A. F., Rothery, S., Dupont, E., & Severs, N. J. (2008). Gap junction remodelling in human heart failure is associated with increased interaction of connexin43 with ZO-1. *Cardiovasc Res*, *77*(4), 757-765. https://doi.org/10.1093/cvr/cvm083

Chen, J., Chen, Z., Narasaraju, T., Jin, N., & Liu, L. (2004). Isolation of highly pure alveolar epithelial type I and type II cells from rat lungs. *Lab Invest*, *84*(6), 727-735. https://doi.org/10.1038/labinvest.3700095

Chen, J., Pan, L., Wei, Z., Zhao, Y., & Zhang, M. (2008). Domain-swapped dimerization of ZO-1 PDZ2 generates specific and regulatory connexin43-binding sites. *EMBO J*, *27*(15), 2113-2123. https://doi.org/10.1038/emboj.2008.138

Chen, W., Sharma, R., Rizzo, A. N., Siegler, J. H., Garcia, J. G., & Jacobson, J. R. (2014). Role of claudin-5 in the attenuation of murine acute lung injury by simvastatin. *Am J Respir Cell Mol Biol*, *50*(2), 328-336. https://doi.org/10.1165/rcmb.2013-0058OC

ClinicalTrials.gov. (May 29, 2020). *A study of granexin (aCT1) gel in the treatment of diabetic foot ulcer*. Retrieved February 8, 2022 from https://clinicaltrials.gov/ct2/show/NCT02667327

Dunn, C. A., & Lampe, P. D. (2014). Injury-triggered Akt phosphorylation of Cx43: a ZO-1-driven molecular switch that regulates gap junction size. *J Cell Sci*, *127*(Pt 2), 455-464. https://doi.org/10.1242/jcs.142497

Ek-Vitorin, J. F., King, T. J., Heyman, N. S., Lampe, P. D., & Burt, J. M. (2006). Selectivity of connexin 43 channels is regulated through protein kinase C-dependent phosphorylation. *Circ Res*, *98*(12), 1498-1505. https://doi.org/10.1161/01.RES.0000227572.45891.2c

Evans, H. M., & Schulemann, W. (1914). The Action of Vital Stains Belonging to the Benzidine Group. *Science*, *39*(1004), 443-454. https://doi.org/10.1126/science.39.1004.443

Fanning, A. S., & Anderson, J. M. (2009). Zonula occludens-1 and -2 are cytosolic scaffolds that regulate the assembly of cellular junctions. *Ann N Y Acad Sci*, *1165*, 113-120. https://doi.org/10.1111/j.1749-6632.2009.04440.x

Fernandez, A. L., Koval, M., Fan, X., & Guidot, D. M. (2007). Chronic alcohol ingestion alters claudin expression in the alveolar epithelium of rats. *Alcohol*, *41*(5), 371-379. https://doi.org/10.1016/j.alcohol.2007.04.010

Francis, R., Xu, X., Park, H., Wei, C. J., Chang, S., Chatterjee, B., & Lo, C. (2011). Connexin43 modulates cell polarity and directional cell migration by regulating microtubule dynamics. *PLoS One*, *6*(10), e26379. https://doi.org/10.1371/journal.pone.0026379

Garcia, J. G. (2009). Concepts in microvascular endothelial barrier regulation in health and disease.

Microvasc Res, *77*(1), 1-3. https://doi.org/10.1016/j.mvr.2009.01.001

Ghatnekar, G. S., Grek, C. L., Armstrong, D. G., Desai, S. C., & Gourdie, R. G. (2015). The effect of a connexin43-based Peptide on the healing of chronic venous leg ulcers: a multicenter, randomized trial. *J Invest Dermatol*, *135*(1), 289-298. https://doi.org/10.1038/jid.2014.318

Giepmans, B. N. (2004). Gap junctions and connexin-interacting proteins. *Cardiovasc Res*, *62*(2), 233-245. https://doi.org/10.1016/j.cardiores.2003.12.009

Giepmans, B. N., & Moolenaar, W. H. (1998). The gap junction protein connexin43 interacts with the second PDZ domain of the zona occludens-1 protein. *Curr Biol*, *8*(16), 931-934. https://doi.org/10.1016/s0960-9822(07)00375-2

Giepmans, B. N., Verlaan, I., & Moolenaar, W. H. (2001). Connexin-43 interactions with ZO-1 and alpha- and beta-tubulin. *Cell Commun Adhes*, *8*(4-6), 219-223. https://doi.org/10.3109/15419060109080727

Grek, C. L., Montgomery, J., Sharma, M., Ravi, A., Rajkumar, J. S., Moyer, K. E., Gourdie, R. G., & Ghatnekar, G. S. (2017). A Multicenter Randomized Controlled Trial Evaluating a Cx43-Mimetic Peptide in Cutaneous Scarring. *J Invest Dermatol*, *137*(3), 620-630. https://doi.org/10.1016/j.jid.2016.11.006

Grek, C. L., Prasad, G. M., Viswanathan, V., Armstrong, D. G., Gourdie, R. G., & Ghatnekar, G. S. (2015). Topical administration of a connexin43-based peptide augments healing of chronic neuropathic diabetic foot ulcers: A multicenter, randomized trial. *Wound Repair Regen*, *23*(2), 203-212. https://doi.org/10.1111/wrr.12275

Gunzel, D., & Fromm, M. (2012). Claudins and other tight junction proteins. *Compr Physiol*, *2*(3), 1819-1852. https://doi.org/10.1002/cphy.c110045

Gunzel, D., & Yu, A. S. (2013). Claudins and the modulation of tight junction permeability. *Physiol Rev*, *93*(2), 525-569. https://doi.org/10.1152/physrev.00019.2012

Haas, A. J., Zihni, C., Ruppel, A., Hartmann, C., Ebnet, K., Tada, M., Balda, M. S., & Matter, K. (2020). Interplay between Extracellular Matrix Stiffness and JAM-A Regulates Mechanical Load on ZO-

1 and Tight Junction Assembly. *Cell Rep*, *32*(3), 107924. https://doi.org/10.1016/j.celrep.2020.107924

Herve, J. C., Bourmeyster, N., Sarrouilhe, D., & Duffy, H. S. (2007). Gap junctional complexes: from partners to functions. *Prog Biophys Mol Biol*, *94*(1-2), 29-65. https://doi.org/10.1016/j.pbiomolbio.2007.03.010

Hunter, A. W., Barker, R. J., Zhu, C., & Gourdie, R. G. (2005). Zonula occludens-1 alters connexin43 gap junction size and organization by influencing channel accretion. *Mol Biol Cell*, *16*(12), 5686-5698. https://doi.org/10.1091/mbc.e05-08-0737

Jiang, J., Hoagland, D., Palatinus, J. A., He, H., Iyyathurai, J., Jourdan, L. J., Bultynck, G., Wang, Z., Zhang, Z., Schey, K., Poelzing, S., McGowan, F. X., & Gourdie, R. G. (2019). Interaction of alpha Carboxyl Terminus 1 Peptide With the Connexin 43 Carboxyl Terminus Preserves Left Ventricular Function After Ischemia-Reperfusion Injury. *J Am Heart Assoc*, *8*(16), e012385. https://doi.org/10.1161/JAHA.119.012385

Kaarteenaho, R., Merikallio, H., Lehtonen, S., Harju, T., & Soini, Y. (2010). Divergent expression of claudin -1, -3, -4, -5 and -7 in developing human lung. *Respir Res*, *11*, 59. https://doi.org/10.1186/1465-9921-11-59

Kakogiannos, N., Ferrari, L., Giampietro, C., Scalise, A. A., Maderna, C., Rava, M., Taddei, A., Lampugnani, M. G., Pisati, F., Malinverno, M., Martini, E., Costa, I., Lupia, M., Cavallaro, U., Beznoussenko, G. V., Mironov, A. A., Fernandes, B., Rudini, N., Dejana, E., & Giannotta, M. (2020). JAM-A Acts via C/EBP-alpha to Promote Claudin-5 Expression and Enhance Endothelial Barrier Function. *Circ Res*, *127*(8), 1056-1073. https://doi.org/10.1161/CIRCRESAHA.120.316742

Kameritsch, P., Pogoda, K., & Pohl, U. (2012). Channel-independent influence of connexin 43 on cell migration. *Biochim Biophys Acta*, *1818*(8), 1993-2001. https://doi.org/10.1016/j.bbamem.2011.11.016

Konsman, J. P., Parnet, P., & Dantzer, R. (2002). Cytokine-induced sickness behaviour: mechanisms and

implications. *Trends Neurosci*, *25*(3), 154-159. https://doi.org/10.1016/s0166-2236(00)02088-9

Laird, D. W. (2006). Life cycle of connexins in health and disease. *Biochem J*, *394*(Pt 3), 527-543. https://doi.org/10.1042/BJ20051922

Lawrence, A. C., & Walters, G. (1959). The extraction of Evans blue (T1824) from plasma and the measurement of plasma volume. *J Clin Pathol*, *12*(2), 123-127. https://doi.org/10.1136/jcp.12.2.123

Lawrenz, M. B., Fodah, R. A., Gutierrez, M. G., & Warawa, J. (2014). Intubation-mediated intratracheal (IMIT) instillation: a noninvasive, lung-specific delivery system. *J Vis Exp*(93), e52261. https://doi.org/10.3791/52261

Leithe, E., Mesnil, M., & Aasen, T. (2018). The connexin 43 C-terminus: A tail of many tales. *Biochim Biophys Acta Biomembr*, *1860*(1), 48-64. https://doi.org/10.1016/j.bbamem.2017.05.008

Maass, K., Ghanem, A., Kim, J. S., Saathoff, M., Urschel, S., Kirfel, G., Grummer, R., Kretz, M., Lewalter, T., Tiemann, K., Winterhager, E., Herzog, V., & Willecke, K. (2004). Defective epidermal barrier in neonatal mice lacking the C-terminal region of connexin43. *Mol Biol Cell*, *15*(10), 4597-4608. https://doi.org/10.1091/mbc.e04-04-0324

Matsuuchi, L., & Naus, C. C. (2013). Gap junction proteins on the move: connexins, the cytoskeleton and migration. *Biochim Biophys Acta*, *1828*(1), 94-108. https://doi.org/10.1016/j.bbamem.2012.05.014

Moitra, J., Sammani, S., & Garcia, J. G. (2007). Re-evaluation of Evans Blue dye as a marker of albumin clearance in murine models of acute lung injury. *Transl Res*, *150*(4), 253-265. https://doi.org/10.1016/j.trsl.2007.03.013

Montgomery, J., Richardson, W. J., Marsh, S., Rhett, J. M., Bustos, F., Degen, K., Ghatnekar, G. S., Grek, C. L., Jourdan, L. J., Holmes, J. W., & Gourdie, R. G. (2021). The connexin 43 carboxyl terminal mimetic peptide alphaCT1 prompts differentiation of a collagen scar matrix in humans resembling unwounded skin. *FASEB J*, *35*(8), e21762. https://doi.org/10.1096/fj.202001881R

Morita, K., Sasaki, H., Furuse, M., & Tsukita, S. (1999). Endothelial claudin: claudin-5/TMVCF

constitutes tight junction strands in endothelial cells. *J Cell Biol*, *147*(1), 185-194. https://doi.org/10.1083/jcb.147.1.185

Nasako, H., Takashina, Y., Eguchi, H., Ito, A., Ishikawa, Y., Matsunaga, T., Endo, S., & Ikari, A. (2020). Increase in Toxicity of Anticancer Drugs by PMTPV, a Claudin-1-Binding Peptide, Mediated via Down-Regulation of Claudin-1 in Human Lung Adenocarcinoma A549 Cells. *Int J Mol Sci*, *21*(16). https://doi.org/10.3390/ijms21165909

O'Quinn, M. P., Palatinus, J. A., Harris, B. S., Hewett, K. W., & Gourdie, R. G. (2011). A peptide mimetic of the connexin43 carboxyl terminus reduces gap junction remodeling and induced arrhythmia following ventricular injury. *Circ Res*, *108*(6), 704-715. https://doi.org/10.1161/CIRCRESAHA.110.235747

Obert, E., Strauss, R., Brandon, C., Grek, C., Ghatnekar, G., Gourdie, R., & Rohrer, B. (2017). Targeting the tight junction protein, zonula occludens-1, with the connexin43 mimetic peptide, alphaCT1, reduces VEGF-dependent RPE pathophysiology. *J Mol Med (Berl)*, *95*(5), 535-552. https://doi.org/10.1007/s00109-017-1506-8

Olk, S., Zoidl, G., & Dermietzel, R. (2009). Connexins, cell motility, and the cytoskeleton. *Cell Motil Cytoskeleton*, *66*(11), 1000-1016. https://doi.org/10.1002/cm.20404

Ongstad, E. L., O'Quinn, M. P., Ghatnekar, G. S., Yost, M. J., & Gourdie, R. G. (2013). A Connexin43 Mimetic Peptide Promotes Regenerative Healing and Improves Mechanical Properties in Skin and Heart. *Adv Wound Care (New Rochelle)*, *2*(2), 55-62. https://doi.org/10.1089/wound.2011.0341

Oyamada, M., Takebe, K., Endo, A., Hara, S., & Oyamada, Y. (2013). Connexin expression and gap-junctional intercellular communication in ES cells and iPS cells. *Front Pharmacol*, *4*, 85. https://doi.org/10.3389/fphar.2013.00085

Persson, S. G., & Ullberg, L. E. (1979). Blood-volume determination with Evans blue dye in foals. *Acta Vet Scand*, *20*(1), 10-15. https://www.ncbi.nlm.nih.gov/pubmed/443134

Radu, M., & Chernoff, J. (2013). An in vivo assay to test blood vessel permeability. *J Vis Exp*(73),

e50062. https://doi.org/10.3791/50062

Rhett, J. M., Jourdan, J., & Gourdie, R. G. (2011). Connexin 43 connexon to gap junction transition is regulated by zonula occludens-1. *Mol Biol Cell*, *22*(9), 1516-1528. https://doi.org/10.1091/mbc.E10-06-0548

Schlingmann, B., Overgaard, C. E., Molina, S. A., Lynn, K. S., Mitchell, L. A., Dorsainvil White, S., Mattheyses, A. L., Guidot, D. M., Capaldo, C. T., & Koval, M. (2016). Regulation of claudin/zonula occludens-1 complexes by hetero-claudin interactions. *Nat Commun*, *7*, 12276. https://doi.org/10.1038/ncomms12276

Schneeberger, E. E., & Lynch, R. D. (2004). The tight junction: a multifunctional complex. *Am J Physiol Cell Physiol*, *286*(6), C1213-1228. https://doi.org/10.1152/ajpcell.00558.2003

Singh, D., Solan, J. L., Taffet, S. M., Javier, R., & Lampe, P. D. (2005). Connexin 43 interacts with zona occludens-1 and -2 proteins in a cell cycle stage-specific manner. *J Biol Chem*, *280*(34), 30416-30421. https://doi.org/10.1074/jbc.M506799200

Sinha, M., & Lowell, C. A. (2016). Isolation of Highly Pure Primary Mouse Alveolar Epithelial Type II Cells by Flow Cytometric Cell Sorting. *Bio Protoc*, *6*(22). https://doi.org/10.21769/BioProtoc.2013

Smith, P., Jeffers, L. A., & Koval, M. (2019). Effects of different routes of endotoxin injury on barrier function in alcoholic lung syndrome. *Alcohol*, *80*, 81-89. https://doi.org/10.1016/j.alcohol.2018.08.007

Smith, P., Jeffers, L. A., & Koval, M. (2021). Measurement of Lung Vessel and Epithelial Permeability In Vivo with Evans Blue. *Methods Mol Biol*, *2367*, 137-148. https://doi.org/10.1007/7651_2020_345

Soder, B. L., Propst, J. T., Brooks, T. M., Goodwin, R. L., Friedman, H. I., Yost, M. J., & Gourdie, R. G. (2009). The connexin43 carboxyl-terminal peptide ACT1 modulates the biological response to silicone implants. *Plast Reconstr Surg*, *123*(5), 1440-1451. https://doi.org/10.1097/PRS.0b013e3181a0741d

Spadaro, D., Le, S., Laroche, T., Mean, I., Jond, L., Yan, J., & Citi, S. (2017). Tension-Dependent Stretching Activates ZO-1 to Control the Junctional Localization of Its Interactors. *Curr Biol*, *27*(24), 3783-3795 e3788. https://doi.org/10.1016/j.cub.2017.11.014

Strauss, R. E., & Gourdie, R. G. (2020). Cx43 and the Actin Cytoskeleton: Novel Roles and Implications for Cell-Cell Junction-Based Barrier Function Regulation. *Biomolecules*, *10*(12). https://doi.org/10.3390/biom10121656

Strauss, R. E., Mezache, L., Veeraraghavan, R., & Gourdie, R. G. (2021). The Cx43 Carboxyl-Terminal Mimetic Peptide alphaCT1 Protects Endothelial Barrier Function in a ZO1 Binding-Competent Manner. *Biomolecules*, *11*(8). https://doi.org/10.3390/biom11081192

Toyofuku, T., Yabuki, M., Otsu, K., Kuzuya, T., Hori, M., & Tada, M. (1998). Direct association of the gap junction protein connexin-43 with ZO-1 in cardiac myocytes. *J Biol Chem*, *273*(21), 12725-12731. https://doi.org/10.1074/jbc.273.21.12725

van Niekerk, G., Isaacs, A. W., Nell, T., & Engelbrecht, A. M. (2016). Sickness-Associated Anorexia: Mother Nature's Idea of Immunonutrition? *Mediators Inflamm*, *2016*, 8071539. https://doi.org/10.1155/2016/8071539

Wang, F., Daugherty, B., Keise, L. L., Wei, Z., Foley, J. P., Savani, R. C., & Koval, M. (2003). Heterogeneity of claudin expression by alveolar epithelial cells. *Am J Respir Cell Mol Biol*, *29*(1), 62-70. https://doi.org/10.1165/rcmb.2002-0180OC

Wang, Z., Li, W., Chen, J., Shi, H., Zhao, M., You, H., Rao, C., Zhan, Y., Yang, Y., & Xie, P. (2016). Proteomic analysis reveals energy metabolic dysfunction and neurogenesis in the prefrontal cortex of a lipopolysaccharide-induced mouse model of depression. *Mol Med Rep*, *13*(2), 1813-1820. https://doi.org/10.3892/mmr.2015.4741

Wustneck, R., Perez-Gil, J., Wustneck, N., Cruz, A., Fainerman, V. B., & Pison, U. (2005). Interfacial properties of pulmonary surfactant layers. *Adv Colloid Interface Sci*, *117*(1-3), 33-58. https://doi.org/10.1016/j.cis.2005.05.001

Yao, L., Xue, X., Yu, P., Ni, Y., & Chen, F. (2018). Evans Blue Dye: A Revisit of Its Applications in

Biomedicine. *Contrast Media Mol Imaging*, *2018*, 7628037. https://doi.org/10.1155/2018/7628037

Zhou, W., Shi, G., Bai, J., Ma, S., Liu, Q., & Ma, X. (2018). Colquhounia Root Tablet Protects Rat Pulmonary Microvascular Endothelial Cells against TNF-alpha-Induced Injury by Upregulating the Expression of Tight Junction Proteins Claudin-5 and ZO-1. *Evid Based Complement Alternat Med*, *2018*, 1024634. https://doi.org/10.1155/2018/1024634

Chapter 6: Future Therapeutic Targets and Injury Models

Introduction

Claudin 4

Claudins are a family of proteins that regulate paracellular permeability to both ions and solutes and are crucial to tight junctions and alveolo-capillary barrier function. There are three highly expressed claudin isoforms in alveolar epithelial cells, claudins 3, 4, and 18. Claudin 4 is exclusively expressed in the airway epithelial, but not endothelial cells that line the alveoli or other distal lung cells (Chen et al., 2005; Kaarteenaho-Wiik & Soini, 2009; LaFemina et al., 2010; Ohta et al., 2012; Wang et al., 2003). Previous studies have shown that increases in the expression of claudin 4 were correlated to higher transepithelial resistance, a measurement of barrier function (Chen et al., 2005; Mitchell et al., 2011). Conversely, suppression of claudin 4 by was associated with decreased in transepithelial resistance (Wray et al., 2009). Surprisingly, global claudin 4 knockout in mice show only a minimal lung impairment. Global loss of claudin 4 at baseline led to lower alveolar fluid clearance and higher solute permeability but unchanged wet:dry lung weight ratios or differences in transepithelial resistance compared with wild-type mice (Kage et al., 2014). However, claudin 4 knockout mice were more susceptible to lung injury after hyperoxia and ventilator-inducted lung injury in an injury severity-dependent manner as well as measured by total protein concentration in bronchoalveolar lavage fluid. Claudin 4 mRNA expression rose significantly after noninjurious levels (20 cm H_2O) and injurious levels (40 cm H_2O) of ventilation as well as with hyperoxia (Kage et al., 2014). Additionally, claudin 4 was associated with greater ARDS severity (Rokkam et al., 2011; Wray et al., 2009). These data suggest that while claudin 4 may have minimal effect on normal lung physiology, claudin 4 may function to protect against different forms of acute lung injury.

Chronic alcohol use decreases the expression of claudin 4 in alveolar cells derived from alcohol-fed rats (Schlingmann et al., 2016). We wanted to test if global claudin 4 knockout mice were more susceptible to alcohol-mediated lung barrier dysfunction, but first needed to establish a baseline for

claudin 4 knockout response to our LPS injury models. Here, we test the systemic and local impact of LPS in claudin 4 knockout mice.

Klebsiella pneumoniae

Klebsiella pneumonia (*K. pneumoniae*) is a Gram-negative, bacterium that is a common cause of antimicrobial-resistant opportunistic infections in hospitalized patients. *K. pneumoniae* is one of the world's leading nosocomial pathogens and some strains have been recognized by the World Health Organization as a critical public health threat (Pendleton et al., 2013; WHO, 2017; Wyres et al., 2020). *K. pneumoniae* has emerged as a major public health threat due to the increasing incidence of hospital-associated infections caused by multidrug-resistant strains and community-acquired infections caused by hypervirulent strains that express newly acquired virulence factors. This virulent strain of bacteria is the third leading cause of hospital-acquired infections and the second leading cause of blood stream infections caused by Gram-negative bacteria (Magill et al., 2014). *K. pneumoniae* can cause severe community-acquired infections in otherwise healthy patients who do not share the same risk factors for hospital-acquired infections (Meatherall et al., 2009). Common and hypervirulent infections of *K. pneumoniae* can cause urinary tract infections, nosocomial pneumonia, endophthalmitis, meningitis, and intraabdominal infections, necrotizing fasciitis, non-hepatic abscess, and pyogenic liver abscesses, all of which may be accompanied by bacteremia or metastatic spread (Russo & Marr, 2019).

An important host risk factor for developing *K. pneumoniae* community-acquired infections is a history of chronic alcoholism, increasing the risk of the patient to develop pneumonia (Ko et al., 2002). The most likely mechanism for developing pneumonia from *K. pneumoniae* is due to aspiration of the bacterium found in the pharyngeal mucosa into the lung. Researchers found that in two of the observed countries, Taiwan and South Africa, community-acquired pneumonia due to *K. pneumoniae* was significantly associated with alcoholism as defined by the patient's physician (Ko et al., 2002). A population-based cross-sectional study found that alcohol consumption per week (OR 1.7, 95% CI 1.04 – 2.8) was independently associated with oropharyngeal carriage of *K. pneumoniae* and that consuming one

more liter of alcohol per week was associated with a 70% increase in odds of *K. pneumoniae* carriage (Dao et al., 2014). Alcohol consumption decreases early- and long-term survival rates in mice after infection with *K. pneumoniae* (Shellito et al., 2001; Zisman et al., 1998). Additionally, alcohol use vastly decreases bacterial clearance of *K. pneumoniae*; 48 h after an intratracheal challenge of the *K. pneumoniae*, alcohol-fed mice had a 37-fold increase in colony forming units isolated in the plasma and a 500-fold increase in the lungs (Zisman et al., 1998).

Given the association between alcoholism and decreased bacterial clearance, decreased survival rate, and the prevalence of *K. pneumoniae*-associated pneumonia, our lab wanted to test whether an interaction existed between alcohol consumption and *K. pneumoniae* and the combined effect on decreasing barrier dysfunction.

Materials and Methods

Mice

Experiments were performed in accordance with the National Institutes of Health Guidelines for the Use of Laboratory Animals guidelines and were approved by the Institutional Animal Care and Use Committee at Emory University School of Medicine. Isogenetic twelve-week-old male C57BL/6 wild-type mice were used for Wild-type experiments (Jackson Laboratory, Bar Harbor, ME). Claudin 4 KO mice were collaborators (Kage et al., 2014). Animals were housed with a maximum of five animals per cage. All animals were kept under constant temperature at 21 °C and under 12 h light-dark cycle with ad libitum access to regular chow diet. In the alcohol group, ethanol was administered by increasing ethanol concentration from 0% to 20% in 5% increments over a two-week period, and then mice were maintained at 20% ethanol for an additional 8 weeks. For instillation experiments, mice were anesthetized via IP injection of xylazine (10 mg/kg) and ketamine (100 mg/kg). Mice were suspended by their incisors on a rodent tilting work stand (Hallowell, Pittsfield, MA) for orotracheal instillation as previously described (Lawrenz et al., 2014). Mice were weighed while awake and prior to receiving a sedative for all weight measurements.

Lipopolysaccharide (LPS) administration

Alcohol- and water-fed mice were administered 5 mg/kg E. coli 055:B5 LPS purchased from Sigma (L2637). Anesthetized mice received an intratracheal instillation (50 µl) of LPS. Results are reported as percent change in weight ± standard error of the mean.

Total lung protein

Recovered bronchoalveolar lavage (BAL) fluid was kept on ice and centrifuged at 1500 × g for 15 min. Supernatant was collected and stored at −20 °C. Total BAL fluid protein was measured using the Pierce BCA Protein Assay Kit (Thermo Fisher Scientific).

Measurement of IL-6 by MILLIPLEX® Multiplex Assay

Bronchoalveolar lavage fluid was collected and centrifuged at 1500 x g for 15 minutes. 50 µl of supernatant was used and analyzed in duplicate in the MILLIPLEX® Multiplex Assay (MCYTOMAG-70K) on a Luminex® platform according to manufacturer's protocol. Standards to determine linear curve along with 2 quality control samples representing high and low levels for IL-6 were included in the assay.

Klebsiella pneumoniae administration and bacterial clearance

Klebsiella pneumoniae was grown in 3% Tryptic Soy Broth (IPM Scientific, Inc.) for 18 h at 37˚C while shaking. Bacteria was centrifuged at 5,000 x g for 15 minutes and washed twice with PBS. After second wash, *Klebsiella pneumoniae* was resuspended in 10 mL PBS and contained 2×10^{10} colony-forming units/mL. *Klebsiella pneumoniae* was diluted from 2×10^{10} to 2×10^{7} (Figure 6.6) and 2×10^{2} – 2×10^{6} (Figure 6.5). 100 µl of the 2×10^{2} and 2×10^{3} dilution was plated onto MacConkey Agar plates to evaluate for proper concentration. Plates should grow 200 and 20 colony-forming units, respectfully.

Anesthetized alcohol- and water-fed mice were given an intratracheal instillation of *Klebsiella pneumoniae* in 50 µl at various concentrations. To evaluate bacterial clearance, bronchoalveolar lavage fluid was harvested and centrifuged at 3,000 x g for 15 minutes. 10 µl of the cell-free lavage fluid was diluted 1:10, and 100 µl, plated onto MacConkey Agar plates overnight at 37˚C, and total number of colony-forming units were counted. Results are reported as percent change in weight ± standard error of

the mean.

Lung permeability as measured by Evans Blue extravasation

24 h after intratracheal treatment, mice were either re-anesthetized for an Evans Blue permeability assay. Mice were placed on a heating pad or kept in the mouse restrainer and the tail was sterilized with an alcohol wipe. 200 µl of 0.5% Evans Blue in PBS was injected into the tail vein with a 30-gauge needle. The mice were allowed to recover on a heating pad for 1 h and then sacrificed while still under anesthesia. 250 µl of blood was collected by cardiac puncture and centrifuged at 1500 × g for 15 min to collect serum. Bronchoalveolar lung lavage (BAL) fluid was collected by flushing the lungs twice via a tracheal tube with 500 µl of ice-cold PBS with protease inhibitors and centrifuged at 1500 x g for 15 minutes to collect cell-free BAL fluid.

Evans Blue in the serum and BAL fluid was analyzed by spectrophotometry (620 nm) (Radu & Chernoff, 2013). Evans Blue readings were corrected for contaminating heme analyzing samples at 740 nm and using the correction factor y = 1.193x +0.007 as previously described (Moitra et al., 2007) and reported as Evans Blue in the BAL and/or normalized to corresponding serum Evans Blue levels.

Statistical Analysis

Comparisons between two groups was performed by unpaired, two-tailed t-test while comparisons between multiple groups were performed by one-way ANOVA with Tukey's multiple comparisons test using GraphPad Prism software. Data are represented as mean ± standard error of the mean and the statistical significance level was set at 0.05.

Results

Claudin 4 KO mice have similar alveolar inflammation response to LPS

To test the extent of acute lung injury in our two-hit model in claudin 4 KO mice, I measured the effect of a direct lung injury on lung airspace protein levels. Total protein was measured in bronchoalveolar lavage (BAL) fluid from claudin 4 KO mice that received an intratracheal administration of either PBS or LPS (Figure 6.1) and was compared to wild-type mice (Smith et al., 2019). LPS injury

increased total BAL protein in both wild-type and claudin 4 KO groups to similar levels. Baseline concentrations of total protein were similar in both groups (274.1 ± 155.7 in Wild-type versus 333.1 ± 172.6 in claudin 4 KO) as were after LPS exposure (806.8 ± 580.8 versus 1315 ± 467.4). This suggests claudin 4 KO have a similar acute response as Wild-type mice to an LPS challenge.

Claudin 4 KO mice are more susceptible to intratracheal injury

As previously discussed, lipopolysaccharide (LPS) administered by intratracheal instillation results in a modest reduction of body weight which is likely due to an inflammation-induced anorexia (Konsman et al., 2002; Smith et al., 2019; van Niekerk et al., 2016; Wang et al., 2016). To evaluate the contribution of claudin 4 on the systemic effects of LPS, claudin 4 KO mice received an intratracheal instillation of PBS or LPS and weighed 24 h later. The data was compared to Wild-type mice who underwent the same experimental conditions (Smith et al., 2019). Wild-type mice lose only 3% body weight with PBS instillation (3.28% ± 2) compared to 8% with LPS (8.68% ± 1.4), while claudin 4 KO mice lose similar weight whether they are given PBS (8.31% ± 1.2) or LPS (7.9% ± 1.3), (Figure 6.2). Claudin 4 mice have a more severe impact to their weight after PBS intratracheal injury than wild-type mice (Figure 6.2) despite similar levels of inflammation in the lung (Figure 6.1)

Alcohol increases levels of IL-6 in lavage fluid after LPS treatment

Wild-type mice were fed either water or alcohol for 8 weeks and given an intratracheal instillation of LPS. Bronchoalveolar lavage was collected and examined by MILLIPLEX® Multiplex Assay using Luminex® for IL-6. Alcohol-fed mice had higher levels of IL-6 in their bronchoalveolar lavage than water-fed mice (Figure 6.3A). IL-6 levels in water-fed and alcohol-fed mice that did not receive an LPS intratracheal treatment were undetectable (data not shown). We next wanted to examine if IL-6 levels would remain elevated even after alcohol withdrawal. Mice that were fed alcohol for 8 weeks were then switched back to water for 2, 4 or 6 weeks before given an LPS treatment and analyzed for IL-6 levels. While levels were still elevated, we did not include water-fed controls for this experiment, so we are unable to determine if the alcohol effect persisted relative to mice that were always fed water (Figure

6.3B).

Klebsiella pneumoniae increases alveolar leak in a dose-dependent manner

To evaluate the systemic effects of increasing concentrations of *Klebsiella pneumoniae* infection, wild-type mice were given an intratracheal instillation of PBS or 10^2, 10^4, or 10^6 ul of *Klebsiella pneumoniae* and evaluated 24 h later for changes in weight. There was no dose-dependent effect of *Klebsiella pneumoniae* on changes in weight (Figure 6.4). Interestingly, mice lost on average 2.3 – 4.3% body weight, lower than what we previously have witnessed with intratracheal instillations of LPS, usually a 5-10% weight loss (Figure 5.1, Figure 6.2), (Smith et al., 2019).

We next wanted to test if increasing *Klebsiella pneumoniae* concentrations would cause a dose-dependent increase in alveolar leakage, as measured by increased Evans Blue permeability. Wild-type mice given an intratracheal administration of PBS or 10^2, 10^4, or 10^6 ul of *Klebsiella pneumoniae* were given an Evans Blue permeability assay 24 h after intratracheal bacterial inoculation. As the concentration of *Klebsiella pneumoniae* was increased, there was a dose-dependent increase in Evans Blue that leaked into the alveolar space (Figure 6.5). This suggests that increasing infection burden likely increases inflammation, leading to increased alveolar leak and barrier disruption.

Alcohol decreases bacterial clearance of *Klebsiella pneumoniae*

Last, we wanted to test the effect of alcohol use on alveolar leak in this new injury model. Alcohol-fed and water-fed wild-type mice received an intratracheal treatment of 10^7 *Klebsiella pneumoniae* and evaluated for clearance of the bacterium in the lavage fluid 24 h later. Alcohol-fed mice had higher levels of *Klebsiella pneumoniae* colony-forming units in their lavage fluid relative to water-fed mouse controls ($p = 0.0526$, Figure 6.6). This data confirms previous reports of alcohol-mediated lung clearance of *Klebsiella pneumoniae* in mice (Zisman et al., 1998) and in rats (Mehta et al., 2011).

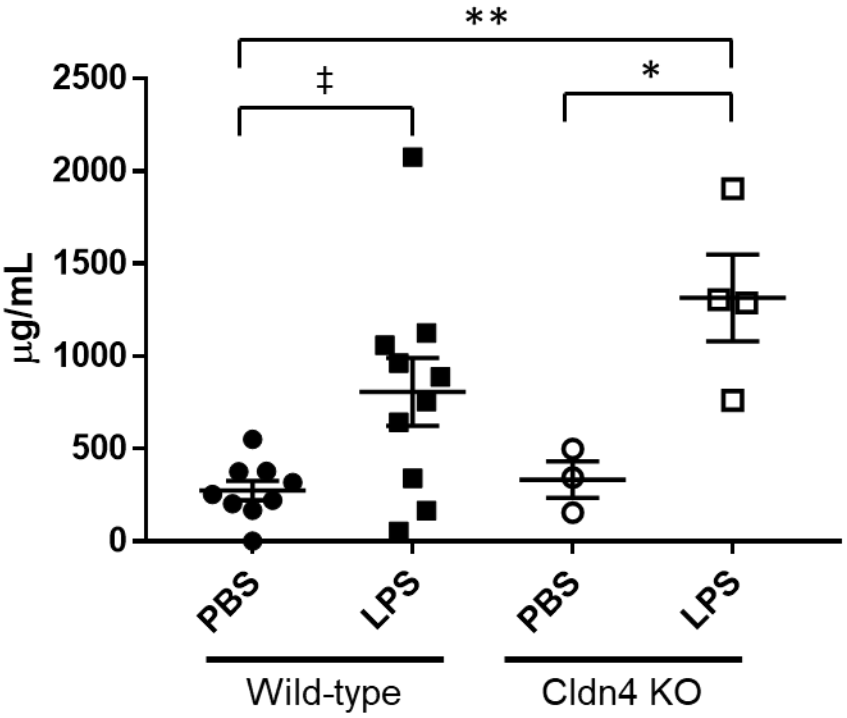

Figure 6.1. Claudin 4 KO mice have similar levels of inflammation in bronchoalveolar lavage to Wild-type mice.

Mice received IT treatment of PBS or LPS at 5mg/kg and BAL was collected 24 h later. Total protein concentration in BAL fluid was measured using the BCA assay. There was no difference in total BAL protein between wild-type and claudin 4 (Cldn4) KO mice with PBS or LPS treatment. Wild-type data were adapted from Smith, et al. (Smith et al., 2019). n = 3-10. *p = 0.029, **p = 0.003, ‡p = 0.0542. Values reported as mean ± standard error of the mean.

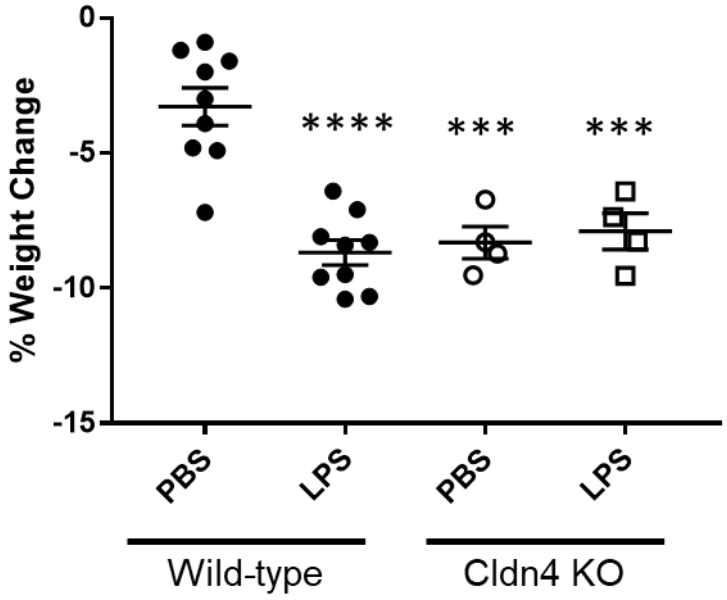

Figure 6.2. Claudin 4 KO mice are more susceptible to saline-induced intratracheal injury than Wild-type mice.

Mice were weighed (pre-weight) and then received an IT treatment of PBS or LPS at 5 mg/kg. Mice were re-weighed 24 h later (post-weight). Data represent % weight change from pre-weight. Wild-type data adapted from Smith, et al. (Smith et al., 2019). n = 4-9. ****$p < 0.0001$ to WT, ***$p < 0.001$ to WT. Values reported as mean ± standard error of the mean.

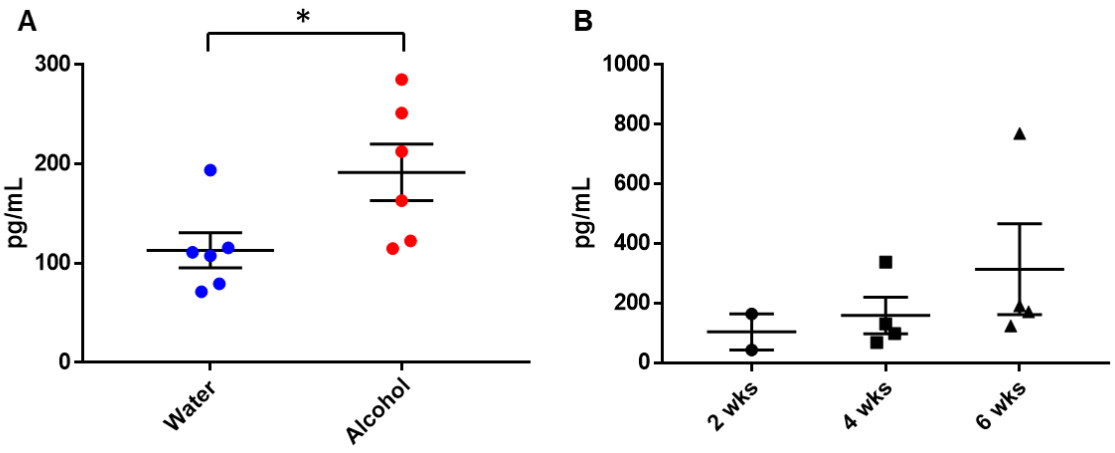

Figure 6.3. LPS-treated, alcohol-fed mice have higher levels of IL-6.

(A) Mice were fed water or alcohol for 8 weeks and then given an IT treatment of LPS at 5 mg/kg. (B) Mice were fed alcohol for 8 weeks and then fed water for 2, 4, or 6 weeks before given an IT treatment of LPS at 5 mg/kg. BAL was collected and analyzed by MILLIPLEX® Multiplex Assay using Luminex® for IL-6. Alcohol-fed mice have higher levels of IL-6 after LPS treatment than water-fed mice and this elevation persists for at least 6 weeks after alcohol withdrawal. n = 2-6. *$p < 0.05$. Values reported as mean ± standard error of the mean.

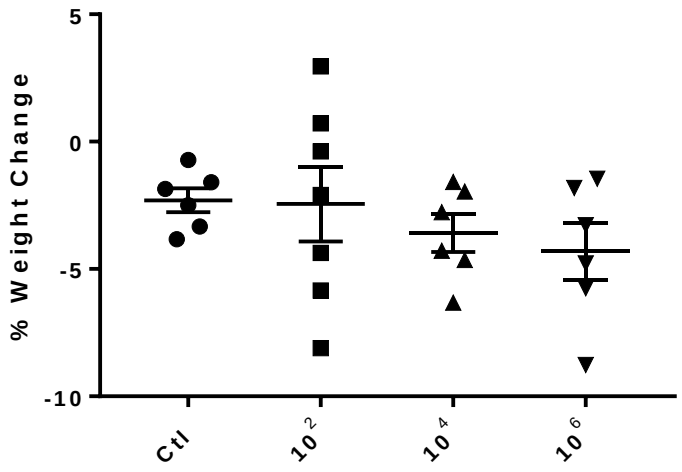

Figure 6.4. No difference in weight changes with increased *Klebsiella* inoculation concentration.

Mice were weighed (pre-weight) and then received 50 µl of PBS (Ctl), 10^2, 10^4, or 10^6 *Klebsiella* via intratracheal instillation. Mice were re-weighed 24 h later (post-weight). Data represent % weight change from pre-weight. n = 6-7. Values reported as mean ± standard error of the mean.

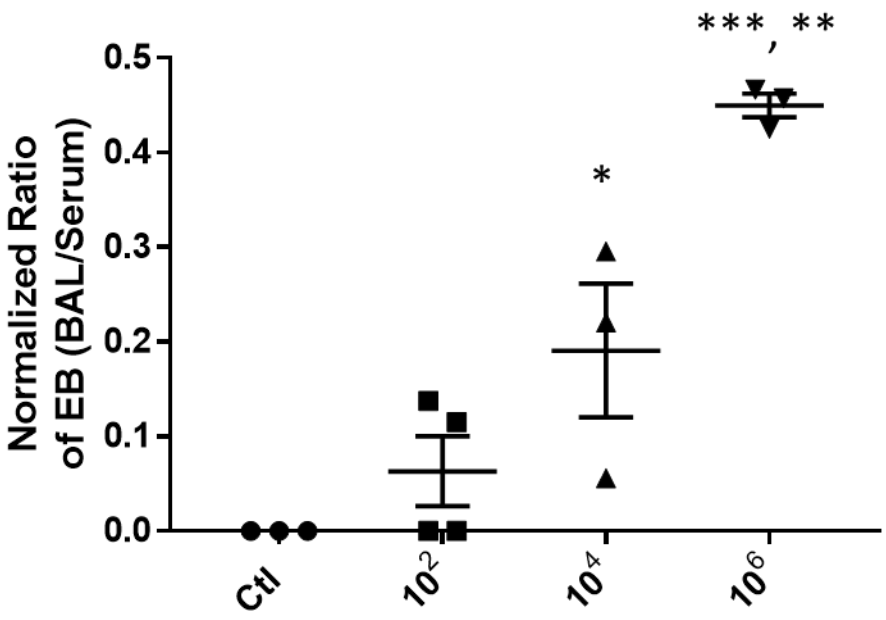

Figure 6.5. Mice have increased alveolar leak with increased *Klebsiella* inoculation concentration.

Mice received an IT treatment of PBS (Ctl), 10^2, 10^4, or 10^6 *Klebsiella*. 24 h later the mice were administered Evans Blue by tail vein injection while anesthetized and allowed to recover for 1 h before BAL and blood were collected. Results were corrected for the presence of heme and are represented as BAL normalized to Evans Blue serum levels. n = 3-4. *$p < 0.05$ to Ctl, ***$p < 0.001$ to Ctl and 10^2, **$p < 0.01$ to 10^4. Values reported as mean ± standard error of the mean.

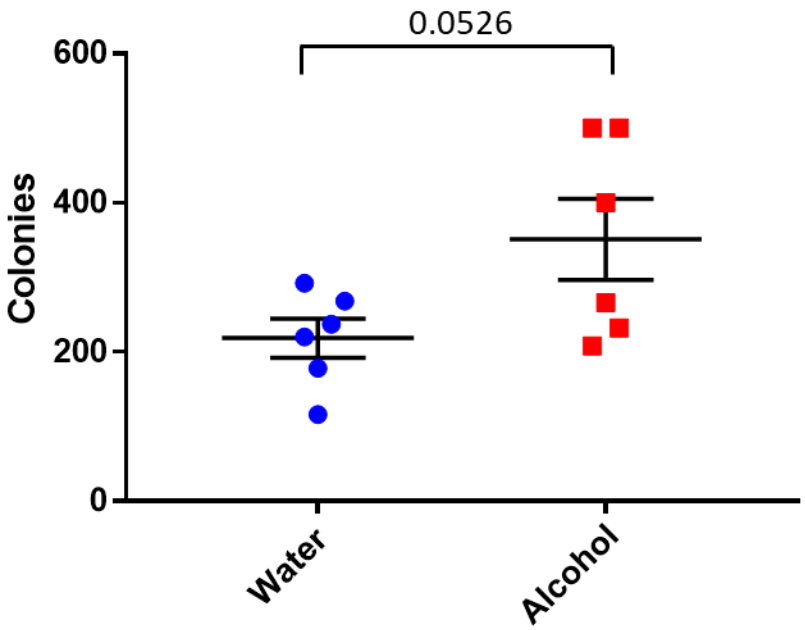

Figure 6.6. Alcohol-fed mice have lower lung clearance of *Klebsiella* infection.

Mice received an intratracheal treatment of 50 µl of 10^7 *Klebsiella pneumoniae*. BAL was collected 24 h later and plated onto MacConkey Agar plates. Plates were incubated at 37˚C for 24 h and then total number of colonies were counted. Alcohol-fed mice had more colonies remaining in their BAL than water-fed mice, indicating decreased lung clearance. n = 6. p = 0.0526. Values reported as mean ± standard error of the mean.

Literature Cited

Chen, S. P., Zhou, B., Willis, B. C., Sandoval, A. J., Liebler, J. M., Kim, K. J., Ann, D. K., Crandall, E. D., & Borok, Z. (2005). Effects of transdifferentiation and EGF on claudin isoform expression in alveolar epithelial cells. *J Appl Physiol (1985)*, *98*(1), 322-328. https://doi.org/10.1152/japplphysiol.00681.2004

Dao, T. T., Liebenthal, D., Tran, T. K., Ngoc Thi Vu, B., Ngoc Thi Nguyen, D., Thi Tran, H. K., Thi Nguyen, C. K., Thi Vu, H. L., Fox, A., Horby, P., Van Nguyen, K., & Wertheim, H. F. (2014). Klebsiella pneumoniae oropharyngeal carriage in rural and urban Vietnam and the effect of alcohol consumption. *PLoS One*, *9*(3), e91999. https://doi.org/10.1371/journal.pone.0091999

Kaarteenaho-Wiik, R., & Soini, Y. (2009). Claudin-1, -2, -3, -4, -5, and -7 in usual interstitial pneumonia and sarcoidosis. *J Histochem Cytochem*, *57*(3), 187-195. https://doi.org/10.1369/jhc.2008.951566

Kage, H., Flodby, P., Gao, D., Kim, Y. H., Marconett, C. N., DeMaio, L., Kim, K. J., Crandall, E. D., & Borok, Z. (2014). Claudin 4 knockout mice: normal physiological phenotype with increased susceptibility to lung injury. *Am J Physiol Lung Cell Mol Physiol*, *307*(7), L524-536. https://doi.org/10.1152/ajplung.00077.2014

Ko, W. C., Paterson, D. L., Sagnimeni, A. J., Hansen, D. S., Von Gottberg, A., Mohapatra, S., Casellas, J. M., Goossens, H., Mulazimoglu, L., Trenholme, G., Klugman, K. P., McCormack, J. G., & Yu, V. L. (2002). Community-acquired Klebsiella pneumoniae bacteremia: global differences in clinical patterns. *Emerg Infect Dis*, *8*(2), 160-166. https://doi.org/10.3201/eid0802.010025

Konsman, J. P., Parnet, P., & Dantzer, R. (2002). Cytokine-induced sickness behaviour: mechanisms and implications. *Trends Neurosci*, *25*(3), 154-159. https://doi.org/10.1016/s0166-2236(00)02088-9

LaFemina, M. J., Rokkam, D., Chandrasena, A., Pan, J., Bajaj, A., Johnson, M., & Frank, J. A. (2010). Keratinocyte growth factor enhances barrier function without altering claudin expression in primary alveolar epithelial cells. *Am J Physiol Lung Cell Mol Physiol*, *299*(6), L724-734. https://doi.org/10.1152/ajplung.00233.2010

Lawrenz, M. B., Fodah, R. A., Gutierrez, M. G., & Warawa, J. (2014). Intubation-mediated intratracheal (IMIT) instillation: a noninvasive, lung-specific delivery system. *J Vis Exp*(93), e52261. https://doi.org/10.3791/52261

Magill, S. S., Edwards, J. R., Bamberg, W., Beldavs, Z. G., Dumyati, G., Kainer, M. A., Lynfield, R., Maloney, M., McAllister-Hollod, L., Nadle, J., Ray, S. M., Thompson, D. L., Wilson, L. E., Fridkin, S. K., Emerging Infections Program Healthcare-Associated, I., & Antimicrobial Use Prevalence Survey, T. (2014). Multistate point-prevalence survey of health care-associated infections. *N Engl J Med*, *370*(13), 1198-1208. https://doi.org/10.1056/NEJMoa1306801

Meatherall, B. L., Gregson, D., Ross, T., Pitout, J. D., & Laupland, K. B. (2009). Incidence, risk factors, and outcomes of Klebsiella pneumoniae bacteremia. *Am J Med*, *122*(9), 866-873. https://doi.org/10.1016/j.amjmed.2009.03.034

Mehta, A. J., Joshi, P. C., Fan, X., Brown, L. A., Ritzenthaler, J. D., Roman, J., & Guidot, D. M. (2011). Zinc supplementation restores PU.1 and Nrf2 nuclear binding in alveolar macrophages and improves redox balance and bacterial clearance in the lungs of alcohol-fed rats. *Alcohol Clin Exp Res*, *35*(8), 1519-1528. https://doi.org/10.1111/j.1530-0277.2011.01488.x

Mitchell, L. A., Overgaard, C. E., Ward, C., Margulies, S. S., & Koval, M. (2011). Differential effects of claudin-3 and claudin-4 on alveolar epithelial barrier function. *Am J Physiol Lung Cell Mol Physiol*, *301*(1), L40-49. https://doi.org/10.1152/ajplung.00299.2010

Moitra, J., Sammani, S., & Garcia, J. G. (2007). Re-evaluation of Evans Blue dye as a marker of albumin clearance in murine models of acute lung injury. *Transl Res*, *150*(4), 253-265. https://doi.org/10.1016/j.trsl.2007.03.013

Ohta, H., Chiba, S., Ebina, M., Furuse, M., & Nukiwa, T. (2012). Altered expression of tight junction molecules in alveolar septa in lung injury and fibrosis. *Am J Physiol Lung Cell Mol Physiol*, *302*(2), L193-205. https://doi.org/10.1152/ajplung.00349.2010

Pendleton, J. N., Gorman, S. P., & Gilmore, B. F. (2013). Clinical relevance of the ESKAPE pathogens. *Expert Rev Anti Infect Ther*, *11*(3), 297-308. https://doi.org/10.1586/eri.13.12

Radu, M., & Chernoff, J. (2013). An in vivo assay to test blood vessel permeability. *J Vis Exp*(73), e50062. https://doi.org/10.3791/50062

Rokkam, D., Lafemina, M. J., Lee, J. W., Matthay, M. A., & Frank, J. A. (2011). Claudin-4 levels are associated with intact alveolar fluid clearance in human lungs. *Am J Pathol*, *179*(3), 1081-1087. https://doi.org/10.1016/j.ajpath.2011.05.017

Russo, T. A., & Marr, C. M. (2019). Hypervirulent Klebsiella pneumoniae. *Clin Microbiol Rev*, *32*(3). https://doi.org/10.1128/CMR.00001-19

Schlingmann, B., Overgaard, C. E., Molina, S. A., Lynn, K. S., Mitchell, L. A., Dorsainvil White, S., Mattheyses, A. L., Guidot, D. M., Capaldo, C. T., & Koval, M. (2016). Regulation of claudin/zonula occludens-1 complexes by hetero-claudin interactions. *Nat Commun*, *7*, 12276. https://doi.org/10.1038/ncomms12276

Shellito, J. E., quan Zheng, M., Ye, P., Ruan, S., Shean, M. K., & Kolls, J. (2001). Effect of alcohol consumption on host release of interleukin-17 during pulmonary infection with Klebsiella pneumoniae. *Alcohol Clin Exp Res*, *25*(6), 872-881. https://www.ncbi.nlm.nih.gov/pubmed/11410724

Smith, P., Jeffers, L. A., & Koval, M. (2019). Effects of different routes of endotoxin injury on barrier function in alcoholic lung syndrome. *Alcohol*, *80*, 81-89. https://doi.org/10.1016/j.alcohol.2018.08.007

van Niekerk, G., Isaacs, A. W., Nell, T., & Engelbrecht, A. M. (2016). Sickness-Associated Anorexia: Mother Nature's Idea of Immunonutrition? *Mediators Inflamm*, *2016*, 8071539. https://doi.org/10.1155/2016/8071539

Wang, F., Daugherty, B., Keise, L. L., Wei, Z., Foley, J. P., Savani, R. C., & Koval, M. (2003). Heterogeneity of claudin expression by alveolar epithelial cells. *Am J Respir Cell Mol Biol*, *29*(1), 62-70. https://doi.org/10.1165/rcmb.2002-0180OC

Wang, Z., Li, W., Chen, J., Shi, H., Zhao, M., You, H., Rao, C., Zhan, Y., Yang, Y., & Xie, P. (2016). Proteomic analysis reveals energy metabolic dysfunction and neurogenesis in the prefrontal

cortex of a lipopolysaccharide-induced mouse model of depression. *Mol Med Rep*, *13*(2), 1813-1820. https://doi.org/10.3892/mmr.2015.4741

WHO. (2017). *Global Priority List of Antibiotic-Resistant Bacteria to Guide Research, Discovery, and Development of New Antibiotics*.

Wray, C., Mao, Y., Pan, J., Chandrasena, A., Piasta, F., & Frank, J. A. (2009). Claudin-4 augments alveolar epithelial barrier function and is induced in acute lung injury. *Am J Physiol Lung Cell Mol Physiol*, *297*(2), L219-227. https://doi.org/10.1152/ajplung.00043.2009

Wyres, K. L., Lam, M. M. C., & Holt, K. E. (2020). Population genomics of Klebsiella pneumoniae. *Nat Rev Microbiol*, *18*(6), 344-359. https://doi.org/10.1038/s41579-019-0315-1

Zisman, D. A., Strieter, R. M., Kunkel, S. L., Tsai, W. C., Wilkowski, J. M., Bucknell, K. A., & Standiford, T. J. (1998). Ethanol feeding impairs innate immunity and alters the expression of Th1- and Th2-phenotype cytokines in murine Klebsiella pneumonia. *Alcohol Clin Exp Res*, *22*(3), 621-627. https://doi.org/10.1111/j.1530-0277.1998.tb04303.x

Chapter 7: Discussion – Conclusion and Future Directions

Overview of Findings

Understanding the molecular and cellular mechanisms that contribute to alcohol-mediated barrier disruption is essential to designing novel therapeutics to prevent or reverse the alveolar epithelial dysfunction. The overarching goal of my dissertation work was to explore how different tight junction proteins contributed to barrier function *in vivo.* To accomplish this goal, I designed with Dr. Prestina Smith a novel assay to evaluate alveolar function in a murine animal model that allowed simultaneous *in vivo* measurement of both epithelial and endothelial barriers (Smith et al., 2019, 2021).

In this dissertation, I chose to investigate the interaction of alcohol with several 'second-hit' injuries, including hydrostatic fluid pressure, direct and indirect models of inflammation, and bacterial pneumonia. I also tested two potential new peptide-based agents that not only can further inform about the molecular mechanisms behind alcoholic lung disease but have significant clinical implications as novel therapeutics.

In Vivo Measurement of Lung Vessel and Epithelial Permeability

Evans Blue is an azo dye that has an extremely high affinity for serum albumin *in vitro* or *in vivo* (Saria & Lundberg, 1983; Wolman et al., 1981) and has long been used in biomedicine to estimate blood volume and vascular permeability (Evans & Schulemann, 1914; Lawrence & Walters, 1959; Persson & Ullberg, 1979; Radu & Chernoff, 2013; Yao et al., 2018). Once the dye is introduced via intravascular injection, Evans Blue bound to albumin remains stably within the vascular walls as albumin cannot normally cross most vascular barriers. Evans Blue can then be quantified fluorescently to measure the extravasation of the dye from the blood vessels into different tissues, including the lung, kidneys, brain, and cancers (Babickova et al., 2017; Maeda et al., 2003; Mammoto et al., 2013; Smith et al., 2019; Yao et al., 2018).

Previous applications of Evans Blue dye have been used to identify leakage of the dye into the combined alveolar and interstitial spaces of mice (Mammoto et al., 2013) or into the alveolar and

interstitial spaces, separately, in rats (Verbrugge et al., 1998). In Chapter 2, we established a novel method using Evans Blue dye to simultaneously measure the function of vascular and epithelial barriers of murine lungs *in vivo.* In Chapter 3, we used this new application of the Evans Blue permeability assay to evaluate the effects of how chronic alcohol consumption affects pulmonary edema in the interstitial and alveolar spaces when coupled with an endotoxin-mediated lung injury. By comparing the alveolar airspace compartment separately from the pulmonary interstitial space, this novel application of the Evans Blue permeability assay can distinguish between edema and barrier disruption of different pulmonary barriers. This application can advance a more targeting understanding of disease pathophysiologies as well as give insight to cellular specificity of new therapeutics.

'Second-hit' Injury Models

Endotoxin-mediated inflammation

Chronic alcohol use negatively impacts the alveolar epithelial barrier whether the additional injury is delivered indirectly (systemically) or directly (locally). In Chapter 3, we used the Evans Blue Permeability assay, established in Chapter 2, to test how alcohol impairs endothelial and epithelial barriers in the lung.

In this study, we find evidence that both airspace and tissue edema are likely drivers in how alcohol-mediated lung dysfunction predisposes the lung to develop Acute Respiratory Distress Syndrome. These findings are in agreement with previous studies that show that chronic alcohol use impairs lung barrier and immune function (Mehta et al., 2013; Price et al., 2017; Schlingmann et al., 2016). We delivered lipopolysaccharide directly onto the alveolar surface (via intratracheal instillation) as a model of inflammatory pneumonia. We compared this model to mice given an intraperitoneal injection of lipopolysaccharide as a model of sepsis, a form of indirect pulmonary injury. Both types of injury caused interstitial edema regardless of endotoxin treatment. However, only the combination of the endotoxin with alcohol use led to a breach in the alveolar epithelial barrier and an increase in macromolecule permeability. The effects of alcohol on permeability alone did not involve inflammation, suggesting the

change in pulmonary barrier function may not have impacted immune cell recruitment (Ward et al., 2015).

When the endotoxin injury is administered directly, the endothelial barrier becomes further compromised. Additionally, direct injury induced a pro-inflammatory response, measured by an increase in total protein content in the bronchoalveolar lavage and an increase in presence and activity of immune cells in the lung tissue. We hypothesize that part of the increase in total protein content included secretion of surfactant and pro-inflammatory cytokines in addition to the increase in alveolar permeability (Fehrenbach et al., 1998). Another interesting finding was the impairment of the pulmonary microvasculature barrier due to alcohol, a finding that is consistent with blood brain barrier disruption in response to alcohol (Haorah et al., 2007; Singh et al., 2007).

Testing the acute and chronic effects of alcohol use on the various pulmonary barriers is vital to understanding the molecular mechanisms and clinical implications of alcoholic lung syndrome as well as determining if both barriers need to be targeted when designing novel therapeutics. The finding that even mild endotoxemia can induce barrier breach and tissue edema suggests the pulmonary damage likely scales with the severity of the injury, such as bacterial or viral pneumonia. In Chapter 6, I begin to explore the effects of alcohol use with bacterial pneumonia.

Bacterial pneumonia

Bacterial toxins can lead to the onset of exacerbation of lung diseases by altering the viability of both the lung epithelial and capillary endothelial surfaces (Hamacher et al., 2017; Lucas et al., 2020; Lucas et al., 2009). Alcohol use is associated with a decreased clearance rate of a bacterial pneumonia in several animal models. Mice given regular access to alcohol had a decreased survival rate when infected with *Klebsiella pneumoniae* (Zisman et al., 1998). Additionally, alcohol consumption reduced the bacterial clearance of *Pseudomonas aeruginosa* infections in mice (Hunt et al., 2014) and in rats (Greenberg et al., 1999). This is consistent with our findings that alcohol-fed mice had a decreased bacterial clearance to *Klebsiella pneumoniae* (Figure 6.6).

Bacterial toxins are capable of causing direct alveolar epithelial and capillary endothelial cell dysfunction and/or death, leading to decreased barrier function and increased pulmonary edema. These toxins can impair alveolar ion channels, form membrane pores, target cell cilia, respiratory mucosa, or tight junction proteins, leading to the significant barrier disruption (Hamacher et al., 2017; Rangel et al., 2015; Repp et al., 2002; Sandoval et al., 2001; Sonnen et al., 2014; Yang et al., 2018). This coincides with our finding that an increased infection burden was associated with increasing levels of alveolar barrier disruption (Figure 6.5).

There are several mechanisms through which excessive alcohol use increases the susceptibility to develop a bacterial pneumonia infection, including impairing the innate immunity within the lower airways (Joshi & Guidot, 2007; Mehta & Guidot, 2012, 2017). Chronic alcohol ingestion impacts the expression of two signaling molecules that regulate immune cells, increasing the expression of TGFβ1 and dampening GM-CSF receptors in alveolar epithelial cells and macrophages (Bechara et al., 2004; Joshi et al., 2006). Critically ill patients that higher ratios of TGFβ1 to GM-CSF had higher mortality, suggesting that the impact of alcohol has a significant role in modifying the immune response (Overgaard et al., 2015). Alcohol consumption in mice suppresses IL-12 and IL-17 release into lung tissue and may be linked to the immunosuppression associated with alcohol abuse (Shellito et al., 2001; Zisman et al., 1998). Here, we found that alcohol-fed mice had increased levels of the pro-inflammatory cytokine IL-6 in bronchoalveolar fluid after an endotoxin injury (Figure 6.3). Alcohol has previously been shown to increase IL-6 in the airway in mouse models (Bailey et al., 2019; Gaydos et al., 2019). This is also consistent with other studies that show that alcohol-dependent patients have significantly higher serum levels of IL-6 as compared to controls (Heberlein et al., 2014; Nicolaou et al., 2004). IL-6 serum levels were associated with alcohol craving and alcohol consumption and IL-6 levels decreased during withdrawal (Heberlein et al., 2014).

Potential Therapeutic for Alcoholic Lung Disease

In this dissertation, I investigated the potential of mimetic peptides to prevent alcohol-mediated

lung dysfunction in a mouse model. The αCT1 peptide has previously been used for a wide variety of novel therapeutic purposes in both tissue engineering and regenerative medicine. αCT1 improved microvascular dysfunction, cardiac function, and edema; provided cardioprotection from ischemia-reperfusion injury; and improved wound healing (Ghatnekar et al., 2015; Grek et al., 2015; Jiang et al., 2019; O'Quinn et al., 2011; Obert et al., 2017; Ongstad et al., 2013; Soder et al., 2009).

αCT1 is a peptide mimetic that can bind to ZO-1 and release it from intracellular Cx43, allowing the tight junction protein to associate with claudins and prevent tight junction degradation in response to injury (Strauss et al., 2021). One mechanism by which chronic alcohol use disrupts alveolar barrier function is by increasing claudin 5 expression, which antagonizes and directly disrupts endogenous claudin 18 binding to ZO-1 (Schlingmann et al., 2016). The specific mechanism is likely through a claudin-claudin interaction that negatively affects the stability and organization of the tight junction scaffold (Lynn et al., 2020). Here, I tested the potential of αCT1 to mitigate the effects of alcoholic lung disease. When delivered after a direct endotoxin injury, αCT1 was able to reverse the deleterious effects of alcohol on alveolar barrier dysfunction (Figure 5.3). This is likely due to αCT1 increasing the intracellular availability of ZO-1 and thereby increasing claudin 18 association at the tight junctions.

Future Directions

Fluid pressure as a novel injury model

There is a critical need to develop additional injury models outside of those that create a state of inflammation. In order to investigate various inflammatory effects of a specific disease or solve a molecular mechanism, an injury model that can promote vascular leak without causing concomitant activation of the immune system. Inducing endothelial injury with increased hydrostatic pressure can also serve as a non-pharmaceutical model for temporarily increasing systemic interstitial pressure or inducing brief systemic hypertension.

While we did not find a volume-dependent effect on alveolar leak at the tested volumes, it is likely the mice excreted the excessive volume to reach steady state fluid homeostasis. This is also

supported by the fact that alcohol is known to induce diuresis (Eiser, 1987; Roberts, 1963). Increasing hydrostatic pressure to induce barrier disruption will still be a viable and novel injury model in both acute (< 4 h) and chronic (> 2 day) fluid burden models.

We found that a small volume of fluid administered intraperitoneally did not induce significant alveolar leak while conscious or under ketamine/xylazine sedation (Figure 4.1). It may be interesting to compare these findings to alternative sedation methods (e.g. avertin, pentobarbital, and isoflurane) (Erhardt et al., 1984; Ho et al., 2011; Stypmann, 2007; Uechi et al., 1998; Yan et al., 2007; Yang et al., 1999) as we found a different pattern of alveolar leak between anesthetized and conscious mice. Additionally, increasing hydrostatic pressure with higher volumes via both intraperitoneal (Figure 4.1) and intravascular (Figure 4.4) routes may induce a more measurable leak response, for example 0.5 – 1 volumes of mouse blood volumes (1-2 mL) (Kaliss & Pressman, 1950). Additionally, it is important to test a bolus injection versus administering fluid over time to allow fluid accommodation if administering a significant volume. While in this dissertation we exclusively tested phosphate-buffered saline, it would be important to test more clinically relevant fluids that are commonly used during fluid resuscitation. A debate exists between using normal saline (0.9% sodium-chloride) compared to a balanced solution (crystalloid fluid), the latter of which are first choice for fluid resuscitation in the presence of hypovolemia, hemorrhage, sepsis, or dehydration (Epstein & Waseem, 2022; Gordon & Spiegel, 2020). These solutions include normal saline (0.9%, 0.45%, and 3%), Lactated Ringers, PlasmaLyte, and Dextrose 5% in water (D5W) (Gordon & Spiegel, 2020).

An additional recommendation for using fluid to induce vascular and epithelial leak would be to calculate a relationship between blood pressure and different volumes of intravascular fluid, then perform an Evans Blue permeability assay at various fluid volumes. Establishing a fluid-pressure curve as it relates to alveolar or endothelial leak would be a novel application of the Evans Blue assay and allow researchers to measure a direct correlation between pressure and barrier dysfunction.

Previously studies have shown that loss of claudin 4 compromises alveolar function by decreasing transepithelial resistance, lower alveolar fluid clearance, and higher solute permeability (Kage

et al., 2014; Wray et al., 2009). Additionally, claudin 4 knockout mice were more susceptible to lung injury after hyperoxia and ventilator-inducted lung injury. Previous studies suggest that while claudin 4 may have a minimal effect on normal lung physiology, the protein may be necessary to protect against various forms of acute lung injury. In this study, we found that claudin 4 knockout mice were more susceptible to non-inflammatory intratracheal injury (Figure 6.1, Figure 6.2). We hypothesize that claudin 4 may be structurally necessary to protect against increased fluid pressures. Establishing whether claudin 4 knockout mice are more susceptible to a hydrostatic fluid injury model may give further insight to the functional role of claudin 4 in the alveolar membrane.

aCT1 therapeutic potential with additional injury models

Collaborators have previously demonstrated that the αCT1 peptide can be administered prior to an LPS injury or to prevent oxidative-stress induced pulmonary injury (data not shown). Here, I demonstrated that αCT1 can be given after a minor inflammatory insult to rescue the deleterious effects of alcohol on alveolar barrier dysfunction (Figure 5.3). Whether αCT1, administered post-insult, can reverse alveolar barrier disruption at dosages closer to clinical sepsis or lethality, or if αCT1 would need to be given prior to the injury as a pre-treatment to prevent significant alveolar leak, remains to be seen.

Additionally, we only tested the endotoxin LPS as a model for inflammatory pneumonia and found a beneficial effect of αCT1. We recommend testing alcohol use with additional injury models, such as bacterial pneumonia (e.g. *Klebsiella pneumoniae*), to evaluate the therapeutic benefit of αCT1 on alveolar barrier defects (Figure 6.5, Figure 6.6). In this dissertation, I demonstrated that increased infection burdens of *Klebsiella pneumoniae* were associated with increased leakage of Evans Blue dye into the bronchoalveolar lavage. While 10^7 inoculations were associated with a high rate of mortality in alcohol-fed mice (data not shown), we suggest using the 10^6 concentration that was still associated with measurable alveolar leak in water-fed mice (Figure 6.5). In addition to also establishing the relationship between bacterial burden concentration and alveolar in leak in alcohol-fed mice, *Klebsiella pneumoniae* should be tested as an injury model when evaluating αCT1 therapeutic potential in vulnerable alcohol-

exposed, damage-primed lungs.

Therapeutic potential of claudin 5

Claudin 5 is necessary and sufficient to diminish alveolar barrier dysfunction in alcohol-exposed alveolar epithelial cells (Schlingmann et al., 2016). Additionally, a peptide inhibitor of claudin 5 (C5) was able to reverse the deleterious effects *in vitro* of alcohol use on epithelial barrier function in alveolar epithelial cells derived from alcohol-fed rats (Schlingmann et al., 2016). In this dissertation, we did not find a therapeutic benefit of C5 *in vivo* (Figure 5.6, Figure 5.7). We only tested 5 mg/kg and 50 mg/kg administered via nebulization one hour after lipopolysaccharide insult, so it is possible a different concentration or direct, intratracheal administration may provide greater therapeutic potential for C5. Additionally, attaching the antennapedia cell internalization sequence (RQPKIWFPNRRKPWKK) from αCT1 (Hunter et al., 2005) to the five amino acid sequence from the second extracellular loop of claudin 5 (EFYDP) may increase C5 incorporation into the alveolar space to target intracellular claudin 5. However, this sequence may drive the peptide entirely intracellular and have minimal impact on interaction between C5 and membrane-associated claudin 5. Investigating alternative integration sequences, like a large hydrophobic sequence, may expand the therapeutic potential of C5.

Literature Cited

Babickova, J., Klinkhammer, B. M., Buhl, E. M., Djudjaj, S., Hoss, M., Heymann, F., Tacke, F., Floege, J., Becker, J. U., & Boor, P. (2017). Regardless of etiology, progressive renal disease causes ultrastructural and functional alterations of peritubular capillaries. *Kidney Int*, *91*(1), 70-85. https://doi.org/10.1016/j.kint.2016.07.038

Bailey, K. L., Wyatt, T. A., Katafiasz, D. M., Taylor, K. W., Heires, A. J., Sisson, J. H., Romberger, D. J., & Burnham, E. L. (2019). Alcohol and cannabis use alter pulmonary innate immunity. *Alcohol*, *80*, 131-138. https://doi.org/10.1016/j.alcohol.2018.11.002

Bechara, R. I., Brown, L. A., Roman, J., Joshi, P. C., & Guidot, D. M. (2004). Transforming growth factor beta1 expression and activation is increased in the alcoholic rat lung. *Am J Respir Crit Care Med*, *170*(2), 188-194. https://doi.org/10.1164/rccm.200304-478OC

Eiser, A. R. (1987). The effects of alcohol on renal function and excretion. *Alcohol Clin Exp Res*, *11*(2), 127-138. https://doi.org/10.1111/j.1530-0277.1987.tb01275.x

Epstein, E. M., & Waseem, M. (2022). Crystalloid Fluids. In *StatPearls*. https://www.ncbi.nlm.nih.gov/pubmed/30726011

Erhardt, W., Hebestedt, A., Aschenbrenner, G., Pichotka, B., & Blumel, G. (1984). A comparative study with various anesthetics in mice (pentobarbitone, ketamine-xylazine, carfentanyl-etomidate). *Res Exp Med (Berl)*, *184*(3), 159-169. https://doi.org/10.1007/BF01852390

Evans, H. M., & Schulemann, W. (1914). The Action of Vital Stains Belonging to the Benzidine Group. *Science*, *39*(1004), 443-454. https://doi.org/10.1126/science.39.1004.443

Fehrenbach, H., Brasch, F., Uhlig, S., Weisser, M., Stamme, C., Wendel, A., & Richter, J. (1998). Early alterations in intracellular and alveolar surfactant of the rat lung in response to endotoxin. *Am J Respir Crit Care Med*, *157*(5 Pt 1), 1630-1639. https://doi.org/10.1164/ajrccm.157.5.9611070

Gaydos, J., McNally, A., & Burnham, E. L. (2019). The impact of alcohol use disorders on pulmonary immune cell inflammatory responses to Streptococcus pneumoniae. *Alcohol*, *80*, 119-130.

https://doi.org/10.1016/j.alcohol.2018.08.016

Ghatnekar, G. S., Grek, C. L., Armstrong, D. G., Desai, S. C., & Gourdie, R. G. (2015). The effect of a connexin43-based Peptide on the healing of chronic venous leg ulcers: a multicenter, randomized trial. *J Invest Dermatol*, *135*(1), 289-298. https://doi.org/10.1038/jid.2014.318

Gordon, D., & Spiegel, R. (2020). Fluid Resuscitation: History, Physiology, and Modern Fluid Resuscitation Strategies. *Emerg Med Clin North Am*, *38*(4), 783-793. https://doi.org/10.1016/j.emc.2020.06.004

Greenberg, S. S., Zhao, X., Hua, L., Wang, J. F., Nelson, S., & Ouyang, J. (1999). Ethanol inhibits lung clearance of Pseudomonas aeruginosa by a neutrophil and nitric oxide-dependent mechanism, in vivo. *Alcohol Clin Exp Res*, *23*(4), 735-744. https://www.ncbi.nlm.nih.gov/pubmed/10235311

Grek, C. L., Prasad, G. M., Viswanathan, V., Armstrong, D. G., Gourdie, R. G., & Ghatnekar, G. S. (2015). Topical administration of a connexin43-based peptide augments healing of chronic neuropathic diabetic foot ulcers: A multicenter, randomized trial. *Wound Repair Regen*, *23*(2), 203-212. https://doi.org/10.1111/wrr.12275

Hamacher, J., Hadizamani, Y., Borgmann, M., Mohaupt, M., Mannel, D. N., Moehrlen, U., Lucas, R., & Stammberger, U. (2017). Cytokine-Ion Channel Interactions in Pulmonary Inflammation. *Front Immunol*, *8*, 1644. https://doi.org/10.3389/fimmu.2017.01644

Haorah, J., Knipe, B., Gorantla, S., Zheng, J., & Persidsky, Y. (2007). Alcohol-induced blood-brain barrier dysfunction is mediated via inositol 1,4,5-triphosphate receptor (IP3R)-gated intracellular calcium release. *J Neurochem*, *100*(2), 324-336. https://doi.org/10.1111/j.1471-4159.2006.04245.x

Heberlein, A., Kaser, M., Lichtinghagen, R., Rhein, M., Lenz, B., Kornhuber, J., Bleich, S., & Hillemacher, T. (2014). TNF-alpha and IL-6 serum levels: neurobiological markers of alcohol consumption in alcohol-dependent patients? *Alcohol*, *48*(7), 671-676. https://doi.org/10.1016/j.alcohol.2014.08.003

Ho, D., Zhao, X., Gao, S., Hong, C., Vatner, D. E., & Vatner, S. F. (2011). Heart Rate and

Electrocardiography Monitoring in Mice. *Curr Protoc Mouse Biol*, *1*, 123-139. https://doi.org/10.1002/9780470942390.mo100159

Hunt, W. R., Zughaier, S. M., Guentert, D. E., Shenep, M. A., Koval, M., McCarty, N. A., & Hansen, J. M. (2014). Hyperglycemia impedes lung bacterial clearance in a murine model of cystic fibrosis-related diabetes. *Am J Physiol Lung Cell Mol Physiol*, *306*(1), L43-49. https://doi.org/10.1152/ajplung.00224.2013

Hunter, A. W., Barker, R. J., Zhu, C., & Gourdie, R. G. (2005). Zonula occludens-1 alters connexin43 gap junction size and organization by influencing channel accretion. *Mol Biol Cell*, *16*(12), 5686-5698. https://doi.org/10.1091/mbc.e05-08-0737

Jiang, J., Hoagland, D., Palatinus, J. A., He, H., Iyyathurai, J., Jourdan, L. J., Bultynck, G., Wang, Z., Zhang, Z., Schey, K., Poelzing, S., McGowan, F. X., & Gourdie, R. G. (2019). Interaction of alpha Carboxyl Terminus 1 Peptide With the Connexin 43 Carboxyl Terminus Preserves Left Ventricular Function After Ischemia-Reperfusion Injury. *J Am Heart Assoc*, *8*(16), e012385. https://doi.org/10.1161/JAHA.119.012385

Joshi, P. C., Applewhite, L., Mitchell, P. O., Fernainy, K., Roman, J., Eaton, D. C., & Guidot, D. M. (2006). GM-CSF receptor expression and signaling is decreased in lungs of ethanol-fed rats. *Am J Physiol Lung Cell Mol Physiol*, *291*(6), L1150-1158. https://doi.org/10.1152/ajplung.00150.2006

Joshi, P. C., & Guidot, D. M. (2007). The alcoholic lung: epidemiology, pathophysiology, and potential therapies. *Am J Physiol Lung Cell Mol Physiol*, *292*(4), L813-823. https://doi.org/10.1152/ajplung.00348.2006

Kage, H., Flodby, P., Gao, D., Kim, Y. H., Marconett, C. N., DeMaio, L., Kim, K. J., Crandall, E. D., & Borok, Z. (2014). Claudin 4 knockout mice: normal physiological phenotype with increased susceptibility to lung injury. *Am J Physiol Lung Cell Mol Physiol*, *307*(7), L524-536. https://doi.org/10.1152/ajplung.00077.2014

Kaliss, N., & Pressman, D. (1950). Plasma and blood volumes of mouse organs, as determined with radioactive iodoproteins. *Proc Soc Exp Biol Med*, *75*(1), 16-20.

https://doi.org/10.3181/00379727-75-18083

Lawrence, A. C., & Walters, G. (1959). The extraction of Evans blue (T1824) from plasma and the measurement of plasma volume. *J Clin Pathol*, *12*(2), 123-127. https://doi.org/10.1136/jcp.12.2.123

Lucas, R., Hadizamani, Y., Gonzales, J., Gorshkov, B., Bodmer, T., Berthiaume, Y., Moehrlen, U., Lode, H., Huwer, H., Hudel, M., Mraheil, M. A., Toque, H. A. F., Chakraborty, T., & Hamacher, J. (2020). Impact of Bacterial Toxins in the Lungs. *Toxins (Basel)*, *12*(4). https://doi.org/10.3390/toxins12040223

Lucas, R., Verin, A. D., Black, S. M., & Catravas, J. D. (2009). Regulators of endothelial and epithelial barrier integrity and function in acute lung injury. *Biochem Pharmacol*, *77*(12), 1763-1772. https://doi.org/10.1016/j.bcp.2009.01.014

Lynn, K. S., Peterson, R. J., & Koval, M. (2020). Ruffles and spikes: Control of tight junction morphology and permeability by claudins. *Biochim Biophys Acta Biomembr*, *1862*(9), 183339. https://doi.org/10.1016/j.bbamem.2020.183339

Maeda, H., Fang, J., Inutsuka, T., & Kitamoto, Y. (2003). Vascular permeability enhancement in solid tumor: various factors, mechanisms involved and its implications. *Int Immunopharmacol*, *3*(3), 319-328. https://doi.org/10.1016/S1567-5769(02)00271-0

Mammoto, A., Mammoto, T., Kanapathipillai, M., Wing Yung, C., Jiang, E., Jiang, A., Lofgren, K., Gee, E. P., & Ingber, D. E. (2013). Control of lung vascular permeability and endotoxin-induced pulmonary oedema by changes in extracellular matrix mechanics. *Nat Commun*, *4*, 1759. https://doi.org/10.1038/ncomms2774

Mehta, A. J., & Guidot, D. M. (2012). Alcohol abuse, the alveolar macrophage and pneumonia. *Am J Med Sci*, *343*(3), 244-247. https://doi.org/10.1097/MAJ.0b013e31823ede77

Mehta, A. J., & Guidot, D. M. (2017). Alcohol and the Lung. *Alcohol Res*, *38*(2), 243-254. https://www.ncbi.nlm.nih.gov/pubmed/28988576

Mehta, A. J., Yeligar, S. M., Elon, L., Brown, L. A., & Guidot, D. M. (2013). Alcoholism causes alveolar

macrophage zinc deficiency and immune dysfunction. *Am J Respir Crit Care Med*, *188*(6), 716-723. https://doi.org/10.1164/rccm.201301-0061OC

Nicolaou, C., Chatzipanagiotou, S., Tzivos, D., Tzavellas, E. O., Boufidou, F., & Liappas, I. A. (2004). Serum cytokine concentrations in alcohol-dependent individuals without liver disease. *Alcohol*, *32*(3), 243-247. https://doi.org/10.1016/j.alcohol.2004.02.004

O'Quinn, M. P., Palatinus, J. A., Harris, B. S., Hewett, K. W., & Gourdie, R. G. (2011). A peptide mimetic of the connexin43 carboxyl terminus reduces gap junction remodeling and induced arrhythmia following ventricular injury. *Circ Res*, *108*(6), 704-715. https://doi.org/10.1161/CIRCRESAHA.110.235747

Obert, E., Strauss, R., Brandon, C., Grek, C., Ghatnekar, G., Gourdie, R., & Rohrer, B. (2017). Targeting the tight junction protein, zonula occludens-1, with the connexin43 mimetic peptide, alphaCT1, reduces VEGF-dependent RPE pathophysiology. *J Mol Med (Berl)*, *95*(5), 535-552. https://doi.org/10.1007/s00109-017-1506-8

Ongstad, E. L., O'Quinn, M. P., Ghatnekar, G. S., Yost, M. J., & Gourdie, R. G. (2013). A Connexin43 Mimetic Peptide Promotes Regenerative Healing and Improves Mechanical Properties in Skin and Heart. *Adv Wound Care (New Rochelle)*, *2*(2), 55-62. https://doi.org/10.1089/wound.2011.0341

Overgaard, C. E., Schlingmann, B., Dorsainvil White, S., Ward, C., Fan, X., Swarnakar, S., Brown, L. A., Guidot, D. M., & Koval, M. (2015). The relative balance of GM-CSF and TGF-beta1 regulates lung epithelial barrier function. *Am J Physiol Lung Cell Mol Physiol*, *308*(12), L1212-1223. https://doi.org/10.1152/ajplung.00042.2014

Persson, S. G., & Ullberg, L. E. (1979). Blood-volume determination with Evans blue dye in foals. *Acta Vet Scand*, *20*(1), 10-15. https://www.ncbi.nlm.nih.gov/pubmed/443134

Price, M. E., Pavlik, J. A., Liu, M., Ding, S. J., Wyatt, T. A., & Sisson, J. H. (2017). Alcohol drives S-nitrosylation and redox activation of protein phosphatase 1, causing bovine airway cilia dysfunction. *Am J Physiol Lung Cell Mol Physiol*, *312*(3), L432-L439.

https://doi.org/10.1152/ajplung.00513.2016

Radu, M., & Chernoff, J. (2013). An in vivo assay to test blood vessel permeability. *J Vis Exp*(73), e50062. https://doi.org/10.3791/50062

Rangel, S. M., Diaz, M. H., Knoten, C. A., Zhang, A., & Hauser, A. R. (2015). The Role of ExoS in Dissemination of Pseudomonas aeruginosa during Pneumonia. *PLoS Pathog*, *11*(6), e1004945. https://doi.org/10.1371/journal.ppat.1004945

Repp, H., Pamukci, Z., Koschinski, A., Domann, E., Darji, A., Birringer, J., Brockmeier, D., Chakraborty, T., & Dreyer, F. (2002). Listeriolysin of Listeria monocytogenes forms Ca2+-permeable pores leading to intracellular Ca2+ oscillations. *Cell Microbiol*, *4*(8), 483-491. https://doi.org/10.1046/j.1462-5822.2002.00207.x

Roberts, K. E. (1963). Mechanism of Dehydration Following Alcohol Ingestion. *Arch Intern Med*, *112*, 154-157. https://doi.org/10.1001/archinte.1963.03860020052002

Sandoval, R., Malik, A. B., Minshall, R. D., Kouklis, P., Ellis, C. A., & Tiruppathi, C. (2001). Ca(2+) signalling and PKCalpha activate increased endothelial permeability by disassembly of VE-cadherin junctions. *J Physiol*, *533*(Pt 2), 433-445. https://doi.org/10.1111/j.1469-7793.2001.0433a.x

Saria, A., & Lundberg, J. M. (1983). Evans blue fluorescence: quantitative and morphological evaluation of vascular permeability in animal tissues. *J Neurosci Methods*, *8*(1), 41-49. https://doi.org/10.1016/0165-0270(83)90050-x

Schlingmann, B., Overgaard, C. E., Molina, S. A., Lynn, K. S., Mitchell, L. A., Dorsainvil White, S., Mattheyses, A. L., Guidot, D. M., Capaldo, C. T., & Koval, M. (2016). Regulation of claudin/zonula occludens-1 complexes by hetero-claudin interactions. *Nat Commun*, *7*, 12276. https://doi.org/10.1038/ncomms12276

Shellito, J. E., quan Zheng, M., Ye, P., Ruan, S., Shean, M. K., & Kolls, J. (2001). Effect of alcohol consumption on host release of interleukin-17 during pulmonary infection with Klebsiella pneumoniae. *Alcohol Clin Exp Res*, *25*(6), 872-881.

https://www.ncbi.nlm.nih.gov/pubmed/11410724

Singh, A. K., Jiang, Y., Gupta, S., & Benlhabib, E. (2007). Effects of chronic ethanol drinking on the blood brain barrier and ensuing neuronal toxicity in alcohol-preferring rats subjected to intraperitoneal LPS injection. *Alcohol Alcohol*, *42*(5), 385-399. https://doi.org/10.1093/alcalc/agl120

Smith, P., Jeffers, L. A., & Koval, M. (2019). Effects of different routes of endotoxin injury on barrier function in alcoholic lung syndrome. *Alcohol*, *80*, 81-89. https://doi.org/10.1016/j.alcohol.2018.08.007

Smith, P., Jeffers, L. A., & Koval, M. (2021). Measurement of Lung Vessel and Epithelial Permeability In Vivo with Evans Blue. *Methods Mol Biol*, *2367*, 137-148. https://doi.org/10.1007/7651_2020_345

Soder, B. L., Propst, J. T., Brooks, T. M., Goodwin, R. L., Friedman, H. I., Yost, M. J., & Gourdie, R. G. (2009). The connexin43 carboxyl-terminal peptide ACT1 modulates the biological response to silicone implants. *Plast Reconstr Surg*, *123*(5), 1440-1451. https://doi.org/10.1097/PRS.0b013e3181a0741d

Sonnen, A. F., Plitzko, J. M., & Gilbert, R. J. (2014). Incomplete pneumolysin oligomers form membrane pores. *Open Biol*, *4*, 140044. https://doi.org/10.1098/rsob.140044

Strauss, R. E., Mezache, L., Veeraraghavan, R., & Gourdie, R. G. (2021). The Cx43 Carboxyl-Terminal Mimetic Peptide alphaCT1 Protects Endothelial Barrier Function in a ZO1 Binding-Competent Manner. *Biomolecules*, *11*(8). https://doi.org/10.3390/biom11081192

Stypmann, J. (2007). Doppler ultrasound in mice. *Echocardiography*, *24*(1), 97-112. https://doi.org/10.1111/j.1540-8175.2006.00358.x

Uechi, M., Asai, K., Osaka, M., Smith, A., Sato, N., Wagner, T. E., Ishikawa, Y., Hayakawa, H., Vatner, D. E., Shannon, R. P., Homcy, C. J., & Vatner, S. F. (1998). Depressed heart rate variability and arterial baroreflex in conscious transgenic mice with overexpression of cardiac Gsalpha. *Circ Res*, *82*(4), 416-423. https://doi.org/10.1161/01.res.82.4.416

Verbrugge, S. J., Vazquez de Anda, G., Gommers, D., Neggers, S. J., Sorm, V., Bohm, S. H., & Lachmann, B. (1998). Exogenous surfactant preserves lung function and reduces alveolar Evans blue dye influx in a rat model of ventilation-induced lung injury. *Anesthesiology*, *89*(2), 467-474. https://doi.org/10.1097/00000542-199808000-00024

Ward, C., Schlingmann, B., Stecenko, A. A., Guidot, D. M., & Koval, M. (2015). NF-kappaB inhibitors impair lung epithelial tight junctions in the absence of inflammation. *Tissue Barriers*, *3*(1-2), e982424. https://doi.org/10.4161/21688370.2014.982424

Wolman, M., Klatzo, I., Chui, E., Wilmes, F., Nishimoto, K., Fujiwara, K., & Spatz, M. (1981). Evaluation of the dye-protein tracers in pathophysiology of the blood-brain barrier. *Acta Neuropathol*, *54*(1), 55-61. https://doi.org/10.1007/BF00691332

Wray, C., Mao, Y., Pan, J., Chandrasena, A., Piasta, F., & Frank, J. A. (2009). Claudin-4 augments alveolar epithelial barrier function and is induced in acute lung injury. *Am J Physiol Lung Cell Mol Physiol*, *297*(2), L219-227. https://doi.org/10.1152/ajplung.00043.2009

Yan, L., Vatner, D. E., O'Connor, J. P., Ivessa, A., Ge, H., Chen, W., Hirotani, S., Ishikawa, Y., Sadoshima, J., & Vatner, S. F. (2007). Type 5 adenylyl cyclase disruption increases longevity and protects against stress. *Cell*, *130*(2), 247-258. https://doi.org/10.1016/j.cell.2007.05.038

Yang, G., Pillich, H., White, R., Czikora, I., Pochic, I., Yue, Q., Hudel, M., Gorshkov, B., Verin, A., Sridhar, S., Isales, C. M., Eaton, D. C., Hamacher, J., Chakraborty, T., & Lucas, R. (2018). Listeriolysin O Causes ENaC Dysfunction in Human Airway Epithelial Cells. *Toxins (Basel)*, *10*(2). https://doi.org/10.3390/toxins10020079

Yang, X. P., Liu, Y. H., Rhaleb, N. E., Kurihara, N., Kim, H. E., & Carretero, O. A. (1999). Echocardiographic assessment of cardiac function in conscious and anesthetized mice. *Am J Physiol*, *277*(5), H1967-1974. https://doi.org/10.1152/ajpheart.1999.277.5.H1967

Yao, L., Xue, X., Yu, P., Ni, Y., & Chen, F. (2018). Evans Blue Dye: A Revisit of Its Applications in Biomedicine. *Contrast Media Mol Imaging*, *2018*, 7628037. https://doi.org/10.1155/2018/7628037

Zisman, D. A., Strieter, R. M., Kunkel, S. L., Tsai, W. C., Wilkowski, J. M., Bucknell, K. A., & Standiford, T. J. (1998). Ethanol feeding impairs innate immunity and alters the expression of Th1- and Th2-phenotype cytokines in murine Klebsiella pneumonia. *Alcohol Clin Exp Res*, *22*(3), 621-627. https://doi.org/10.1111/j.1530-0277.1998.tb04303.x